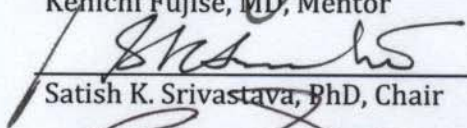The Dissertation Committee for Abhijnan Chattopadhyay Certifies

that this is the approved version of the following dissertation:

STUDY ON THE PHYSICAL AND FUNCTIONAL INTERACTION

BETWEEN FORTILIN AND PEROXIREDOXIN I
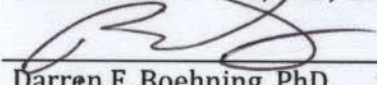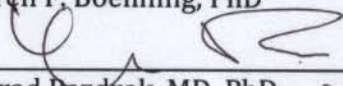
Committee:

_____
Kenichi Fujise, MD, Mentor
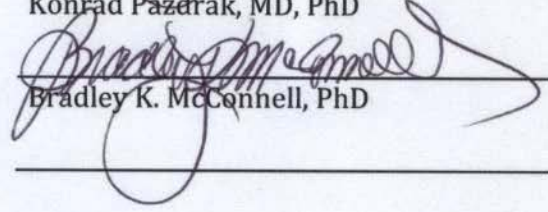
_____
Satish K. Srivastava, PhD, Chair

_____
Darren F. Boehning, PhD

_____
Konrad Pazdrak, MD, PhD

_____
Bradley K. McConnell, PhD

_____

_____
Dean, Graduate School

STUDY ON THE PHYSICAL AND FUNCTIONAL INTERACTION

BETWEEN FORTILIN AND PEROXIREDOXIN I

BY

Abhijnan Chattopadhyay, BSc, MSc

Dissertation

Presented to the Faculty of the Graduate School of

The University of Texas Medical Branch

in Partial Fulfillment

of the Requirements

for the Degree of

Doctor of Philosophy

The University of Texas Medical Branch

October, 2013

DEDICATION

To my parents who have made me everything that I am today.

ACKNOWLEDGEMENTS

First and foremost, I would like to express my deepest thanks and gratitude to my mentor Dr Kenichi Fujise without whose constant support and encouragement this research project would not have been completed. For the preceding four years, Dr Fujise has served as an inspiration for me to work harder, to go the extra mile, to do something conventional wisdom warns against and at the same time helped me maintain the highest standards of scientific conduct – something he upholds and embodies. Dr Fujise accepted me into his research laboratory at a difficult time for me and I would remain forever indebted to him for his generosity and the confidence he showed in me. He has always taught me to look at the bigger picture and that scientific research is not just designing and performing experiments day in and day out, but a continuous process aimed at looking at something greater. Thank you, Dr Fujise, for being an outstanding mentor.

I would like to extend my personal thanks to each and every member of the Fujise laboratory, particularly Dr Yanjie Chen and Dr Decha Pinkaew, for sharing their expertise and experiences with me and giving me the confidence to trust the results of my own experiments. The scientific discussions we have had in the lab and over lunch at the MRB 7th floor lunch room have been some of the most engrossing discussions I have ever had. Special thanks go out to my friend and fellow graduate student Hung Doan who started this journey around four months before I did and has been by my side ever since I joined the Fujise lab. From teaching me the basics of cell culture to those of fundamental laboratory techniques, Hung has been an integral part of my scientific education. The extensive discussions which we have had over the years have not only enhanced my understanding of my project and science as a whole, but also enriched me as a person. I would also like to take this opportunity to thank my other colleagues in the Fujise laboratory – Dr Wei Liu, Dr Nattaporn Wanachottrakul, Patuma Sinthujaroen, Barbara Rolls as well as our outstanding administrative coordinators Heather Foster, Suzan Allman and Codi Hurd.

I would like to recognize and appreciate the help and support of the members of my Supervisory Committee – Chairman Dr Satish K. Srivastava whose words of wisdom have encouraged me to look at science with a broader perspective; Dr Darren F. Boehning whose insightful questions have made me pause and dig

STUDY ON THE PHYSICAL AND FUNCTIONAL INTERACTION BETWEEN FORTILIN AND PEROXIREDOXIN I

Publication No._____

Abhijnan Chattopadhyay, PhD
The University of Texas Medical Branch, 2013

Supervisor: Kenichi Fujise

Abstract:

Apoptosis or programmed cell death is a highly regulated cellular process which is essential for the development of an organism as well as for tissue and organ maintenance. Dysregulation of apoptosis is responsible for a variety of disease phenotypes from cancer to neurodegenerative and cardiovascular diseases. Fortilin (FT) is an anti-apoptotic protein that prevents apoptotic cell death under various conditions of cellular stress including UV, chemical and oxidative stress. However, the molecular mechanism of this pro-survival action under conditions of oxidative stress has yet to be elucidated. Using an immunoprecipitation and mass spectrometry-based screening approach, we identified a number of potential fortilin interacting proteins, including the anti-oxidant enzyme peroxiredoxin I (Prx I). Prx I is a thioredoxin-dependent peroxidase enzyme that is known to be protective against reactive oxygen species (ROS)-induced cell death. We confirmed the interaction between FT and Prx I by using various approaches, including reverse co-immunoprecipitation, direct binding and co-localization studies in cultured cells as well as animal tissue and demonstrated that FT stabilizes Prx I in U2OS cells by preventing its proteasomal degradation. Furthermore, our results showed that wild type FT, but not a point mutant of FT that does not bind to Prx I, enhances the enzymatic activity of Prx I. Further investigations revealed that FT inhibits the deactivating phosphorylation of Prx I by the serine/threonine kinase Mst1 in a dose-dependent manner. Additionally, the anti-apoptotic activity of FT under oxidative stress was found to be dependent on its interaction with Prx I. Finally, we demonstrated that a liver-specific knockout of FT exacerbates ethanol-induced oxidative liver damage. Taken together, our data confirm a novel interaction between FT and Prx I that positively regulates the functions of both proteins, leading to increased cytoprotection and may be explored in future as a therapeutic target in oxidative stress-induced pathological conditions.

TABLE OF CONTENTS

LIST OF TABLES

LIST OF FIGURES

LIST OF ABBREVIATIONS

ABTS	2,2'-azino-bis(3-ethylbenzothiazoline-6-sulphonic acid)
ADP	Adenosine diphosphate
ALB	Albumin
ALP	Alkaline phosphatase
ALT	Alanine aminotransferase
APAF1	Apoptotic protease activating factor-1
ARE	Antioxidant response element
Asn	Asparagine
As$_2$O$_3$	Arsenius oxide
ATM	Ataxia-telangiectasia mutated
ATP	Adenosine triphosphate
BA	Bile acids
Bad	Bcl-2-associated death promoter
Bak	Bcl-2 homologous antagonist killer
Bax	Bcl-2-associated X protein
Bcl-2	B-cell lymphoma 2
BH	Bcl-2 homology
BHT	Butylated hydroxytoluene
Bid	BH3-interacting-domain death agonist
Bim	Bcl-2-like protein 11
BLF	Basal lavage fluid
BMP	Bone morphogenic protein
Bok	Bcl-2 related ovarian killer
53BP1	p53-binding protein
BRF	Biomolecular Resource Facility
BUN	Blood urea nitrogen
Caspases	Cysteine-aspartic proteases or cysteine-dependent aspartate-directed proteases
Cdc2/CDK1	Cyclin-dependent kinase 1/Cell division control protein 2 homolog
CEDs	Cell Death proteins
C. elegans	*Caenorhabditis elegans*
co-IP	co-immunoprecipitation
Chk	Checkpoint kinase
CHOL	Cholesterol
CHX	Cycloheximide
Cys	Cysteine
DAPI	4',6-diamidino-2-phenylindole
DEPC	Diethylpyrocarbonate or diethyl carbonate
DISC	Death Inducing Signaling Complex
DNA	Deoxyribonucleic acid
DPBS	Dulbecco's phosphate buffered saline
dpc	Days post-coitus

DR	Death receptor
DTNB	5,5'-dithiobis(2-nitrobenzoic acid)
DTT	Dithiothreitol
E. coli	*Escherichia coli*
EDTA	Ethylenediaminetetraacetic acid/tetraacetate
eEF1A	Eukaryotic translation elongation factor 1A
eEF1Bβ	Eukaryotic translation elongation factor 1Bβ
EGFR	Epidermal growth factor receptor
EGTA	Ethylene glycol tetraacetic acid
ELISA	Enzyme-linked immunosorbet assay
ER	Endoplasmic reticulum
FADD	Fas-activated death domain
FBS	Fetal bovine serum
FIP	Fortilin interacting protein
FT	Fortilin
GAPDH	Glyceraldehyde-3-phosphate dehydrogenase
GDP	Guanosine diphosphate
GEF	Guanine nucleotide exchange factor
GM-CSF	Granulocyte macrophage-colony stimulating factor
GR	Glutathione reductase
GSH	Glutathione
GSSG	Reduced glutathione
GTP	Guanosine triphosphate
HA	Hemagglutinin
HCl	Hydrochloric acid
H&E	Hematoxylin and eosin
HEK	Human embryonic kidney
HEPES	4-(2-hydroxyethyl)-1-piperazineethanesulfonic acid
HF	Heart failure
4-HNE	4-hydroxynonenal
H_2O_2	Hydrogen peroxide
HRF	Histamine-releasing factor
HSP	Heat shock protein
IAP	Inhibitors of apoptosis
IB	Immunoblot
IgE	Immunoglobulin E
IgG	Immunoglobulin G
IL	Interleukin
IgM	Immunoglobulin M
IP	Immunoprecipitation
JNK	c-Jun N-terminal kinase
kDa	Kilodalton
MALDI-TOF	Matrix-associated laser desorption ionization/time of flight
MAP	Microtubule-associated protein
MCL-1	Myeloid cell leukemia sequence 1
MDA	Malondialdehyde

Mdm2	Mouse double minute 2 homolog
$MgCl_2$	Magnesium chloride
μM	Micromolar
mM	Millimolar
MOI	Multiplicity of infection
MOMP	Mitochondrial outer membrane pores
mRNA	Messenger RNA
MS	Mass Spectrometry
Mst1	Serine/threonine kinase 4
MT	Microtubule
NaCl	Sodium chloride
NAD	Nicotinamide adenine dinucleotide
NADH	Reduced Nicotinamide adenine dinucleotide
NaF	Sodium fluoride
NAD(P)	Nicotinamide adenine dinucleotide phosphate
NAD(P)H	Reduced Nicotinamide adenine dinucleotide phosphate
Na,K-ATPase	Sodium, potassium ATPase
NaOH	Sodium hydroxide
NBF	Neutral buffered formalin
NF-κB	Nuclear factor kappa-light-chain-enhancer of activated B cells
nM	Nanomolar
Npm1	Nucleophosmin/nucleoplasmin family member 1
NQO2	NAD(P)H dehydrogenase, quinone 2
Nrf2	Nuclear factor-E2-related factor 2
Na_3VO_4	Sodium orthovanadate
PBS	Phosphate buffered saline
PCR	Polymerase chain reaction
pI	Isoelectric point
PLA	Proximity ligation assay
PLK	Polo-like kinase
PMSF	Phenylmethylsulphonyl fluoride
Prx	Peroxiredoxin
PUMA	p53-upregulated modulator of apoptosis
qRT-PCR	Quantitative real-time polymerase chain reaction
Rheb	Ras-homolog enriched in brain
RNA	Ribonucleic acid
ROS	Reactive Oxygen Species
SDHA	Succinate dehydrogenase subunit A
SDS	Sodium dodecylsulphate
Ser	Serine
SMAC	Second mitochondrial activator of caspases
SPR	Surface Plasmon resonance
Srx	Sulfiredoxin
5-SSA	5-Sulphosalicylic acid
SUMO	Small ubiquitin-like modifier

TBA	Thioburbituric acid
TBIL	Total bilirubin
TCTP	Translationally controlled tumor protein
TEMED	Tetramethylethylenediamine
TGF	Transforming growth factor
Thr	Threonine
TNFα	Tumor necrosis factor alpha
TRAF6	Tumor Necrosis Factor receptor-associated factor 6
Tris	Tris(hydroxymethyl)aminomethane
Trx	Thioredoxin
TrxR	Thioredoxin reductase
TSC22	Transforming growth factor-β stimulated clone-22
TUNEL	Terminal deoxynucleotidyl transferase
UPR	Unfolded protein response
UTMB	University of Texas Medical Branch
UTR	Untranslated region
VDR	Vitamin D3 receptor
WB	Western blot
X-Gal	5-bromo-4-chloro-3-indolyl-β-D-galactopyranoside

CHAPTER I: BACKGROUND AND SIGNIFICANCE

1.1. APOPTOSIS

Apoptosis or programmed cell death is a highly regulated process responsible for tissue maintenance and development of an organism. Dysregulation of apoptosis is implicated in a wide range of human pathological conditions including cancer, cardiovascular and neurodegenerative diseases. Apoptosis has come into research focus ever since the inhibition of apoptosis was identified by Hanahan and Weinberg as a hallmark of cancer in 2000 and reinforced in 2011 [Hanahan and Weinberg, 2000; Hanahan and Weinberg, 2011]. Additionally, the importance of apoptosis during embryonic development cannot be overstated: it is an essential process right from the beginning of life when embryonic structures start forming and then die in a programmed manner at pre-destined time points during the course of development. After birth and throughout the life of the organism, apoptosis plays an important role in tissue maintenance and homeostasis. Apoptotic stimuli can arise from within or from outside the cell, in the form of death signals and developmental cues or from simple needs to maintain normal tissue and organ function. The key word in understanding apoptosis is that it is a highly *regulated* process, which makes it different from the other major forms of cell death such as autophagy and necrosis. Autophagy or "self eating" is induced primarily by nutrient starvation and necrosis is induced by pathogen infection or toxic shock.

Another crucial difference between apoptosis and necrosis is the fact that apoptosis, unlike necrosis, does not engage the inflammatory cascade of the cell. The following cartoon (Fig. 1) demonstrates the major differences between the three major forms of cell death.
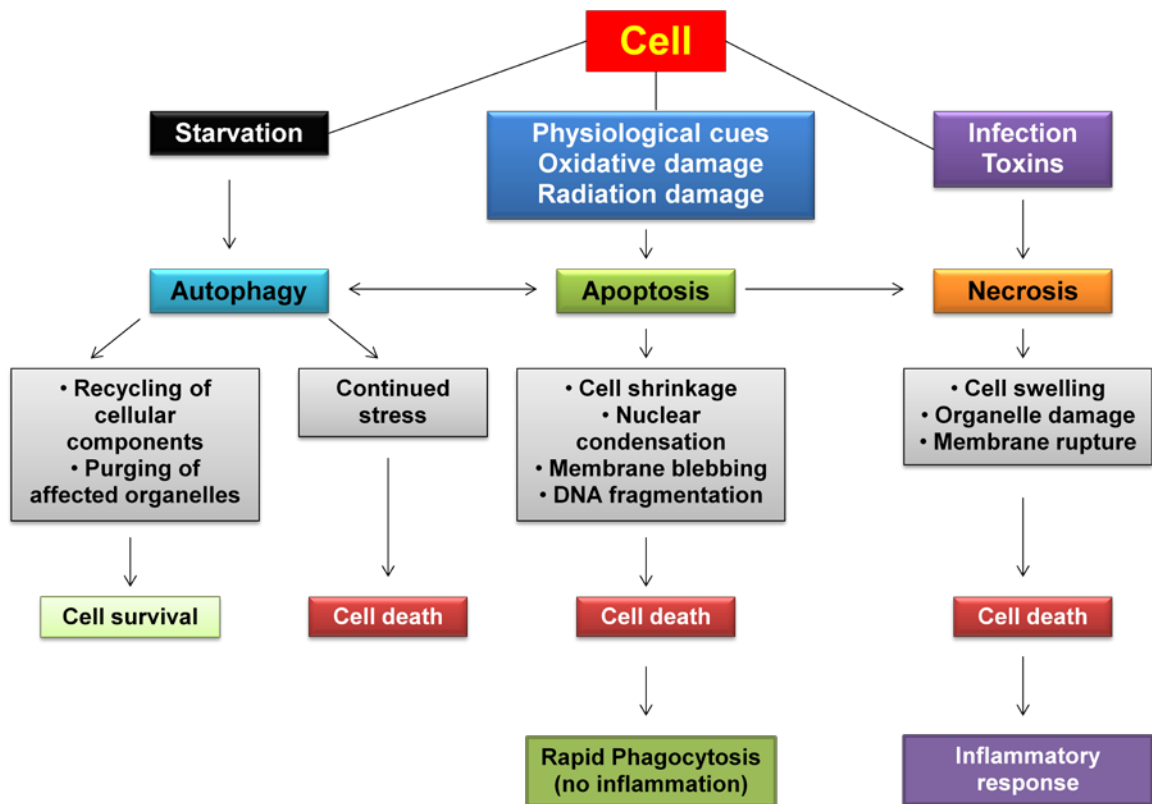
Figure 1: Overview of autophagy, apoptosis and necrosis. Key features and differences among the three major pathways of cell death.

Necrosis is characterized by changes in cellular morphology such as cell swelling, organelle disruption and membrane rupture, eventually leading to the

release of the cellular contents in the extracellular milieu and subsequent activation of the inflammatory cascade. Apoptosis, on the other hand, is characterized by membrane blebbing, loss of plasma membrane asymmetry, shrinkage in cell size, chromatin condensation and nuclear and DNA fragmentation. One of the classical ways to experimentally visualize apoptosis is to collect DNA from the dead cells and perform electrophoresis on it and observe a characteristic ladder-like appearance of the fragmented DNA.

Based on the molecular effectors of the process, apoptosis can be loosely discussed in terms of two major pathways – the so-called Cell Extrinsic Pathway and the so-called Cell Intrinsic Pathway [Ashkenazi *et al.* 2002]. The principal effectors of apoptosis at the molecular level are caspases, which are cysteine-aspartate proteases that bring about the cleavage of proteins crucial for cell survival, eventually leading to apoptotic cell death. Caspases were initially characterized in *C. elegans* as "*C. elegans* Death proteins" or CEDs. Based on their function, caspases can be subdivided into two classes: initiator caspases and executor caspases. The major function of initiator caspases (caspase-2, 8, 9, 10) is to cleave the zymogen or pro-caspase forms of the executor caspases and activate them. The activated executor caspases 3, 6 and 7, finally cleave proteins crucial for cell survival, including structural proteins and enzymes that are important for cell viability.

1.1.1. THE CELL EXTRINSIC PATHWAY OF APOPTOSIS:

The extrinsic pathway of apoptosis is primarily activated by cues from outside the cell, usually in a ligand-receptor interaction mechanism. The process is initiated by the binding of a pro-death ligand (e.g. Fas ligand for immune cells) to death receptors DR4 and DR5. Activation of the death receptor (via the Fas-activated death domain or FADD) leads to the formation of the Death Inducing Signaling Complex (DISC). DISC then recruits a series of membrane-associated proteins to form the Death Complex. This complex then leads to activation of pro-caspases 8 and 10 into activated caspases 8 and 10. These caspases then cleave the pro-apoptotic Bcl-2 family protein Bid, which engages the mitochondria through the activation of pro-apoptotic Bad and Bax. Dimerization of Bax within the mitochondrial membrane leads to mitochondrial membrane permeabilization and release of cytochrome –c into the cytosol. The point where Bad and Bax are engaged in the process is where the extrinsic pathway begins cross-talk with the intrinsic pathway, as discussed below.

1.1.2. THE CELL INTRINSIC PATHWAY OF APOPTOSIS

The cell intrinsic pathway of apoptosis is activated primarily from within the cell through DNA damage or developmental cues. Generation of reactive oxygen

4

species (ROS) causes rupture of the mitochondrial membrane and release of cytochrome-c into the cytosol. Alternatively, the DNA damage response activates the tumor suppressor gene p53 which activates transcription of pro-apoptotic proteins PUMA and Noxa, followed by Bax and Bad, leading to Bax dimerization in the mitochondrial membrane and subsequent loss of mitochondrial membrane integrity. This is the point where the cell extrinsic and cell intrinsic pathways communicate with each other (Fig. 2). Cytochrome-c along with apoptosis activating factor-1 (APAF1) forms the so-called apoptosome complex and cleaves pro-caspase 9 to activate the initiator caspase 9, which then cleaves and activates the executioner caspase 3. The executioner caspases 3, 6 and 7 then bring about cleavage of proteins crucial for cell viability, causing cell death, followed by rapid phagocytosis by circulating macrophages.

1.1.3. OTHER MECHANISMS OF APOPTOSIS ACTIVATION

Along with the two major pathways of apoptosis discussed above, there also exist other pathways of apoptosis including one activated by endoplasmic reticulum (ER) stress. ER stress, brought about by either calcium ions or heat shock or protein glycosylation inhibitors, leads to activation of the initiator pro-caspase 12. Long term ER stress, however, leads to cleavage and activation of it into caspase 12 via an unfolded protein response (UPR)-mediated process [Zinzsner *et al.* 1998; Feng *et al.* 2003; Ling *et al.* 2007], thus potentiating the apoptotic cascade.
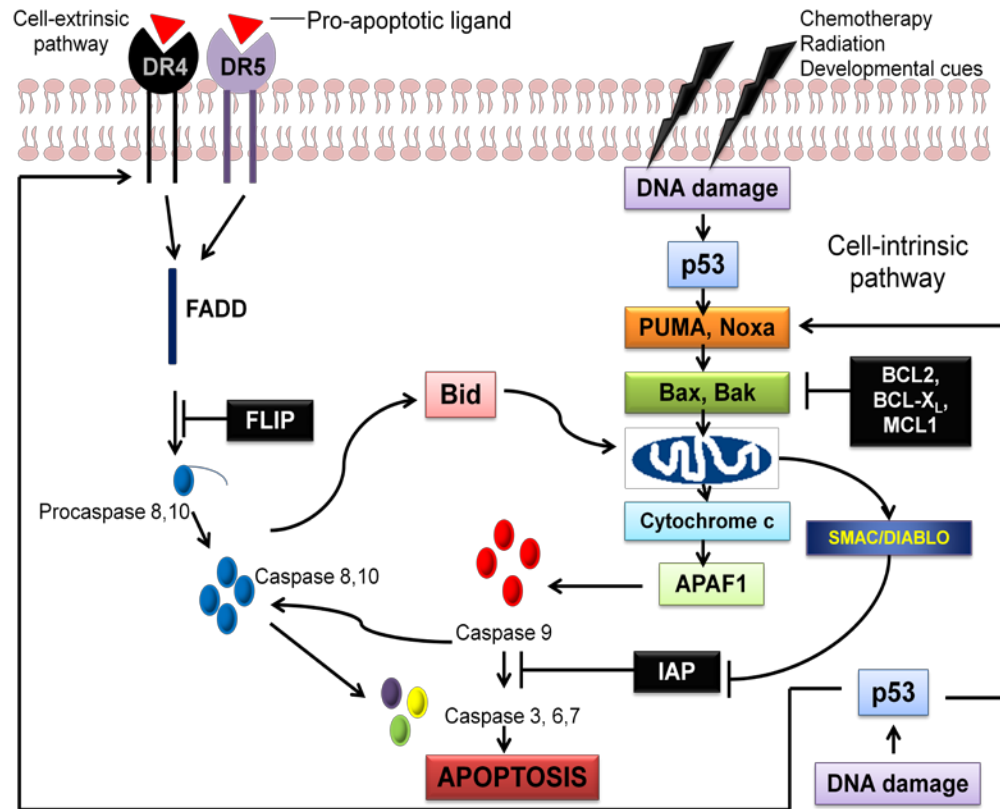
Figure 2: The two major pathways of apoptosis. Brief overview of the two major pathways of apoptosis.

1.1.4. p53 AND APOPTOSIS

While p53 is a known regulator of apoptosis, the exact mechanism of apoptosis activation by p53 is not exactly clear. Radiation or ROS-induced DNA damage causes activation of checkpoint kinases Chk1 or Chk2, whose role is to phosphorylate and induce self-ubiquitinylation of the p53 inhibitor Mdm2, thereby abrogating its inhibitory effect on p53. p53 then translocates to the nucleus and

upregulates transcription of genes like p21, Bcl-2 and Bax. If the stress is too high for the cell to handle, p53 initiates full scale activation of apoptosis by upregulating transcription of pro-apoptotic genes PUMA, Noxa and Bax. These genes then lead to cytochrome-c release via mitochondrial membrane permeabilization.

1.1.5. OXIDATIVE STRESS AND APOPTOSIS

Reactive oxygen species (ROS) are oxygen-containing highly reactive molecules that are generated as by-products of cellular metabolism as well as during cellular respiration in presence of molecular oxygen. The high reactivity of ROS is attributed to the presence of unpaired electrons in the species. Although important in intracellular signaling, elevated levels of ROS are dangerous for the cell as they cause tremendous oxidative damage to proteins and DNA, leading to either cell death or disease states. ROS can be generated by metabolic pathways, heat, chemicals – especially chemotherapeutic drugs and ionizing radiation. Under physiological conditions, the toxic effects of ROS, such as superoxide anion and hydroxyl radicals are prevented by the ROS scavenger enzymes: superoxide dismutase, glutathione peroxidase, catalase and members of the peroxiredoxin (Prx) family. However, when the ROS load overwhelms the antioxidant capacity of the cell, the resultant oxidative stress leads to oxidation of membrane phospholipids, proteins and DNA, eventually leading to cell death. ROS-induced cell death could be both apoptotic and necrotic. ROS such as superoxide anions ($\cdot O_2^-$) and hydroxy

radicals (·OH) have been reported by some authors to be responsible for a variety of disease states like ischemia-reperfusion injury, neurodegeneration and aging [Tsutsui *et al.* 2008], by causing oxidative damage to cellular proteins, lipids and nucleic acids. Furthermore, elevated levels of lipid peroxides and 8-iso-prostaglandin F2α, major biochemical markers of ROS generation, have been observed in the plasma and pericardial fluid of patients with heart failure, with good positive correlation to disease progression [Belch *et al.* 1991; Mallat *et al.* 1998].

ROS can lead to apoptosis by either causing structural damage to mitochondrial membrane, leading to permeabilization and release of cytochrome-c or by causing damage to the mitochondrial electron transport chain, which in turn leads to p53 activation via Chk1 and Chk2 and subsequent p53-mediated upregulation of pro-apoptotic genes. Ionizing radiation and chemotherapeutic drugs bring about cellular apoptosis via these mechanisms. Acute or chronic alcohol-induced liver damage also occurs via ethanol-mediated ROS generation and causes apoptotic as well as necrotic cell death.

1.1.6. INHIBITION OF APOPTOSIS

Apoptosis is a highly regulated process and its regulation is crucial for survival of the cell as well as to prevent formation of cancerous lesions. The regulation is achieved at the molecular level by the balance between pro- and anti-

apoptotic proteins. While p53, Bax, Bak, Bid, PUMA, Noxa, and Apaf-1 etc are all pro-apoptotic factors, there are two important families of apoptosis inhibitor proteins that regulate the apoptotic pathways, as discussed below:

1.1.6.1. THE BCL-2 FAMILY OF PROTEINS

The family is named after the first member of the family - B-cell leukemia (Bcl)-2, which was originally identified in B-cell leukemias. Bcl-2 contains four Bcl-2 homology (BH) domains. In fact all proteins in this family contain one or more BH domains; Bcl-2 itself contains four such domains – BH1, BH2, BH3 and BH4. Interestingly, the family consists of both pro- and anti-apoptotic proteins. The difference between the two groups is that all the anti-apoptotic Bcl-2 proteins contain all four BH domains while the pro-apoptotic proteins are either BH3-only proteins (Bid, Bim, Bad, PUMA, Noxa) or multi-domain BH-containing proteins (Bax, Bak, Bok). These pro-apoptotic proteins either embed directly within the mitochondrial membrane (Bax, Bim), forming the mitochondrial outer membrane pore (MOMP) or favor formation of MOMP while some of the other proteins, inhibit anti-apoptotic Bcl-2 family proteins.

Some major anti-apoptotic Bcl-2 family proteins include Bcl-2 itself, Bcl-xL, Bcl-w and myeloid cell leukemia (MCL)-1. All these proteins contain four BH domains and are primarily thought to function by preventing loss of mitochondrial

membrane integrity. As important regulators of apoptosis, they are crucial in diseases like cancer and atherosclerosis.

1.1.6.2. THE INHIBITORS OF APOPTOSIS PROTEIN FAMILY (IAP)

Another very important family of anti-apoptotic proteins is the inhibitors of apoptosis protein (IAP) family. IAPs specifically function by directly inhibiting the action of caspases 3, 7 and 9. All the eight mammalian IAPs, including Survivin, X-linked IAP (XIAP), cytosolic IAP (cIAP)-1, cIAP-2, Ts-IAP, ML-IAP, NIAP and Apollon, contain a zinc-binding Baculovirus IAP Repeat (BIR) domain and a RING domain at the C-terminus. The BIR domain is crucial for their ability to directly inhibit caspases. IAPs can be regulated by post-translational modifications like phosphorylation and ubiquitinylation. They are also inactivated by interactions with the Second Mitochondrial Activator of Caspases (SMAC) and the Omi proteins. IAPs additionally inhibit pro-survival pathways involved in TRAF6/NF-kB signaling and TGF/JNK pathway.

1.2. FORTILIN: A NOVEL REGULATOR OF APOPTOSIS

In 2001, Li and others [Li *et al.* 2001] identified a novel negative regulator of apoptosis called fortilin (FT) which does not share any structural or sequence

homology with either Bcl-2 or IAP groups of anti-apoptotic proteins. FT is therefore, in a novel class of anti-apoptotic proteins and I will dedicate the next few subsections to provide more information about this protein.

1.2.1. DISCOVERY

Fortilin (FT), also known as translationally controlled tumor protein (TCTP), IgE-dependent histamine releasing factor (HRF), p21/23 was discovered in 1983 in Ehrlich ascites tumor cells [Yenofsky *et al.* 1983] and also in mouse erythroleukemia [Chitpatima *et al.* 1988]. The original name of the protein – TCTP – is derived from the observation that mRNA of TCTP is rapidly translated into the protein upon stimulation with growth factors. While present in relatively low levels in resting cells, its expression level increases dramatically in proliferating cells. For example, in proliferating *Saccharomyces cerevisiae*, there exist close to 100,000 molecules of the protein as compared to 60,000 molecules of actin [Norbeck *et al.* 1997]. While the protein had been identified in 1983, no proper function could be attributed to it till 1995, when MacDonald and co-workers identified it as an immunoglobulin-dependent histamine releasing factor (HRF) [MacDonald *et al.* 1995]. Six years later, in a seminal paper [Li *et al.* 2001] TCTP was identified to be a potent anti-apoptotic protein and renamed as *fortilin* (Latin *fortis* – strong). For the remainder of this dissertation, I will refer to the protein as fortilin (FT).

11

1.2.2. GENETIC ORGANIZATION

FT is encoded by the TPT1 gene, containing five introns and six exons in humans, mouse, rat and rabbit. The gene has a classical TATA-box and a number of highly conserved promoter elements. Exon 6 constitutes the 3'-UTR of the FT mRNA.

1.2.3. FORTILIN mRNA:

All mammalian tissues express two FT mRNAs which differ only by the lengths of their 3'-UTRs, the shorter of the two being usually the more prominent one [Thiele *et al.* 2000]. It contains a highly GC-enriched 5'-UTR while the 3'-UTR is slightly more AU-rich and contains some AUUUA elements. A GC-rich 5'-UTR is characteristic of a high degree of secondary structure and it begins with a 5'-oligopyrimidine tract (5'-OPT). All these constitute classical features of translationally controlled mRNAs.

1.2.4. SEQUENCE ANALYSIS OF FORTILIN

FT is a 172-amino acid containing polypeptide that has a high degree of sequence conservation among diverse taxonomic groups (Fig. 3). Mouse and human FT share ~95% homology and the phylogeny of FT sequences is consistent with

established evolutionary models [Hinojosa-Moya *et al.* 2008]. FT, however, has no sequence homology with known families of anti-apoptotic proteins – the Bcl-2 family and the IAP family, thus establishing itself as a novel type of anti-apoptotic protein. FT does not contain any DNA-binding domains, nuclear localization sequence [Kamitani *et al.* 1997], hydrophobic transmembrane anchor or signal sequence. Two highly conserved cysteine residues (Cys^{28} and Cys^{172}) are present in FT and are predicted to be involved in disulphide bond formation. Additionally, FT contains a conserved Asn^{51}-X^{52}-Ser^{53} sequence stretch, representing a potential glycosylation site, which is yet to be verified experimentally. However, the calculated and observed molecular weights of FT are different (19kDa and 23 kDa respectively) and this difference has been attributed by some researchers to the possible glycosylation of FT.

1.2.5. STRUCTURE AND DOMAINS OF FORTILIN:

The solution NMR structure of FT reveals the presence of three α-helices and eleven β-strands [Feng *et al.* 2007]. The β-strands β-1, β-2 and β-11 form the β-sheet A, strands β-3, β-4, β-10, β-9, β-8 and β-7 form β-sheet B while β-strands β-5 and β-6 form β-sheet C. β-sheets A and B together form a β-barrel, into which the α-hairpin structure formed by the anti-parallel α2 and α3 helices and containing a short loop are packed (Fig. 4A). The protein also contains a long loop from residues T^{39} to V^{66}, which links strands β-5 and β-6. Fortilin contains three domains, with

```
TCTP_Trypanosoma_brucei          MKIFRDILTNAEVVCDNDKPMDVL-----DEIVYAVQGRYIEIG--GED----YGISANA
TCTP_Arabidopsis_thaliana        MLVYQDLLTGDELLSDSFPYKEIE-----NGILWEVEGKWVTVG-AVDV---NIGANPSA
TCTP_Hevea_brasiliensis          MLVYQDLLTGDELLSDSFPYKEIH-----NGILWEVEGKWVVQG-AVDV---DIGANPSA
TCTP_Plasmodium_knowlesi         MKVYKDVFTNDEVCSDSYNQEDPFGIADFREIAFEVKSNKRIK---GNDD---YGIADNS
TCTP_Caenorhabditis_elegans      MLIYKDIFTDDELSSDSFPMKLVD------DLVYEFKGKHVVRK-EGEIV--LAGSNPSA
TCTP_Brugia_malayi               MLIFKDAFTDDELASDSFPMKLVD------GLIWEFKGRQVVRR-EGEIQ--LAGANPSA
TCTP_Schistosoma_mansoni         MIVYKDMITEDEMFTDSHCPRVVA------DFFYEVDSRFTTV--SSNVDGRLIGANPSG
TCTP_Schizosaccharomyces_pombe   MLLYKDVISGDELVSDAYDLKEVD------DIVYEADCQMVTVKQGGDV---DIGANPSA
TCTP_Drosophila_melanogaster     MKIYKDIITGDEMFADTYKMKLVD------DVIYEVYGKLITR-QGDDIK--LEGANASA
TCTP_Danio_rerio                 MIIYKDIITGDEMFSDIYKIKESE-----NGMMLEVEGKMITR-AEGDIDDALIGGNASA
TCTP_Homo_sapiens                MIIYRDLISHDEMFSDIYKIREIA-----DGLCLEVEGKMVSR-TEGNIDDSLIGGNASA
TCTP_Mus_musculus                MIIYRDLISHDELFSDIYKIREIA-----DGLCLEVEGKMVSR-TEGAIDDSLIGGNASA
                                 * :::* ::   *:   *                .           .              *    ..


TCTP_Trypanosoma_brucei          DEDAAEGAAGDVADEKQRVIDVVHNNRYTETN--YDKNSYMAHIRGYMKQLLEKIEDEGA
TCTP_Arabidopsis_thaliana        EEGG---EDEGVDDSTQKVVDIVDTFRLQEQPT-YDKKGFIAYIKKYIKLLTPKLSEED-
TCTP_Hevea_brasiliensis          EGAD---EDEGVDDQAVKVVDIVDTFRLQEQPA-FDKKQFVTYMKRFIKLLTPKLDEEK-
TCTP_Plasmodium_knowlesi         EE-----AVDGMGADVEQVIDIVDSFQLTSTS--LSKKEYSVYIKNYMQKILKYLEEKKP
TCTP_Caenorhabditis_elegans      EEGA---EDDGSDEHVERGIDIVLNHKLVEMNCYEDASMFKAYIKKFMKNVIDHMEKNNR
TCTP_Brugia_malayi               EGED---GDEGSEECVERGIDFVLNHRLQEMNCYEDLVTFKSYCKSFMKKVVELMQKNGK
TCTP_Schistosoma_mansoni         EG-G---EDENVDDTSKRVIDLVHANGFISVP--FDQKSYKAHLNLYLKTIIERLQKTDP
TCTP_Schizosaccharomyces_pombe   ED-A---EEN-AEEGTETVNNLVYSFRLSPTS--FDKKSYMSYIKGYMKAIKARLQESNP
TCTP_Drosophila_melanogaster     EE-A----DEGTDITSESGVDVVLNHRLTECFAFGDKKSYTLYLKDYMKKVLAKLEEKSP
TCTP_Danio_rerio                 EV-A----DEGCDSTSVSGVDIVLNHKLQETS--YDKKSYTAYIKDYMKAVKAKLQESAP
TCTP_Homo_sapiens                EG-P---EGEGTESTVITGVDIVMNHHLQETS--FTKEAYKKYIKDYMKSIKGKLEEQRP
TCTP_Mus_musculus                EG-P---EGEGTESTVVTGVDIVMNHHLQETS--FTKEAYKKYIKDYMKSLKGKLEEQKP
                                 :                   :.*               :   :  . ::: :    :..


TCTP_Trypanosoma_brucei          KK----AFQTNAAAFVKKVI--KEIDEYQFFIPEGNEEDPDNGMIVLCKWD----GETPT
TCTP_Arabidopsis_thaliana        ----QAVFKKGIEGATKFLL--PRLSDFQFFVGEGMH---DDSTLVFAYYKEG--STNPT
TCTP_Hevea_brasiliensis          ----QESFKKNIEGATKFLL--SKLSDLQFFVGESMH---DDGSLVFAYYRGG--ATDPT
TCTP_Plasmodium_knowlesi         DR--VDVFKTKAQPLIKHIL--TNFDDFEFYMGESLD---MDAGLTYSYYKGE--EVTPR
TCTP_Caenorhabditis_elegans      DKADVDAFKKKIQGWVVSLLAKDRFKNLAFFIGERAAEGAENGQVAIIEYRDVDGTEVPT
TCTP_Brugia_malayi               SEAEISEFKRKIPAWVVSLLSKDRFKQLQFFIGERMAEGQGEGQVAVVEYRDEEDGEVPY
TCTP_Schistosoma_mansoni         DK--VPLLKSQVNKYMKNVL--DNFDQYEFYMGPPSN---PDAMIVLMNFRED--GMTPY
TCTP_Schizosaccharomyces_pombe   ER--VPVFEKNAIGFVKKIL--ANFKDYDFYIGESMD---PDAMVVLMNYRED--GITPY
TCTP_Drosophila_melanogaster     DQ--VDIFKTNMNKAMKDIL--GRFKELQFFTGESMD---CDGMVALVEYREINGDSVPV
TCTP_Danio_rerio                 NR--VDPFMANAPAEVKKIL--GNIKNFQFFTGESMN---PDGMIGLLDFRED--GVTPY
TCTP_Homo_sapiens                ER--VKPFMTGAAEQIKHIL--ANFKNYQFFIGENMN---PDGMVALLDYRED--GVTPY
TCTP_Mus_musculus                ER--VKPFMTGAAEQIKHIL--ANFNNYQFFIGENMN---PDGMVALLDYRED--GVTPF
                                     :          ::     .:.:   *:             :.  :    :         *


TCTP_Trypanosoma_brucei          FYFWKDGLKGERV
TCTP_Arabidopsis_thaliana        FLYFAHGLKEVKC
TCTP_Hevea_brasiliensis          FLYFAYALKEVKC
TCTP_Plasmodium_knowlesi         FVYISDGLYEEKF
TCTP_Caenorhabditis_elegans      LMLVKEAIIEEKC
TCTP_Brugia_malayi               LMLVKEALIEEKQ
TCTP_Schistosoma_mansoni         FVFFKDGLT----
TCTP_Schizosaccharomyces_pombe   MIFFKDGLVSEKF
TCTP_Drosophila_melanogaster     LMFFKHGLEEEKC
TCTP_Danio_rerio                 MISFKDGLEIEKC
TCTP_Homo_sapiens                MIFFKDGLEMEKC
TCTP_Mus_musculus                MIFFKDGLEMEKC
                                 :      .:
```

Figure 3: Sequence alignment of Fortilin. FT protein sequences from various organisms were aligned using Clustal Omega alignment algorithm (http://www.ebi.ac.uk/Tools/msa/clustalo/).

14

domains 1 and 3 being more hydrophobic than domain 2 (Fig. 4B). Domain 1 is responsible for its antiapoptotic action and a majority of its other functions, as will be discussed in more details in later sections.

Figure 4: Solution NMR structure and domains of Fortilin. A. Solution NMR structure of FT showing the three α-helices, eleven β-strands and the loop regions (Adapted from Feng *et al.* 2007). **B.** Domains of FT, domains 1 and 3 are more hydrophobic than domain 2.

1.2.6. Subcellular localization

Under steady state FT is reported to be predominantly localized in the cytosol and in the nucleus to a lesser extent (further discussed in section 3.2.11). However, when stimulated by hydrogen peroxide, it is seen to translocate to the nucleus, which was surprising, given that FT does not contain a nuclear localization

signal. Munirathnam and colleagues investigated the sequence of FT and reported the presence of potential sites of modification by small ubiquitin-like modifier (SUMO). They demonstrated that SUMOylation was crucial for the translocation of FT into the nucleus and that mutation of a lysine residue in the putative SUMOylation motif inhibited this translocation [Munirathnam and Ramaswamy, 2012].

1.2.7. Expression of fortilin in various tissues

Primary Northern blot analysis of FT transcript levels from different tissues in mice reveals that FT message is present ubiquitously in all tissues, with relatively higher expressions in liver, kidney, small intestine, skeletal muscle, and testis (Fig. 5A). Analysis of FT protein levels in different cell lines indicates very low basal expression levels in normal cells like human embryonic kidney (HEK) 293T cells and mouse fibroblasts (NIH-3T3). In contrast, an upregulation of FT is observed in tumors of epithelial origin like non-small cell lung cancer (H1299), breast cancer (MCF7), cervical cancer (HeLa) and lung adenocarcinoma (A549) and low FT levels in soft tissue tumors (Fig 5B) like promyelocytic leukemia (ML1a) and osteosarcoma (U2OS). It is interesting to note that FT message levels are rather low in normal lung tissue, but the expression increases in lung adenocarcinoma.
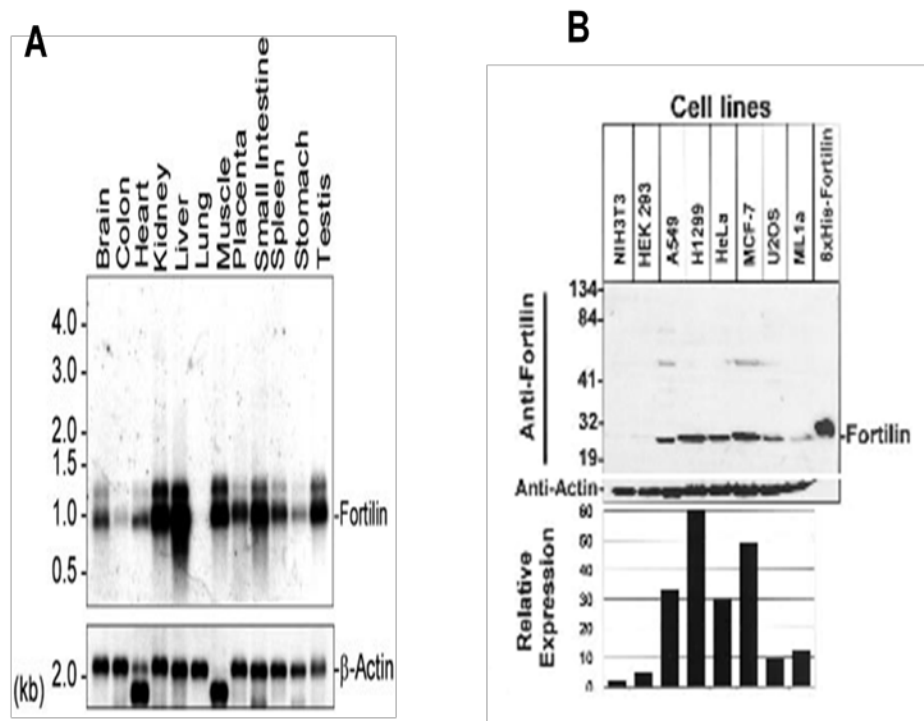
Figure 5: Tissue distribution of Fortilin mRNA and protein. A. Northern blot analysis of FT message levels in various tissues in mice with liver, small intestine, kidney and testis showing highest expression levels. **B.** Western blot analysis of FT protein levels in different cell lines, with epithelial tumors like MCF7 and A549 showing higher expression than soft tissue tumors like U2OS and normal cells like HEK293T. (This research was originally published in The Journal of Biological Chemistry. Li, F., Zhang, D., Fujise K. 2001; Characterization of fortilin, a novel antiapoptotic protein. *J. Biol. Chem*. 276(50), 47542-47549. © the American Society for Biochemistry and Molecular Biology)

1.2.8. GENERAL FUNCTIONS OF FORTILIN:

1.2.8.1. CYTOKINE-LIKE ACTIVITY

While it was discovered by Yonefsky *et al* in 1983, [Yonefsky *et al.* 1983], no definite function could be attributed to FT till 1995 when MacDonald *et al*

[MacDonald *et al.* 1995] demonstrated that FT acted as an IgE-dependent histamine releasing factor (HRF) that is present outside macrophages [Liu *et al.* 1986] and activated monocytes [Pasmans *et al.* 1994]. Other researchers have demonstrated its presence in bronchoalveolar lavage fluid (BLF) from patients afflicted with eosinophilic pneumonia and asthma [Yoneda *et al.* 2004], in nasal washings [MacDonald *et al.* 1987] and finally, in fluids from skin blisters obtained from patients with late allergic reaction [Warner *et al.* 1986]. Further evidence of the cytokine-like activity of FT is provided by observations that recombinant human FT is able to induce basophils to secrete IL-4 and IL-13 [Schroeder *et al.* 1997] also and human bronchial epithelial cells to secrete IL-8 and GM-CSF [Yoneda *et al.* 2004]. Subsequent to activation by anti-IgE antibody, Schroeder demonstrated a dose-dependent increase in IL-4, IL-13 and histamine secretion by basophils primed with various concentrations of FT. The authors therefore hypothesized that FT may bind to a specific receptor and modulate the IgE-dependent secretion of cytokines by basophils, suggestion an important role in chronic allergic inflammation. Similarly, Yoneda reported that FT could successfully stimulate secretion of IL-8 and GM-CSF from both human bronchial cell primary cultures and cell lines. They also detected the secretion of FT itself from bronchial epithelial cells upon stimulation with hydrogen peroxide but not IL-1 or tumor necrosis factor α (TNFα), thus proposing a role of oxidative stress in inducing FT secretion. The same group reported a significantly high level of FT in the basal lavage fluids (BLF) from patients suffering from asthma and even higher levels in patients with idiopathic eosinophilic

pneumonia. More recent studies have demonstrated that the dimerization of FT via its N-terminal is essential for its cytokine-like activity [Kim *et al.* 2009].

1.2.8.2. MICROTUBULE-STABILIZING PROTEIN:

As reported by Gachet in 1999, FT binds to the microtubule (MT) system of the cell during G1, S, G2 and early mitosis phase of the cell cycle [Gachet *et al.* 1999]. FT remains attached to the mitotic spindle during metaphase and the association ends during metaphase to anaphase transition. Furthermore, FT interacts with α- and β-tubulin and shows some similarity with the tubulin-binding domain of the microtubule associated protein MAP-1B. More recent work has indicated that the interaction between FT and MTs is indirect and not a classical MAP-MT interaction [Bazile *et al.* 2009]. Additionally, FT has been reported to interact with F-actin filaments and downregulation of FT has been demonstrated to cause dramatic changes in cell shape in HeLa cells. Tsarova and others have recently reported the existence of a cofilin-like specific actin interacting site on FT that has higher affinity for G-actin than F-actin and is unable to prevent actin depolymerization by cofilin [Tsarova *et al.* 2010]. These authors have further theorized that FT would direct cofilin to F-actin, thereby increasing its activity in invasive tumors.

1.2.8.3. INTERACTIONS WITH TRANSLATIONAL MACHINERY

FT interacts with both the translation elongation factor eEF1A and its guanine nucleotide exchange factor (GEF) eEF1Bβ and inhibits guanine dissociation at the elongation step during protein synthesis [Cans *et al.* 2003; Langdon *et al.* 2004]. FT, therefore, acts as a novel regulator of the elongation step of protein translation by preferentially stabilizing the GDP-bound form of eEF1A and simultaneously inhibiting the GDP exchange process facilitated by eEF1Bβ.

1.2.8.4. ROLE AS A HEAT SHOCK PROTEIN WITH CHAPERONE-LIKE ACTIVITY

In 2001, Mak *et al* [Mak *et al.* 2001] demonstrated that FT is one of the three most highly upregulated genes in the nematode parasite *Trichinella spiralis* larvae post-heat shock. Additionally, the solution structure of FT exhibited structural homology with a family of guanine nucleotide-free chaperones which binds to the GTP/GDP free form of Rab proteins [Thaw *et al.* 2001; superseded by Feng *et al.* 2007]. The ability of FT to bind to and stabilize MCL-1 [Liu *et al.* 2005] further supported the chaperone-like activity of FT. This led Gnanasekar and others to explore the idea that FT may act as a heat shock protein (HSP). They demonstrated that FT indeed acts as an HSP by preventing thermal denaturation of proteins in *E. coli*, and overexpression of FT protects bacterial cells from heat-induced cell death [Gnanasekar *et al.* 2009].

1.2.8.5. QUESTIONABLE ROLE OF FORTILIN AS A GUANINE NUCLEOTIDE EXCHANGE FACTOR (GEF)

FT had been reported to be a GEF for the Ras homologue enriched in brain (Rheb) in both *Drosophila* and mammalian cells [Hsu *et al.* 2008] since it was shown to be structurally similar to the Rab family GEF Mss4 [Thaw *et al.* 2001]; the validity of this claim has, however, been questioned by a subsequent study [Rehmann *et al.* 2008] and remains controversial.

1.2.8.6. FORTILIN IN EMBRYONIC DEVELOPMENT

Knockout mutants of FT in Drosophila show lower cell number and arrested development. Multiple groups have demonstrated that homozygous knockouts of FT (FT$^{-/-}$) in mice are embryonically lethal, while heterozygous i.e. FT$^{-/+}$ mice are viable without any deleterious phenotype. Chen and others in 2007 observed that FT$^{-/-}$ embryos are smaller in size with the epiblast suffering the highest amount of apoptosis starting around embryonic stage day 6.5 and the embryos dying around day 9.5-10.5. In 2009, Koide *et al* demonstrated that FT has a bimodal expression pattern during mouse embryonic development, with FT transcript levels reaching a peak around 9.5 days post coital (dpc), then decreasing around 12 dpc and again increasing to levels comparable to 9.5 dpc [Koide *et al.* 2009]. They showed that FT$^{-/-}$ mice blastocysts are unable to attach and outgrow and die prematurely. FT

knockout mice are therefore embryonically lethal around 3.5 dpc via overactivation of bone morphogenic protein (BMP) pathway.

In Xenopus embryos, FT acts as an inhibitor of BMP4 induced transcription of the genes Vent1, Vent2 and Msx1. In the absence of FT, mouse embryonic fibroblasts are subjected to extensive apoptosis by overactivation of BMP4 by overexpression of Msx1. All the above observations taken together indicate that FT is required for early embryonic development and that deletion or defects in the FT gene may be responsible for embryonic death *in vivo*, thereby underscoring the importance of FT as a crucial factor in early embryonic development. Some studies have also suggested a possible role for FT during embryo implantation in mice [Li *et al.* 2011].

A potential role for FT in cell proliferation was suggested by Johansson and others who demonstrated that FT forms a complex with endogenous nucleophosmin/nucleophosmin family member 1 (Npm1) during mitosis in embryonic stem cells [Johansson *et al.* 2011]. The same group had previously demonstrated that FT interacts with the phosphorylation-sensitive RNA-binding protein nucleolin, which is one of the most highly expressed non-ribosomal proteins in the nucleolus of a cell [Johansson *et al.* 2010]. Further evidence of the involvement of FT in cellular growth and proliferation is provided by the fact that FT is critical for peripheral T cell maintenance and T-cell antigen receptor-mediated cell proliferation [Wu *et al.* 2009].

1.2.8.7. FORTILIN IN DNA DAMAGE SENSING AND REPAIR:

In 2012, Zhang and others reported an upregulation of FT protein, especially in the nucleus, when regular human cells were exposed to a DNA-damaging agent like gamma radiation [Zhang *et al.* 2012] and this upregulation was dependent on the ataxia-telangiectasia mutated (ATM) kinase and the DNA-dependent protein kinase. They further demonstrated a direct interaction of FT with the DNA binding subunits Ku70 and Ku80 of the DNA-dependent protein kinase and also with p53. FT seemed to colocalize with DNA damage marker proteins γH2A.X, 53BP1, and p-ATM, underscoring its potential role in DNA damage sensing. Depletion of FT enhanced radiation-induced genomic damage and reduced nuclear levels and DNA-binding capacity of Ku70 and Ku80. The authors therefore proposed a potential role for FT in the maintenance of DNA stability under radiation stress.

1.2.8.8. OTHER REPORTED PROTEIN INTERACTIONS OF FORTILIN

FT has been reported to interact with a wide variety of proteins. It has already been mentioned that FT binds to F-actin and α- and β-tubulin. Researchers have shown that FT physically interacts with and stabilizes MCL-1[Zhang *et al.* 2002; Liu *et al.* 2005]. I will elaborate on this interaction in a later subsection. A yeast two hybrid screen in 2002 identified as a putative client for the Polo-like kinase (PLK) and the phosphorylation of FT by PLK is reported to decrease its

microtubule-stabilizing activity [Yarn *et al.* 2002]. FT also interacts with the third cytoplasmic domain of the α-subunit of the Na,K-ATPase [Kim *et al.* 2008] and suppression of the Na,K-ATPase induces systemic hypertension in FT-overexpressing mice. As an extension of the same study, Jung have observed that binding of FT to the Na,K-ATPase leads to release and activation of the tyrosine kinase Src [Jung *et al.* 2011]. This in turn leads to transcriptional activation of the epidermal growth factor receptor (EGFR) and eventually leads to transformation in human breast cancer cells. This study demonstrated the ability of FT to induce tumorigenesis by affecting multiple cell signaling pathways. The interaction with the Na,K-ATPase is also considered responsible for the development of cataracts in FT transgenic mice [Kim *et al.* 2009].

Among other protein interactions of FT, Rid and colleagues have demonstrated that upon stimulation with H_2O_2, FT translocates from the cytosol into the nucleus and interacts with the ligand-binding domain of the vitamin D3 receptor (VDR) [Rid *et al.* 2010]. FT also has a very important physical and functional interaction with the tumor suppressor protein p53, which I will discuss in details in the subsequent subsections.

1.2.8.9. FORTILIN – A NOVEL ANTI-APOPTOTIC PROTEIN

Ascribing a definite function to FT had been a challenge for scientists for a number of years, till 2001 when Li and colleagues unambiguously demonstrated

that FT is an anti-apoptotic protein that protects cells from etoposide-induced cytotoxicity (Fig. 6A&B) [Li *et al.* 2001]. The anti-apoptotic function of FT comparable to that of MCL1 and BcL-xL in U2OS and HeLa cells [Li *et al.* 2001] and this action is both dose and time-dependent. FT was identified as a novel and specific interacting partner for the anti-apoptotic protein MCL1 and a potential role for MCL1 as a FT chaperone was suggested [Zhang *et al.* 2002]. However, the anti-apoptotic activity of the two proteins was found to be independent of each other [Graidist *et al.* 2004]. Other groups have suggested that FT may regulate the function of MCL-1 by controlling the stability of the latter [Liu *et al.* 2005]. FT has been shown to interact with the anti-apoptotic protein BcL-xL via its N-terminal region and the same region is also responsible for its anti-apoptotic action since the deletion of this domain abrogates the anti-apoptotic action of FT [Yang *et al.* 2005]. Further evidence of the anti-apoptotic action of FT is provided by the observation that downregulation of FT results in tumor reversion [Tuynder *et al.* 2003] and apoptosis of prostate cancer cells [Gnanasekar *et al.* 2009] and that FT is implicated in tumor growth and metastasis in colon cancer cells [Ma *et al.* 2010]. Additionally, studies have shown that FT prevents apoptosis induced by transforming growth factor-β stimulated clone-22 (TSC-22), a pro-apoptotic protein by destabilizing it [Lee *et al.* 2008]. More recently, Diraison and others have identified FT as a novel glucose-inducible protein that can protect pancreatic beta cells from hyperglycemia-induced apoptosis [Diraison *et al.* 2011].
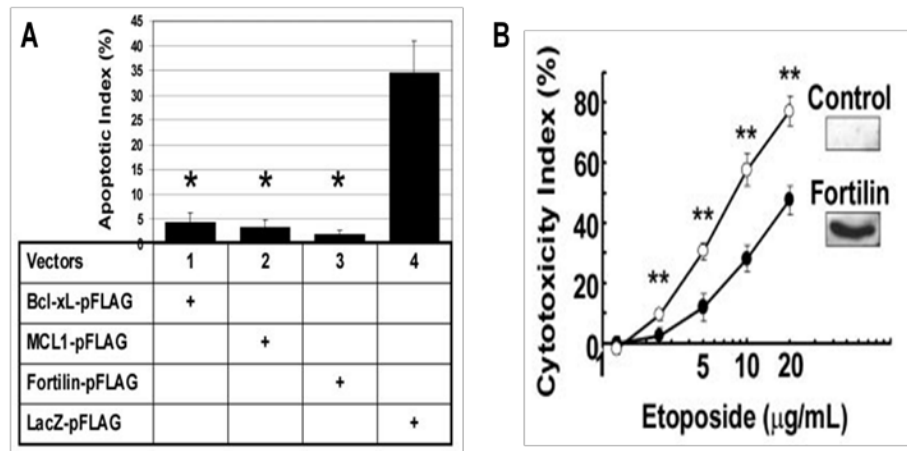
Figure 6: Anti-apoptotic action of fortilin. A. Transient overexpression of FT in U2OS cells leads to prevention of etoposide-induced cytotoxicity and this anti-apoptotic action is comparable to Bcl-xL and MCL-1. **B.** Stable overexpression of FT is also able to protect U2OS cells from etoposide induced apoptosis in a dose dependent manner. (This research was originally published in The Journal of Biological Chemistry. Li, F., Zhang, D., Fujise K. 2001; Characterization of fortilin, a novel antiapoptotic protein. *J. Biol. Chem.* 276(50), 47542-47549. © the American Society for Biochemistry and Molecular Biology)

1.2.8.10. PREVENTION OF CALCIUM ION-INDUCED APOPTOSIS

FT is an acidic protein (calculated pI= 4.84) which binds calcium ions via two high affinity sites (E58/E60) in its N-terminal region and prevents Ca^{2+} induced apoptosis in U2OS cells [Graidist *et al.* 2007]. The authors of the study speculated that binding of Ca^{2+} ions, released from the endoplasmic reticulum upon stimulation by thapsigargin, to FT leads to sequestration of the ions from the calcium ion-

induced apoptotic signaling cascades. They further noted that binding to Ca^{2+} ions induces a significant change in the secondary structure of FT.

1.2.8.11. FORTILIN AND OXIDATIVE STRESS INDUCED APOPTOSIS

In a screening study to identify genes that conferred cells with ability to protect cells against H_2O_2, Rid identified FT as a protein that prevented oxidative stress-induced cell death [Rid *et al.* 2010]. More recently, Lucibello also identified FT as a factor that prevents normal and cancer cells from arsenius oxide (As_2O_3)-induced oxidative cell death [Lucibello *et al.* 2011]. They also demonstrated that FT is upregulated by chronic exposure to As_2O_3. This is a significant observation, given that resistance to chemotherapeutic agents that cause ROS-induced death is an important mechanism of cancer cell survival. Additionally, as already mentioned, treatment with hydrogen peroxide causes translocation from the cytosol to the nucleus where it interacts with the ligand-binding domain of VDR.

1.2.8.12. MECHANISM OF ANTI-APOPTOTIC ACTION

While several groups have reported the ability of FT to protect cells from apoptosis induced by various stimuli, including chemotherapeutic drugs, ROS-inducing agents and UV radiation, the exact mechanism of this anti-apoptotic ability

could not be clearly established. In one of the earliest studies on this topic, it was proposed that FT inhibits dimerization of the pro-apoptotic protein Bax in the mitochondrial membrane, based on the structural similarity between the H2-H3 helices of FT and the H5-H6 helices of Bax [Susini *et al.* 2008]. However, due to the lack of any demonstrated physical interaction between FT and Bax, the mechanism of antagonism of Bax dimerization by FT is not clear. Other known protein interactions of FT cannot satisfactorily explain its anti-apoptotic action; its protective ability has been shown to be independent of MCL-1. Despite reports of the ability of FT to protect cells from apoptosis induced by TSC-22, it is yet to be elucidated whether direct interaction between the two proteins is essential for the destabilization of TSC-22. However, despite all these efforts, the exact molecular mechanism of the anti-apoptotic effect of FT could not be established. In parallel to reports by Rho and others, Chen and co-workers demonstrated that FT directly interacts with the tumor suppressor protein p53 and inhibits p53-mediated upregulation of the pro-apoptotic Bax, thereby preventing apoptosis under UV stress [Rho *et al.* 2011; Chen *et al.* 2011]. Almost immediately following the publication of these two reports, Amson also confirmed the same observation, by showing that FT promotes ubiquitinylation and subsequent degradation of p53 by blocking the self-ubiquitinylation of the p53-regulator Mdm2 [Amson *et al.* 2011]. They further reported the repression of FT expression by p53, thus pointing to clear antagonism between the two proteins at the level of both expression and function.

However, while the repression of p53 by FT is the final step in its ability to prevent apoptosis, the exact molecular events leading up to that final step are yet to be elucidated. The reported interactions of FT with known partners cannot therefore clearly explain its protective action, especially under conditions of oxidative stress. This calls for a need to identify novel protein partners of FT which would successfully explain its ability to protect cells against oxidative stress-induced apoptosis.

1.2.9. PHYSICAL AND FUNCTIONAL INTERACTION BETWEEN FORTILIN AND PEROXIREDOXIN I: A NOVEL INTERACTION

In our efforts to identify novel interacting partners of FT that may satisfactorily explain the anti-apoptotic action of FT under oxidative stress, I employed an immunoprecipitation and Mass Spectrometry-based screening approach to identify other fortilin interacting proteins (FIPs) and identified the anti-oxidant, pro-survival protein peroxiredoxin I (Prx I) as a direct interacting partner of FT (described in details in Chapter III). Peroxiredoxins I-VI are a class of six thioredoxin-dependent anti-oxidant enzymes which are expressed in a broad range of organisms ranging from bacteria to mammals. A major function common to all peroxiredoxins is the catalytic degradation of hydrogen peroxide, a potent source of reactive oxygen species (ROS) which can be highly toxic to the cells [Chae *et al.* 1993; Chae *et al.* 1994; Chae *et al.* 1994]. The catalytic core of Prxs contain

conserved cysteine residues (Cys^{52} in case of Prx I) which carry out the redox degradation of peroxides, getting oxidized to sulfinic acids, before being reduced back to the active thiol state [Woo *et al.* 2003]. Peroxiredoxin gene expression, especially Prx I (22 kDa), is upregulated under oxidative stress and also involved in the regulation of cell cycle as well as differentiation [Immenschuh and Baumgart-Vogt, 2005]. Prx I knockout mice develop hemolytic anemia with hemoglobin instability as well as increased hematopoietic malignancies [Neumann *et al.* 2003].

1.2.10. PEROXIREDOXINS IN CELL PROLIFERATION AND APOPTOSIS:

Peroxiredoxins have been implicated to have a role in cell proliferation and increased cell survival. A correlation between Prx I expression and cell proliferation has been shown by a significantly high Prx I gene expression in Ras-transformed epithelial cells [Prosperi *et al.* 1993] and lowering of Prx I levels in DMSO-induced growth arrested HL60 human promyelocytic cells. There are evidences of Prx I interacting with oncogenic products c-Abl and c-Myc, both of which are crucial for the regulation of cell proliferation [Wen *et al.* 1997], thus indicating a possible role for Prx I in the cell cycle. Prx I overexpression has been shown to induce an increase in cell size and to have a protective role against apoptosis under conditions of oxidative stress, thereby confirming its role as a pro-survival cue. Prx I gene expression level is known to be upregulated under oxidative stress, via the

interaction of the transcription factor NF-E2-related factor 2 (Nrf2) with the antioxidant response element (ARE) [Nguyen *et al.* 2003].

Another important regulator of Prx I is sulfiredoxin (Srx) which is responsible for reducing hyperoxidized Prx I to its active reduced state [Bae *et al.* 2011]. Just as increased Prx I expression is correlated with increased survival, endogenous Prx I and Prx II levels have been shown to be lowered in rat hepatocytes undergoing apoptotic death via ROS-generation and NF-κB activation, upon treatment with glycochenodeoxycholic acid [Chu *et al.* 2003].

1.2.11. PRX I AS A MODEL FORTILIN INTERACTING PROTEIN (FIP)

Both FT and Prx I have been known to be pro-survival as well as have a role in combating oxidative stress. Additionally, there have been reports of peroxiredoxin expression levels changing in FT-overexpressing transgenic mice hearts [Cheon *et al.* 2008] and of both Prx and FT levels changing concomitantly in neonatal rat cardiomyocytes exposed to H_2O_2 [Cullingford *et al.* 2006], which point to a possible interaction between Prx I and FT, as also indicated by our preliminary data. The detected interaction, if indeed true, could potentially explain the protective effect of FT under oxidative stress. The upregulation of Prx I in Ras-transformed epithelial cells and the concomitant upregulation of FT and Prx I under oxidative stress also point to a possible functional and/or regulatory correlation

between the two. I performed confirmatory Western blots using specific antibodies against Prx I to demonstrate that Prx I is a true FIP and the interaction between Prx I and FT therefore merited further investigation.

1.3. SIGNIFICANCE OF THE STUDY:

While FT is a multi-functional protein, its most crucial function seems to be inhibition of apoptosis, underscored by the massive embryonic apoptosis and consequent death in FT-null mice. Chen and colleagues were the first to conclusively demonstrate that FT was indeed anti-apoptotic and that the inhibition of p53-mediated Bax upregulation was the crucial step in its regulation of apoptosis. Our primary goal in this study was to identify a novel set of FIPs, which would successfully explain anti-apoptotic action of FT. I indeed identified a set of novel FIPs, including Prx I and throughout the course of the current study I sought to answer the question whether this interaction is important in modulating cellular response to oxidative stress. A rigorous molecular understanding of this novel protein interaction is crucially important to target these proteins or their interaction for therapeutic purposes in diseases where either protein has been implicated. For example, it has been described before that FT is upregulated in tumors of epithelial origin and that it would be a defense mechanism cancer cells employ to combat chemotherapeutic drugs that cause cell death by ROS generation. It is of paramount importance to investigate whether this ability of FT to protect

cells from ROS-induced cell death is mediated via Prx I, which being an anti-oxidant enzyme, appears to be a natural candidate for the job. Investigation of this novel interaction can potentially establish a platform for designing therapeutics for diseases where ROS has been implicated. In diseases like heart failure (HF) where ROS has been shown to cause death of cardiomyocytes, the study eventually may be instrumental in developing specific targets to stimulate interactions of FT with Prx I which would result in cardioprotection and offer a novel approach for the successful treatment of HF. Investigating the molecular mechanism of HF by analyzing a potentially protective novel protein-protein interaction certainly offers an unexplored avenue for the treatment of HF, challenging the current paradigm and opening up other areas of research in the fields of ROS biology and HF. A similar approach could also be employed against acute ethanol-induced liver damage, where ROS is implicated and Prx I knockout has been shown to exacerbate the disease. On the other hand, blocking the apparently protective FT-Prx I interaction may offer a novel therapeutic approach against growth of cancer cells. The strong potential of this study to offer novel therapeutic targets in ROS-induced inflammatory diseases makes it highly significant from the perspectives of basic as well translational biomedical research.

1.4. INNOVATION

Innovation in this project is evident in the topic of research, the concepts and hypotheses to be tested and the approaches to be used. The list of novel FIPs I

identified via a systemic, unbiased, comprehensive proteomic study has not been published in FT literature till date. Furthermore, to the best of our knowledge, this is the first instance where the potentially crucial FT-Prx I interaction has been detected. While Prx I and FT have been shown individually to have a protective role against ROS-induced apoptosis, the potentially protective effect of the interaction between the two proteins has not been reported in literature. The research in the current project is innovative because it focuses on a novel interaction as a potential protective mechanism against apoptosis. The systematic proteomic, biochemical and functional studies of the anti-apoptotic action of FT via its interaction with Prx I under oxidative stimulus were unique and sought to answer a fundamental question, which has the potential to change the current paradigm in research and treatment of diseases where ROS has been implicated.

1.5. GOAL OF THE PROJECT AND WORKING HYPOTHESIS

The overall goal of the project was to understand the protective action of FT under conditions of oxidative stress. Combining our co-immunoprecipation and Mass Spectrometry-based screening approach (for details see Chapter III), a number of novel fortilin interacting proteins (FIPs) were identified, including the pro-survival anti-oxidant enzyme peroxiredoxin I (Prx I). Based on our preliminary data, I constructed a working hypothesis that *anti-apoptotic function of fortilin under*

oxidative stress is dependent on its interaction with peroxiredoxin I. The hypothesis was tested using different experiments in the subsequent chapters. In Chapter III, I verified the identity of Prx I as a true FIP by performing reverse co-immunoprecipitation of FT and Prx I, followed by the demonstration of direct binding between them and determination of the dissociation constant (K_D) of the interaction. In the next part of this chapter, I investigated whether the two proteins were physically close enough to interact within the cell by immunofluorescence and proximity ligation assay (PLA). In chapter IV, I investigated whether and how the downregulation of FT affects the expression and/or stability of Prx I followed by determining the effect of addition on pure recombinant FT to Prx I in an *in vitro* peroxidase assay and then investigating the mechanism by which FT may alter the activity of Prx I. The last portion of the chapter was dedicated to investigating the effect of Prx I on the function of FT under ROS stress. I employed a FT mutant incapable of binding to Prx I to evaluate how the anti-apoptotic action of FT under oxidative stress depends on its interaction with Prx I. Having demonstrated the binding between FT and Prx I and investigating the biological significance of that binding in-cell, chapter V was dedicated to testing the protective action of the FT-Prx I interaction in a mouse model of alcohol-induced oxidative damage. I generated a liver-specific FT knockout mouse and tested whether the absence of FT led to increased oxidative damage as compared to wild type mice when they were subjected to acute liver damage via alcohol consumption.

Upon successful completion of these experiments, I was able to establish the biological significance of the FT-Prx I interaction and lay important groundwork for exploring this interaction for translational studies in future, which is the ultimate goal of this dissertation.

CHAPTER II: METHODS

This chapter provides details of all the reagents, buffers, chemicals and scientific methods and protocols employed to perform all the experiments described in the current dissertation.

2.1. BUFFERS:

Lysis buffer for Immunoprecipitation (IP): IP was performed using a buffer consisting of 20mM 4-(2-hydroxyethyl)-1-piperazineethanesulfonic acid (HEPES) pH = 7.4, 35mM sodium chloride (NaCl) and 0.001% NP-40 (non-ionic detergent), supplemented with protease inhibitor cocktail (Roche Applied Science, Indianapolis, IN), phosphatase inhibitor cocktail (Sigma-Aldrich, St. Louis, MO) and 1mM phenylmethylsulphonyl fluoride (PMSF) (Sigma-Aldrich, St. Louis, MO).

Immunoprecipitation Wash Buffer: IP wash buffer was prepared using 20mM HEPES (pH = 7.4), 150mM NaCl and 0.01% NP-40.

Immunoprecipitation Elution Buffer: The immunoprecipitates were eluted using 4X SDS loading buffer - 50mM Tris-HCl, 0.1% glycerol, 1% sodium dodecyl

sulphate and 8μg/mL bromophenol blue (All the chemicals were purchased from Fisher Scientific, Waltham, MA)

Peroxidase assay buffer: Peroxidase assay was performed using a buffer containing 50mM HEPES-NaOH, pH = 7.0, with 1mM ethylenediamine tetraacetate (EDTA).

Radioimmunoprecipitation assay (RIPA) buffer: Cell lysates were prepared by lysing cells in RIPA buffer containing 50mM Tris-HCl pH = 7.4, 1mM EDTA, 150 mM NaCl, 0.1 % SDS, 0.5 % sodium deoxycholate and 1% Triton X-100, supplemented with 5μg/mL aprotinin, 5μg/mL leupeptin and 1mM phenylmethylsulphonyl fluoride (PMSF).

Proximity Ligation Assay (PLA) Buffer A: PLA wash buffer A contained 10mM Tris-HCl pH 7.4, 150mM NaCl and 0.05% Tween 20. (All reagents were supplied by the manufacturers – Olink Bioscience, Uppsala, Sweden).

Proximity Ligation Assay (PLA) Buffer B: PLA wash buffer B contained 200mM Tris-HCl pH 7.5 and 100mM NaCl. (All reagents were supplied by the manufacturers – Olink Bioscience, Uppsala, Sweden).

Kinase Buffer: Kinase buffer was prepared with 50mM Tris-HCl pH 7.4 and 10mM $MgCl_2$. Immediately before use, the buffer was supplemented with 1mM dithiothreitol (DTT) and 20μM ATP.

2.2. ANTIBODIES:

Primary antibodies for Immunoblotting: I utilized the following antibodies for the different immunoblotting experiments: Rabbit anti-fortilin antibody (MBL International), , mouse anti-GAPDH antibody (Fitzgerald Scientific), mouse anti-FLAG M2 antibody and anti-FLAG M2 agarose matrix (Sigma-Aldrich, Saint Louis, MO), rabbit anti-hemagglutinin (HA) antibody (Bethyl Laboratories, Montgomery, TX), rat anti-HA matrix beads and mouse anti-Protein C matrix beads (Roche Applied Science, Indianapolis, IN), goat anti-Peroxiredoxin I, V and VI (Abnova, Taiwan), anti-Peroxiredoxin II, III and IV, mouse anti-TOPO IIβ antibody, mouse anti-Succinate dehydrogenase subunit A (SDHA) antibody, goat anti-calnexin antibody (Santa Cruz Biotechnology, Santa Cruz, CA), rabbit anti-phosphothreonine antibody (Cell Signaling Technology, Danvers, MA).

Secondary antibodies for Immunoblotting: Secondary antibodies used for immunoblotting included goat anti-mouse, goat anti-rabbit and donkey anti-goat IR680 and IR800 dyes (LI-COR Biosciences, Lincoln, NE).

Primary antibodies for Immunofluorescence and PLA: Mouse anti-TPT1 antibody and goat anti-Prx I antibody (Abnova, Taiwan), goat anti-Prx IV antibody (Santa Cruz Biotechnology, Santa Cruz, CA) and rabbit anti-E-cadherin antibody (Abcam PLC, Cambridge, MA) were used for immunofluorescence and PLA experiments.

Secondary antibodies for Immunofluorescence and PLA probes: I used donkey anti-mouse, donkey anti-rabbit and donkey anti-goat AlexaFluor® 488 and AlexaFluor® 568 dyes (Invitrogen, Grand Island, NY) for immunofluorescence. Specialized mouse PLUS and goat MINUS PLA probes (Olink Bioscience, Uppsala, Sweden) were used for the PLA.

2.3. CELL CULTURE:

U2OS cells and HEK293T cells were grown in Dulbecco's Minimum Essential Medium (DMEM), supplemented with 10% fetal bovine serum, 1% non-essential amino acids and 1% L-Glutamine (Hyclone, Thermo Fisher Scientific Inc, Waltham, MA), at 37^0C in presence of 5% CO_2 in a CO_2 incubator (Sanyo, Japan). Cells were washed with Dulbecco's phosphate buffered saline (DPBS, Cellgro, Manassas, VA). When appropriate, stable cell lines were generated by treatment with antibiotics including zeocin and puromycin (InvivoGen, San Diego, CA) and geneticin (G418 sulphate, Cellgro, Manassas, VA).

2.4. CLONING:

2.4.1. CLONING OF HA-FORTILIN:

I cloned the human FT gene from a human lymphocyte cDNA library using reverse transcription PCR to isolate the gene and inserted it into the pcDNA4 vector. I further cloned the N-terminus in-frame with the influenza hemagglutinin epitope, to generate an HA-FT vector.

2.4.2. Cloning of Peroxiredoxin constructs:

I cloned the human Prx I, II, III, IV, V and VI genes directionally into the p3X-FLAG CMV14 vector (Fig. 7A). A list of primers used for the cloning process is provided in Table 2 and the PCR products for each of the constructs are shown in Fig. 7B. The different PCR primers used for the construction of the peroxiredoxin constructs have been described in Table 1.

2.4.3. CLONING AND EXPRESSION OF RECOMBINANT WILD TYPE AND MUTANT FT:

Wild type and mutant human FT gene, TPT1, were cloned into the pENTRY-IBA51 entry vector (IBA BioTAGnology, St. Louis, MO) and then transformed into *E.*

coli. Following colony selection on a kanamycin-X-Gal agar plate, 10 clones were selected for miniprep and restriction digestion. As shown in Fig. 8A, all the clones contained inserts of the desired size; the sequences of the clones were confirmed and one clone each was selected for further studies. Clone 1 was then subcloned into the pESG-IBA5 acceptor vector to generate the destination vector. Followed by colony selection on an ampicillin-X-Gal agar plate, 4 clones were selected for miniprep and restriction digestion. As shown in Fig. 8B, all the clones contained inserts of the desired size; the sequences of the clones were confirmed and one clone each was selected for further studies. The plasmids were purified using a maxiprep kit (Qiagen) and transfected into HEK293T cells. Stable expression of the plasmids was achieved by selection using the antibiotic G418 sulphate.

2.4.4. IDENTIFICATION OF A FORTILIN POINT MUTANT THAT FAILS TO INTERACT WITH PRX I:

Various FT point mutants (I3R, D6A, L7R, D16A, R21A, D71A, H76A, Y91A, P108A, R110A and G166L) were created from a human cDNA library by site directed mutagenesis and cloned into the pcDNA4-HisMax vector. The HA-tagged plasmids were transiently transfected into U2OS cells along with WT FT and HA-Empty vector. Anti-HA IP was carried out using anti-HA agarose beads and lysates from the different transfectants, the beads were washed with wash buffer and subjected to immunoblotting using anti-HA and anti-Prx I antibodies.
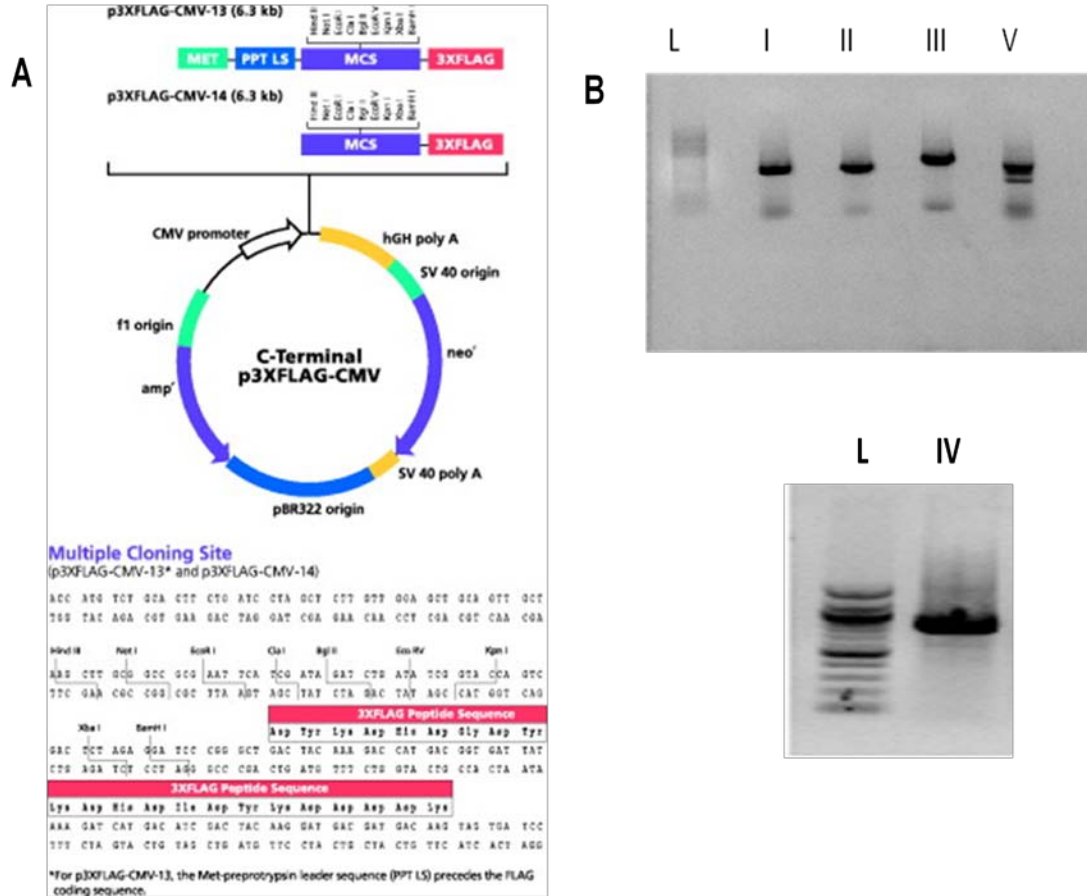
Figure 7: Cloning of Prx constructs into the p3X-FLAG CMV 14 vector. A. The vector map for p3X-FLAG CMV14 vector (courtesy: **WWW.SIGMAALDRICH.COM**) **B.** Polymerase Chain Reaction (PCR) products for Prx I-V constructs.

2.5. RECOMBINANT PROTEINS:

Wild type and mutant human streptavidin-tagged FT were transfected into HEK293T cells using the plasmids generated in 2.4.3 and stable selection as

achieved by treatment with G418 sulphate. The proteins were purified using affinity chromatography on Strep-Tactin® Superflow ™ Column (Novagen, San Diego, CA) and further purified by buffer exchange into PBS. Details of the purification procedure are described in section 2.5.1.

Table 1: List of primers used for cloning of Prx I-VI-FLAG

Gene	Primers	Restriction enzyme
Prx I	Fwd: 5'-GC*GAATTC*GCGATGTCTTCAGGAAATGCT-3'	EcoRI
	Rev:5'GCG*GGATCC*GCGCTTCTGCTTGGAGAAATATT-3'	BamHI
Prx II	Fwd: 5'-GC*GAATTC*GCGATGGCCTCCGGTAACGCG-3'	EcoRI
	Rev: 5'-GCG*GGATCC*GCGATTGTGTTTGGAGAAATATT-3'	BamHI
Prx III	Fwd: 5'-GC*GAATTC*GCGATGGCGGCTGCTGTAGGA-3'	EcoRI
	Rev: 5'-GCG*GGATCC*GCGCTGATTTACCTTCTGAAAGT-3'	BamHI
Prx IV	Fwd: 5'- GCG*AAGCTT*GCGATGGAGGCGCTGCCGCTGC-3'	HindlIII
	Rev:5'-GC*TCTAGA*GCGATTCAGTTTATCGAAATACTTCAG-3'	XbaI
Prx V	Fwd: 5'-GC*GAATTC*GCGATGGGACTAGCTGGCGTG-3'	EcoRI
	Rev: 5'- GCG*GGATCC*GCGGAGCTGTGAGATGATATT-3'	BamHI
Prx VI	Fwd: 5'-*AAGCTT*ATGCCCGGAGGTCTGCTTCT-3'	HindlIII
	Rev: 5'- *TCTAGA*AGGCTGGGGTGTGTAGCGG-3'	XbaI

Table 1: List of primers used for cloning of Prx I-VI-FLAG. Primers used for cloning Prx I-VI into the p3X-FLAG CMV14 vector.
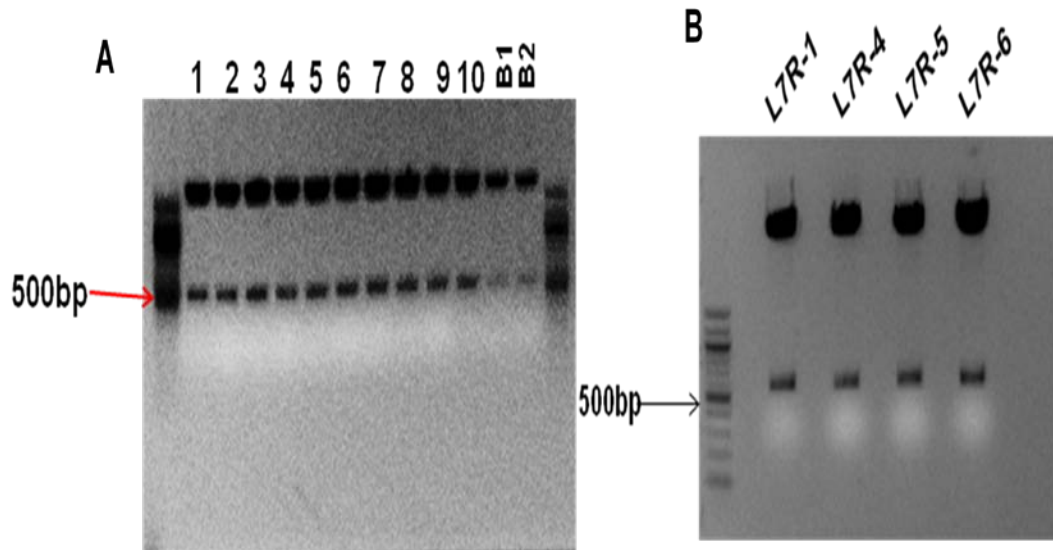
Figure 8: Cloning of FT-L7R-Strep. A. Restriction digestion of generated donor vectors. Clones B1 and B2 represent blue colonies from the X-Gal plate, used as negative control. **B.** Restriction digestion of generated acceptor vectors. In both cases, the clones were digested with XbaI and HindIII.

Pure recombinant human Prx I and thioredoxin (Trx), both purified from *E. coli* and thioredoxin reductase (TrxR) purified from rat liver were purchased from Sigma-Aldrich (St. Louis, MO). All the lyophilized proteins were reconstituted in 1mL of sterile deionized water. Pure recombinant human serine/threonine kinase 4 (Mst1) with GST and His_6 tags, was purchased from ProQinase GmbH (Freiburg, Germany).

2.5.1. PURIFICATION OF WILD TYPE AND RECOMBINANT FORTILIN FROM HEK293T CELLS:

HEK2983T cells stably overexpressing WT-FT-Strep or FT-L7R-Strep were maintained in 400μg/mL G418S till they were 100% confluent and then harvested by trypsinization. The cells were centrifuged at 5000 rpm for 5 minutes at 4 °C and resuspended in 4 ml Buffer W per 10^9 cells, supplemented with protease inhibitors. Cells were frozen in liquid nitrogen and thawed at 37 °C. The process was repeated five times, after which the cells were subjected to sonication to shear the DNA. The lysate was then subjected to centrifugation at 14,000 rpm for 5 minutes at 4 °C and the clear supernatant was used for affinity chromatography to purify fortilin.

To start the affinity purification process, the top and then the bottom caps were removed from the Strep-Tactin® Superflow ™ Column and the excess storage buffer was allowed to drain off. The column was then equilibrated by adding 2ml of Buffer W. The cell lysate was then added to the column and allowed to completely enter the column, following which, the column was washed 5 times with 1 CV of Buffer W. The wash fractions were collected and then, the bound protein was eluted as six 500μL fractions using Buffer E. After measuring the protein contents of the fractions (Fig. 9), they were analyzed by immunoblotting to determine the purity of the samples. Fractions 3-6 appeared to contain the highest amounts of WT or mutant FT. The fractions were pooled and concentrated using a centrifugal filter

unit (EMD Millipore, Billerica, MA). The concentrated protein samples were further

purified by buffer exchange into PBS using a ZebaTM Spin Desalting Columns

(Thermo Scientific, Waltham, MA).
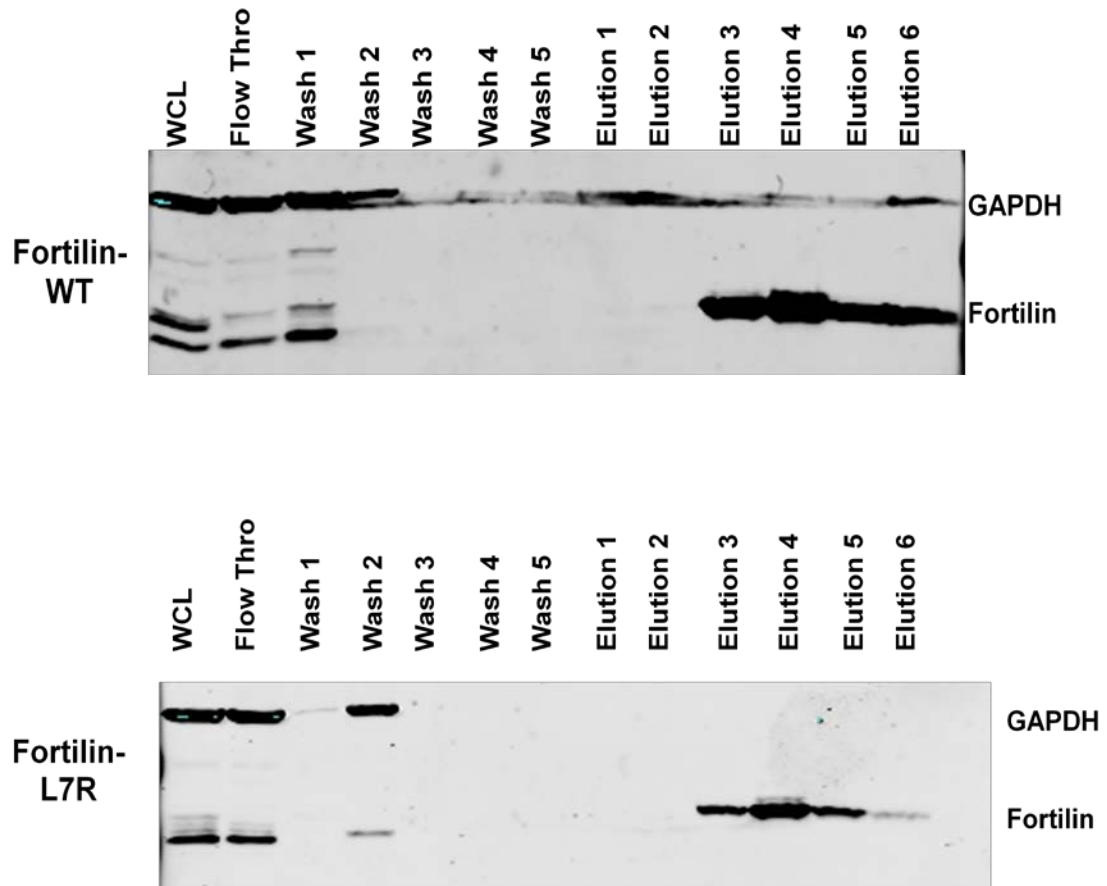
Figure 9: Purification of FT(WT)-Strep and FT-L7R-Strep. Top. Purification of WT FT using biotin column. Column washes and elution fractions were immunoblotted against anti-FT and anti-GAPDH antibodies. **Bottom.** Purification of FT-L7R using biotin column. Column washes and elution fractions were immunoblotted against anti-FT and anti-GAPDH antibodies.

2.6. IMMUNOBLOTTING:

Protein concentrations in the whole cell lysates or purified proteins were determined using a Bio-Rad Protein Assay kit. Whole cell lysates were diluted 1:10 and loaded along with the immunoprecipitated samples on 12% SDS Polyacrylamide Bis-Tris gels and subjected to SDS polyacrylamide gel electrophoresis. The samples were then transferred onto nitrocellulose membranes (Bio-Rad) at constant voltage of 35V overnight at 4 degrees Celsius or at constant current of 350mA for one hour at room temperature. The membranes were blocked with 5% skim milk (EMD Millipore, Billerica, MA) and finally incubated with primary antibodies (dilution range 1:250-1:10000) of choice at 4^0C overnight. The membranes were washed and incubated with secondary antibodies (dilution 1:10000) conjugated to IR680 dye and IR800 dye (Licor Corp, Lincoln, NE). Protein bands were visualized using the LI-COR imaging system.

2.7. IMMUNOPRECIPITATION:

2.7.1. IMMUNOPRECIPITATION USING CELL LYSATE:

Appropriate cells were washed with phosphate-buffered saline (PBS) and harvested by incubating at 37^0C for 5 minutes with 0.25% Trypsin-EDTA solution,

followed by centrifugation at 1000rpm for 5 minutes. The cells were lyzed using an equal volume of lysis buffer -20mM HEPES (pH = 7.4), 35mM NaCl and 0.001% NP-40, supplemented with protease inhibitor cocktail - followed by sonication thrice at an intermediate setting. Clear cell lysate was obtained by centrifuging the crude cell lysate at 14,000rpm for 20 minutes at 4^0C. For IP using the anti-HA and anti-Protein C beads, the clear lysate was mixed with the beads and the reaction was allowed to occur overnight at 4^0C on an end-over-end rotator, followed by three washes with wash buffer (20mM HEPES (pH = 7.4), 150mM NaCl and 0.01% NP-40) for 5 minutes in each case. The anti-FLAG agarose beads were precipitated and then washed thrice with lysis buffer to remove residual glycerol. For IP using the anti-FLAG agarose beads, the clear lysate was mixed with the beads and the reaction was allowed to occur overnight at 4^0C, followed by three washes with lysis buffer (20mM HEPES (pH = 7.4), 35mM NaCl and 0.001% NP-40) for 5 minutes in each case. In all cases, the immunoprecipitated mixture was eluted by treatment with 4X SDS loading buffer, followed by boiling the sample for 5 minutes. Sepharose 6B beads (Sigma) were used as a negative control.

2.7.2. IMMUNOPRECIPITATION USING MOUSE LIVER LYSATE:

Mice were sacrificed and their livers were harvested and washed in PBS and frozen at -80^0C. 1mg of tissue was lyzed in lysis buffer supplemented with protease inhibitors and phosphatase inhibitors and then homogenized using a hand held

tissue homogenizer. The crude lysate was then cleared by centrifugation lysate at 14,000rpm for 20 minutes at 4^0C. IP was carried out using mouse anti-Prx I antibody (Abcam, Cambridge, MA). Briefly, equal amounts of liver lysate were mixed with either 10μg of mouse anti-Prx I antibody or 10μg of normal mouse IgG and sheep anti-mouse magnetic Dynabeads ® (Novex by Life Technologies, Oslo, Norway) and allowed to rotate overnight at 4^0C on an end-over-end rotating platform. The beads were then collected by brief centrifugation and application of a magnetic field and then washed three times with lysis buffer for 5 minutes in each case. The immunoprecipitated protein complexes were then eluted by treatment with 4X SDS loading buffer for 20 minutes at room temperature, following which the eluate was collected by application of magnetic field to the beads. The eluate was then boiled for 5 minutes and analyzed by immunoblotting.

2.8. PROTEOMIC ANALYSIS OF THE IMMUNOPRECIPITATED COMPLEXES:

10mg of protein from U2OS-HA-Empty or U2OS-HA-FT cells was obtained after lysing the cells in lysis buffer. The lysates were mixed with the anti-HA agarose beads and the reaction was allowed to occur overnight at 4^0C on an end-over-end rotator, followed by three washes with wash buffer (20mM HEPES (pH = 7.4), 150mM NaCl and 0.01% NP-40) for 10 minutes in each case. The mixtures were eluted into 4X SDS loading buffer and boiled for 5 minutes. The proteins were

resolved on a large format 10% SDS Polyacrylamide gel and stained with SYPRO Ruby. The protein bands were visualized under UV light and protein bands observed differentially in the U2OS-HA-FT lane as opposed to the U2OS-HA-Empty lanes were excised and submitted for identification by Matrix Assisted Laser Desorption Time-of-Flight (MALDI-TOF/TOF) Mass Spectrometry at the UTMB Biomolecular Resource Facility (BRF).

2.9. IMMUNOFLUORESCENCE:

Wild type U2OS cells were plated on glass cover slips and fixed using 1% paraformaldehyde-PBS solution (USB Labs) followed by permeabilization in a 0.1% Triton-X solution. The cells were incubated overnight at 4^0C in a humidifying chamber with primary antibodies against FT, Prx I and both. The cells were washed and incubated with donkey anti-mouse AlexaFluor 488 and donkey anti-goat AlexaFluor 568 fluorescent tagged secondary antibodies. The cells were subjected to confocal microscopy on a Zeiss LSM 510 UV Meta Laser42 Scanning Confocal Microscope and images were obtained using the Zeiss LSM software.

2.10. PROXIMITY LIGATION ASSAY (PLA):

PLA was performed on U2OS cells using PLA kit (Olink Bioscience, Uppsala, Sweden) as per manufacturer's instructions. Briefly, 15000-20000 U2OS cells were plated on each well of a 16-well chamber slide and incubated for 24 hours at 37^0C in a humidified 5% CO_2 incubator. After 24 hours, the medium was aspirated and the cells were gently washed with PBS followed by aspiration the PBS and removal of the chambers, leaving the silicone around the cells. Cells were fixed using 4% paraformaldehyde solution and incubated at room temperature for 10 minutes without agitation, followed by three successive washes with PBS for 5 minutes in each case. The cells were then permeabilized using 0.5% Triton X-100 in PBS for 10 minutes at room temperature and washed with 0.05% Tween 20 in PBS thrice for 5 minutes each. The next step was to block non-specific sites on the cells by adding the proprietary Duolink II Blocking Solution to each well and incubating the cells in blocking solution for 30 minutes at 37^0C in a pre-heated humidified chamber consisting of an empty pipet tip box with distilled water. Primary antibodies against FT, Prx I, Prx IV and E-cadherin were diluted 1:100 in Duolink II antibody diluent, added to cells and incubated for 1 hour at 37^0C in a pre-heated humidified chamber consisting of an empty pipet tip box with distilled water. The cells were washed in Buffer A thrice for 5 minutes each. Cells were then incubated for 1 hour at 37^0C with PLA probes diluted 1:5 in Duolink II antibody diluent and washed with wash buffer A twice for 5 minutes each. Cells were then incubated with ligation mixture for 30 minutes at 37^0C, followed by two washes in wash buffer A for 2 minutes in each

case. The cells were then subjected to rolling circle amplification using Duolink Polymerase for 100 minutes at 37^0C in darkness, following which they were washed twice with wash buffer B for 10 minutes each and dipped in 0.1X buffer B. The silicone was then completely removed from the slides and Duolink II mounting medium with DAPI was added to a cover slip and placed gently over the cells making sure there were no air bubbles under the cover slip. The cover slip was fixed and sealed and the slide was stored at -20^0C till it was used for confocal microscopy.

2.11. FORTILIN-PRX I BINDING STUDIES:

Pure recombinant FT and Prx I were used to perform direct binding studies using Blitz instrument (forteBio, Menlo Park, CA). The principle behind the experiment was to load biotinylated FT onto streptavidin-coated biosensors and then monitor the association between the FT on the biosensors with increasing concentrations of pure recombinant Prx I and then the dissociation of the same using PBS, using the Surface Plasmon Resonance (SPR) technology.

2.11.1. BIOTINYLATION OF FORTILIN:

FT was biotinylated using 10mM NHS-PEG$_4$-Biotin (Thermo Scientific, Waltham, MA) as per manufacturer's instructions, after the purified FT was dialyzed

53

into PBS. The mixture was incubated at room temperature for 30 minutes. The excess biotin reagent was removed by using a desalting column. The biotinylated FT was then conjugated to streptavidin-tagged biosensors for 10 minutes at room temperature. The overall steps of the FT-Prx I binding studies were as follows:

Step 1: Baseline correction with PBS – 30 seconds

Step 2: Loading step – binding of FT to the biosensors – 10 minutes

Step 3: Second baseline with PBS – 30 seconds

Step 4: Association step with Prx I – 3 minutes

Step 5: Dissociation step with PBS – 5 minutes

Each set of 5 steps was repeated for increasing concentrations of Prx I from $0\mu M$, $312.5\mu M$, $625\mu M$, $1250\mu M$, $2500\mu M$ and $5000\mu M$. K_D values were calculated from the resulting kinetics curves. The experiment was repeated thrice and the average K_D from three experiments was noted.

2.12. SUBCELLULAR FRACTIONATION:

I used commercially available kits to extract the desired cellular fractions: NE-PER Nuclear Extraction Kit (Pierce, Rockford, IL) to extract nuclear and cytosolic fractions, Mitochondrial Extraction Kit (Pierce, Rockford, IL) to isolate mitochondrial fraction and the Imgenex Endoplasmic Reticulum Enrichment Kit to

enrich the ER fraction as per manufacturer's instructions. A brief overview of each extraction is presented below:

2.12.1. ISOLATION OF NUCLEAR AND CYTOPLASMIC FRACTIONS:

U2OS cells were harvested using trypsin-EDTA and collected by centrifugation at 500g for 5 minutes. The cells were washed with PBS and then collected by centrifugation at 500g for 3 minutes. Care was taken to ensure that the pellet was as dry as possible. The pellet was then resuspended in ice cold Cytoplasmic Extraction Reagent I (CER I), supplemented with protease inhibitors, by vortexing at the highest setting for 15 seconds. After addition of ice cold CER II to the cells, the cells were once again vortexed at the highest setting for 5 seconds and then incubated on ice for 1 minute. The cells were further vortexed at the highest setting for 5 seconds and then centrifuged at 16000g for 5 minutes. The supernatant, which was the cytoplasmic extract, was immediately transferred to a pre-cooled tube and stored at -80^{0}C till further use. The pellet from the previous centrifugation step was resuspended in ice cold Nuclear Extraction Reagent (NER), vortexed at the highest setting for 15 seconds and then placed on ice. The sample was left on ice for a total of 40 minutes during which it was vortexed for 15 seconds every 10 minutes. The sample was then centrifuged at 16000g for 10 minutes. The supernatant from this step, which was the nuclear extract, was stored at -80^{0}C till further use.

2.12.2. ISOLATION OF MITOCHONDRIAL FRACTION:

U2OS cells were harvested by trypsinization, washed with PBS and resuspended in Reagent A and incubated on ice for 2 minutes and then homogenized using a Dounce homogenizer. After adding Reagent C to it, the lysate was centrifuged at 700g for 10 minutes at 4^0C to pellet and discard the nuclei and cellular debris. The supernatant was further centrifuged at 12000g for 15 minutes at 4^0C and the mitochondria were pelleted, washed with Reagent C and then further centrifuged at 12000g for 5 minutes at 4^0C to get purified mitochondrial fraction.

2.12.3. ISOLATION OF ER-ENRICHED FRACTION:

U2OS cells were homogenized in 1X Isosmotic Homogenization Buffer supplemented with protease inhibitors using a Dounce homogenizer. The lysate was centrifuged at 1000g for 10 minutes at 4^0C to pellet the nuclei and cellular debris. After careful removal of the thin layer of lipid floating at the top, the supernatant was further centrifuged at 12000g for 15 minutes at 4^0C to pellet and discard the mitochondria and cellular debris. This supernatant was the total ER fraction. It was then centrifuged at 90000g for 1 hour at 4^0C. The supernatant was discarded and the pellet was resuspended in 1X Suspension Buffer, supplemented with protease inhibitors and stored at -80C till further use.

2.13. CONSTRUCTION OF FORTILIN-DEFICIENT U2OS CELLS:

U2OS cells were transfected with lentiviral particles harboring shRNA against FT and control shRNA (pLKO.1-puro Control, Sigma-Aldrich, St. Louis, MO). Briefly, 1.6×10^4 U2OS cells were plated on each well of a 96-well plate and incubated 18-20 hours at 37^0C in presence of 5% CO_2 in a CO_2 incubator (Sanyo). The medium was then removed, followed by addition of 110μL of medium containing 8μg/mL of hexadimethrine bromide. Lentiviral particles were added to the wells at a multiplicity of infection (MOI) of 25 and incubated 18-20 hours at 37^0C in presence of 5% CO_2 in a CO_2 incubator. I also prepared some control wells without any lentivirus. The next day, media containing the viral particles was removed and replaced with 120μL of fresh media. The next day, media was removed and replaced with media containing 2.5μg/mL puromycin. From this time on, media was replaced with fresh puromycin-containing media every 3-4 days until resistant colonies were identified. 10 puromycin resistant colonies were selected and expanded to assay for knockdown of FT. After confirming FT knockdown in these polyclonal cells, I prepared monoclonal cells with downregulated FT (U2OS-sh-FT).

2.14. Prx I STABILITY ASSAY:

2×10^5 of each of U2OS-sh-Control and U2OS-sh-FT cells were plated in each well of a 6-well plate and allowed to grow overnight at 37^0C. The cells were then

washed with PBS and incubated with culture medium containing 100μg/mL CHX and harvested at different time points – 0, 2, 4, 8, 12 and 24 hours post-CHX treatment. The culture medium was replaced every 12 hours since CHX degrades after 12 hours. The cells harvested at various time points were lyzed using 100μL of RIPA buffer, followed by sonication and centrifugation at 14000rpm for 15 minutes at 4^0C. Total protein concentration was measured using a Bio-Rad Protein Assay kit and 10μg of each lysate was loaded onto a 12% SDS polyacrylamide gel for immunoblotting. The samples were immunoblotted with primary antibodies against FT, Prx I and GAPDH as loading control. Band intensities of the proteins were determined using the Licor imaging system software and Prx I expression index was determined as the ratio of band intensities of Prx I and GAPDH at each particular point.

2.15. PEROXIDASE ASSAY:

Peroxidase assay was performed by preparing reaction mixtures having the following final concentrations: 200μM NADPH, 3μM Trx, 1.5μM TrxR and requisite amount of Prx I and FT (1μg each when used separately and equimolar amounts when used together). Mixed every component and added buffer to them to prepare a master mix and pipetted the mixture into each well of a black-bottomed of a 96-well μClear-Plate (Greiner Bio-One). We added the protein components or buffer as

required, to obtain a final volume of 200μL. The reaction was initiated by adding 100μM H_2O_2 to each well simultaneously using a multi-channel pipet, making sure to avoid bubbles. We measured the NADPH absorbance immediately at 340nM for 30 minutes at 30^0C. The reaction buffer was used as blank for the measurement.

2.16. DNA FRAGMENTATION ELISA:

Apoptosis levels were determined in different cell types using a DNA fragmentation ELISA kit (Roche Applied Science, Indianapolis, IN). Briefly, cells under different treatment conditions were lysed and centrifuged at 200g for 10 minutes, following which the lysate was added to each well of the microcentrifuge plate along with positive control, negative control and background control (wash buffer only). Immunoreagent was prepared using anti-histone antibody (biotin-labeled) and anti-DNA-POD antibody (peroxidase conjugated) and added to each well. The mixture was allowed to incubate for 2 hours at room temperature with gentle shaking (300rpm). Subsequently, the solution was removed by suction and the wells were washed thrice with incubation buffer. 2,2'-azino-bis(3-ethylbenzothiazoline-6-sulphonic acid (ABTS) solution was added to each well and incubated on plate shaker at 250rpm until color development was sufficient for photometric analysis. The reaction was then stopped by adding ABTS stop solution and colorimetric analysis was performed at 405nm against ABTS solution plus ABTS stop solution as blank. For each sample there were three assay replicas. Average of

these readings was corrected by subtracting the reading for background (ABTS solution plus incubation buffer).

2.17. MAINTENANCE OF VERTEBRATE ANIMALS:

All the animals were housed in the Animal Resource Center (ARC) in the Medical Research Building and monitored by ARC veterinary staff. When there was a need to remove the animals from the ARC, animal cages were covered with a gown for removal from the room. Outside of the cages was sprayed with Cavicide, wiped down, and covered for transport back to the room. The surgical space was decontaminated by Cavicide and 70% ethanol and wiped down. Personal protective equipments were used by the personnel. All the experimental procedures concerning animals were approved by the Institutional Animal Care and Use Committee (IACUC) at UTMB prior to the experiments being performed.

2.18. ORAL GAVAGE:

Oral gavage of ethanol was performed using a gavage needle, with mice under general anesthesia using isoflurane inhalation to minimize trauma to the animals.

2.19. EUTHANASIA:

Mice were euthanized by asphyxiation using carbon dioxide until effective. Death was ascertained by bilateral thoracotomy. These methods are consistent with the recommendations of the American Veterinary Medical Association (AVMA) Guidelines on Euthanasia and UTMB IACUC policies.

2.20. GENERATION OF *CRE⁺/⁻LFL⁺/⁺* MICE:

The Cre recombinase-LoxP system was utilized to specifically knockout FT from only the liver of mice. Briefly, Cre is a 38kDa recombinase enzyme that was first demonstrated in 1981 to have the ability to carry out unique site-specific recombination in the bacteriophage P1 [Sternberg and Hamilton, 1981]. This unique site, called the LoxP (locus of X-over P1) site, is a 34bp stretch of nucleotides containing an asymmetric 8bp sequence (*GCATACAT*) flanked between two 13bp palindromic sequences (*ATAACTTCGTATA* and *TATACGAAGTTAT*). In presence of the Cre recombinase, cells containing LoxP sites in their genome can undergo recombination via cleavage of the double stranded DNA at both LoxP sites by Cre and subsequent rejoining of the strands catalyzed by DNA ligase. If the two LoxP sites on the same chromosome are direct repeats of one another, this recombination results in deletion of the intervening sequence. This strategy is utilized obtain targeted deletion of selected genes in mice [Gu *et al.* 1994]. By putting the Cre gene

under the action of specific promoters, the spatial and temporal expression of Cre can be controlled as desired. For example, by designing a construct where the Cre is expressed under the liver-specific albumin promoter (Alb-Cre), desired genes can be deleted only in the liver, leaving the function of the gene unaffected in the rest of the organism (Fig. 10). Genetically, our desired mice would contain at least one copy of the Cre recombinase transgene under the liver-specific albumin promoter (*Alb-Cre$^{+/+}$*or *Alb-Cre$^{+/-}$*) and two copies of the FT floxed allele (*LFL$^{+/+}$*) to give an overall genotype of *Alb-Cre$^{+/+}$LFL$^{+/+}$*or *Alb-Cre$^{+/-}$LFL$^{+/+}$*. Mice from the C57BL/6J strain overexpressing the Cre-transgene (*Alb-Cre$^{+/+}$LFL$^{-/-}$*) were purchased from Jackson Laboratory (Bar Harbor, ME) and crossed with *Alb-Cre$^{-/-}$LFL$^{+/+}$* mice (growing colony in the Fujise Laboratory) to generate *Alb-Cre$^{+/-}$LFL$^{+/-}$* mice. These doubly heterozygous mice in the F1 generation were self-crossed to generate, among others, *Alb-Cre$^{+/-}$LFL$^{+/+}$* mice. No *Alb-Cre$^{+/+}$LFL$^{+/+}$* mice were obtained in the F2 generation. The breeding strategy is described in Fig. 11. Only 8-week old male *Alb-Cre$^{+/-}$LFL$^{+/+}$* (sample) or *Alb-Cre$^{-/-}$LFL$^{+/+}$* (control) mice were used for future experiments.

2.21. GENOTYPING OF MICE:

At 3 weeks of age, the distal 5mm was snipped off from the tails of all the mouse pups under general anesthesia and used for genotyping.

A

FT is knocked out in the liver
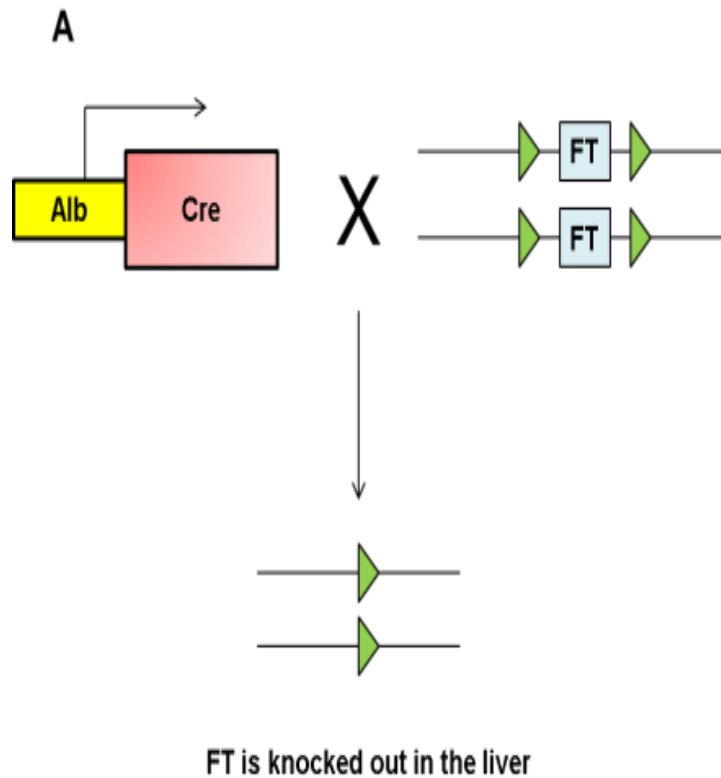
Figure 10: Schematic representation of the generation of *Alb-Cre⁺/⁻LFL⁺/⁺* mice. The Cre transgene under the control of the liver-specific albumin (Alb) promoter recognizes the two loxP sites (green triangles) and deletes the intervening fortilin sequence, thus knocking out FT from the liver.

2.21.1. DNA EXTRACTION FOR GENOTYPING:

The tail pieces were incubated overnight at 50^0C with shaking at 300rpm in lysis buffer containing 10mM Tris-HCl pH 8.0, 25mM EDTA, 100mM NaCl, 1% SDS and 1:100 Proteinase K. The lysate was subsequently centrifuged for 5 minutes at

14000rpm and the clear lysate was treated with phenol/chloroform/isoamyl alcohol (25:24:1) and vortexed until it became cloudy. It was then centrifuged at 14000rpm for 10 minutes and the top layer was transferred to a phase-lock gel tube. Phenol/chloroform/isoamyl alcohol (25:24:1) was added to it and the tubes were allowed to rock gently at room temperature for 15 minutes, following which they were centrifuged for 5 minutes at 14000rpm and the upper layer was carefully transferred to a new tube. DNA was precipitated using isopropanol and the pellet was washed carefully twice with 70% ethanol and once with 100% ethanol, following which the pellet was allowed to dry for 20 minutes. It was subsequently dissolved in nuclease-free water and incubated at 50^0C for 30 minutes before the DNA concentration was determined. This DNA was used to perform genotyping PCR using primers specific for Alb-Cre and LoxP-Fortilin-LoxP (LFL) genes.

2.21.2. PCR FOR GENOTYPING:

2.21.2.1. PCR CONDITIONS FOR CRE TRANSGENE:

Primers: 5'-GCG GTC TGG CAG TAA AAA CTA TC-3' (Forward)

5'-GTG AAA CAG CAT TGC TGT CAC TT-3' (Reverse)

PCR conditions: 94^0C for 3.00 min

94^0C for 0.30 min

56^0C for 1.00 min

72^{0}C for 1.00 min

72^{0}C for 2 min

10^{0}C Forever

Steps 2-4 were repeated for 34 cycles.

2.21.2.2. PCR CONDITIONS FOR LFL:

Primers: 5'-TGG ACC CTG ACT TTC ATC ACC TC-3' (Forward)

5'-GTC ATC TAA CCT TAC CCC AGT AAG C-3' (Reverse)

PCR conditions: 94^{0}C for 3.00 min

94^{0}C for 0.30 min

54^{0}C for 1.00 min

72^{0}C for 1.00 min

72^{0}C for 3 min

10^{0}C Forever

Steps 2-4 were repeated for 34 cycles.
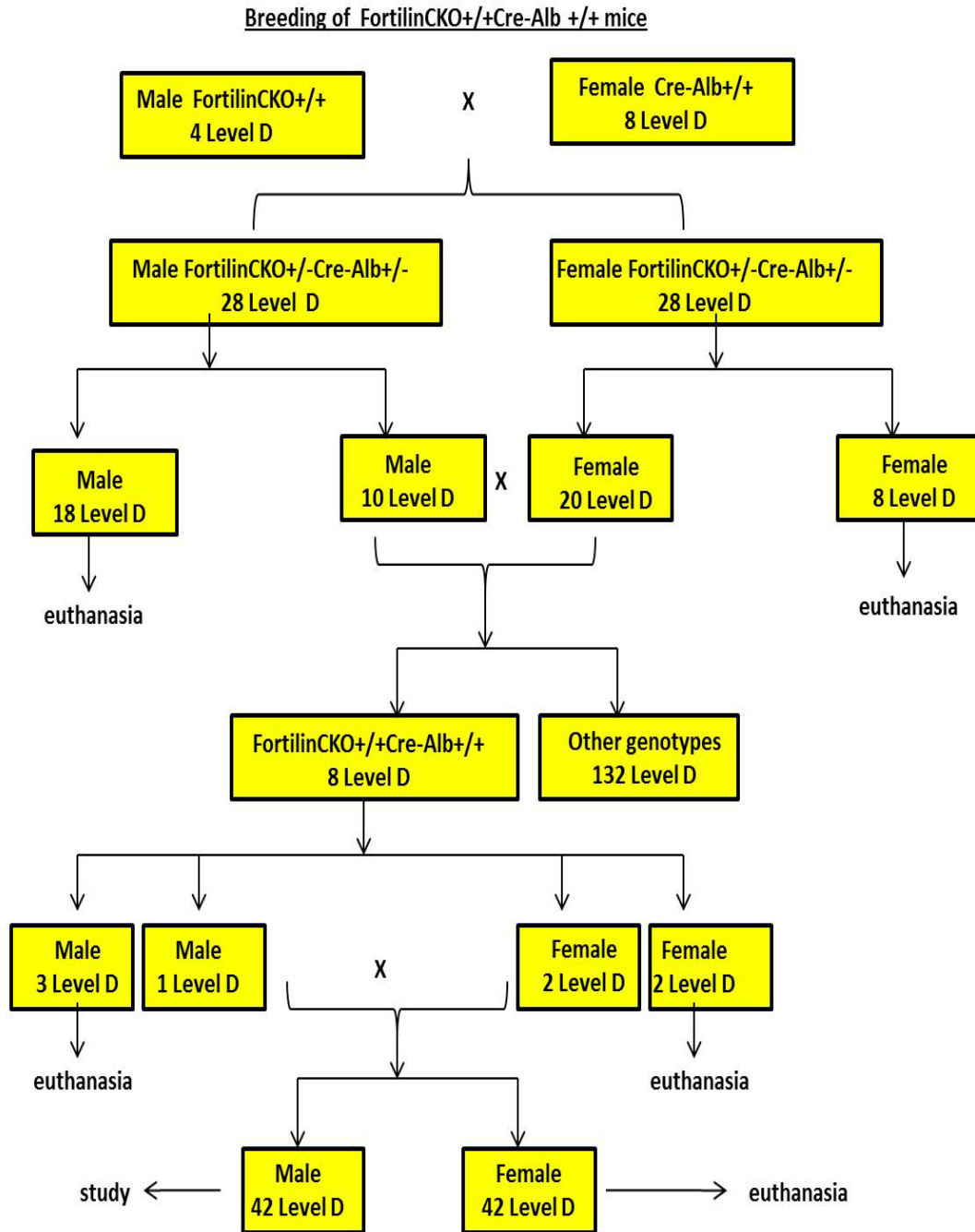
Figure 11: Breeding Strategy for generation of *Alb-Cre⁺/⁻LFL⁺/⁺* mice. The above flowchart describes the breeding strategy to generate *Cre⁺/⁻LFL⁺/⁺* mice.

2.22. Estimation of Liver Profile Parameters in Mouse Blood

Liver profile parameters – alkaline phosphatase (ALP), alanine aminotransferase (ALT), bile acids (BA), total bilirubin (TBIL), albumin (Alb), blood urea nitrogen (BUN) and cholesterol (Chol) – were determined in mouse blood using a VetScan mammalian liver profile disc (Abaxis, Union City, CA) on a VetScan VS2 instrument.

2.22.1. Estimation of Lipid Peroxidation by Quantification of Malondialdehyde (MDA) in Ethanol-Treated Mice:

Lipid peroxidation in the liver and kidneys of *Alb-Cre+/-LFL+/+* and *Alb-Cre-/- LFL+/+* mice was estimated by measuring MDA production using a OxiSelect™ TBARS Assay Kit (Cell Biolabs Inc., San Diego, CA). The principle of the assay involves samples with known (standards) or unknown concentrations of MDA to be treated with thiobarbituric acid (TBA) at 95^0C. The adduct thus formed can be then quantified fluorimetrically using a predetermined MDA standard curve. Briefly, liver and kidney samples were perfused with PBS following harvesting from sacrificed mice. Tissues were resuspended in 500μL PBS containing 1X butylated hydroxytoluene (1X BHT) and then homogenized on ice. The samples were centrifuged at 10000g for 5 minutes to collect the supernatant. Protein

concentration of the supernatants was determined using Bio-Rad protein assay. A standard curve was prepared using MDA standards in the range 125μM – 0μM. 100μL of tissue lysate or MDA standards were added to separate microcentrifuge tubes and treated with 100μL SDS lysis solution and incubated at room temperature for 5 minutes. 250μL of TBA reagent was added to each tube and incubated at 95^0C for 60 minutes, following which they were cooled to room temperature and spun down at 3000rpm for 15 minutes and removed the supernatants for further analysis. 300μL of the supernatants was mixed with 300μL of n-butanol, vortexed vigorously for 1-2 minutes and then centrifuged for 5 minutes at 10000g. The supernatant, i.e. the butanol fraction was used for further analysis. 150μL of the MDA standards and the samples were transferred to a 96-well microplate and the samples were read in duplicate using a fluorimetric plate reader at 540nm excitation and 590nm emission wavelength. MDA concentrations in the liver and kidney samples were estimated by comparison with the standard curve and the estimated MDA amount was normalized to the protein content of the sample.

2.22.2. ESTIMATION OF TOTAL CELLULAR GLUTATHIONE LEVEL IN MOUSE LIVER HOMOGENATE:

Total cellular glutathione (GSH) level was estimated in mouse liver homogenate using a Glutathione Assay Kit (Sigma-Aldrich, St. Louis, MO). The principle of the assay involves a kinetic reaction between GSH and 5,5'-dithiobis(2-

nitrobenzoic acid) (DTNB) to TNB and the oxidized GSH (GSSG) is converted back to GSH by glutathione reductase (GR) and NADPH. The 5-thio-2-nitrobenzoic acid (TNB) formed is yellow in color and can be estimated colorimetrically at 412nm. The reactions involved are as follows:

1. $2GSH + DTNB \rightarrow GSSG + 2TNB$

2. $GSSG + NADPH + H^+$ ------------------------------- Glutathione reductase $\rightarrow 2GSH + NADP^+$

Combined reaction:

$DTNB + H^+$ ------------------------------------- Glutathione reductase / GSSG/GSH $\rightarrow 2TNB + NADP^+$
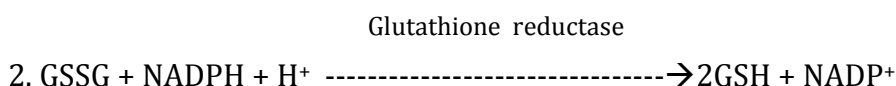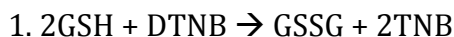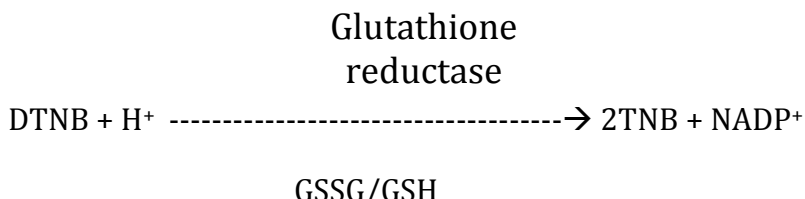
Mouse liver samples were perfused with PBS and then flash-frozen in liquid nitrogen immediately after excision from the animal. The tissue was then ground into a fine powder using a mortar and pestle with liquid nitrogen. $300\mu g$ of the powder was mixed with 3 volumes of 5% 5-SSA solution ($900\mu L$) and vortexed, following which another 7 volumes of 5% 5-SSA were added to it. The samples were homogenized using a Dounce homogenizer till an even suspension was obtained. The suspension was left at 2-8^0C for 10 minutes and then centrifuged at 10000g for 10 minutes. Reactions were setup using 95mM potassium phosphate buffer, pH 7.0, 0.95mM EDTA, 0.038mg/mL ($48\mu M$) NADPH, 0.031mg/mL DTNB, 0.115units/mL glutathione reductase and 0.24% 5-sulfosalicylic acid and various known

concentrations of TNB or unknown samples. 5% SSA was used as reagent blank. The samples were incubated 5 minutes at room temperature and then 50μL of the diluted NADPH solution was added to the reaction mixtures, followed by mixing by pipeting. The absorbance of the solutions at 412nm was followed kinetically for 5 minutes using a spectrophotometer. Nanomoles of GSH per μg of protein in each sample were calculated using the ratio of the slope generated by the sample and the slope calculated from the standard curve for 1nmole of GSH.

2.22.3. HISTOPATHOLOGICAL AND IMMUNOLOGICAL STAINING OF ETHANOL-INDUCED TISSUE DAMAGE IN MOUSE LIVER:

Freshly harvested mouse liver, kidney and heart were perfusion-fixed using 10% neutral buffered formalin (NBF) in PBS and then fixed overnight in 10% NBF, following which they were transferred to 70% ethanol in PBS till further analysis. Liver tissue was analyzed at the Histology Core Facility at the MD Anderson Cancer Center, Smithsville. Briefly, the liver tissue was cut into 5μM sections and stained with, as required, hematoxylin and eosin (H&E) stain and anti-4-hydroxynonenal (4-HNE) antibody (Abcam, Cambridge, MA).

2.23. STATISTICAL ANALYSIS:

All data were expressed as means ± SD. Statistical analysis of the results will be performed by Dunnett's test for multiple comparisons and Student's t-test for single comparisons, using Microsoft Excel. Unless mentioned otherwise, a p-value <0.001 was considered statistically significant.

CHAPTER III: PROTEOMIC SCREENING AND ANALYSIS TO IDENTIFY NOVEL FORTILIN INTERACTING PROTEINS (FIPs) AND CONFIRMATION OF PEROXIREDOXIN I AS A TRUE FIP

3.1. INTRODUCTION:

FT is a highly conserved 172-amino acid polypeptide with anti-apoptotic function comparable to that of MCL1 and BcL-xL in HeLa cells [Li *et al.* 2001] and is overexpressed in human cancers, mostly cancers of epithelial origin [Li *et al.* 2001]. FT prevents hydrogen peroxide-induced cell death in multiple cell lines [Nagano-Ito s*et al.* 2009] and is also seen to be upregulated under oxidative stress. The ability of FT to lower the sensitivity of FT-overexpressing cells to oxidative stress has prompted Lucibello and colleagues [Lucibello *et al.* 2011] to propose FT to be an important stress response molecule. Additionally, some studies have shown FT to be translocated from the cytoplasm to the nucleus upon treatment with hydrogen peroxide, where it interacts directly with the ligand binding domain of the endogenous vitamin D3 receptor (VDR) [Rid *et al.* 2010]. While there is a growing body of evidence on the anti-apoptotic function of FT, the molecular mechanism of such function has not been clearly elucidated, especially under the conditions of oxidative stress. The primary goal in the current study was to identify novel

interacting partners of FT which may be able to explain the anti-apoptotic behavior of FT under oxidative stress.

3.2. RESULTS:

Our strategy to identify potential FIPs was to overexpress FT with an HA tag in U2OS cells and then immunoprecipitate HA-FT using anti-HA agarose beads, along with its complement of interacting partners. The immunoprecipitated complex was then resolved using SDS-PAGE and the protein bands that would preferentially get pulled down with HA-FT but not with the empty-HA vector would be considered as potential FIPs.

3.2.1. OPTIMIZATION OF FORTILIN IMMUNOPRECIPITATION:

I cloned the human FT gene from a human lymphocyte cDNA library using reverse transcription PCR to isolate the gene and inserted it into the pcDNA4 vector (Fig. 12A). I further cloned the N-terminus in-frame with the influenza hemagglutinin epitope, to generate an HA-FT vector. U2OS cells were selected for stable transfection of HA-FT vector since these osteosarcoma cells express low levels of endogenous FT (Fig. 12B). U2OS cells were transfected with the HA-FT vector and also the control vector (referred to as HA-Empty henceforth) and grown
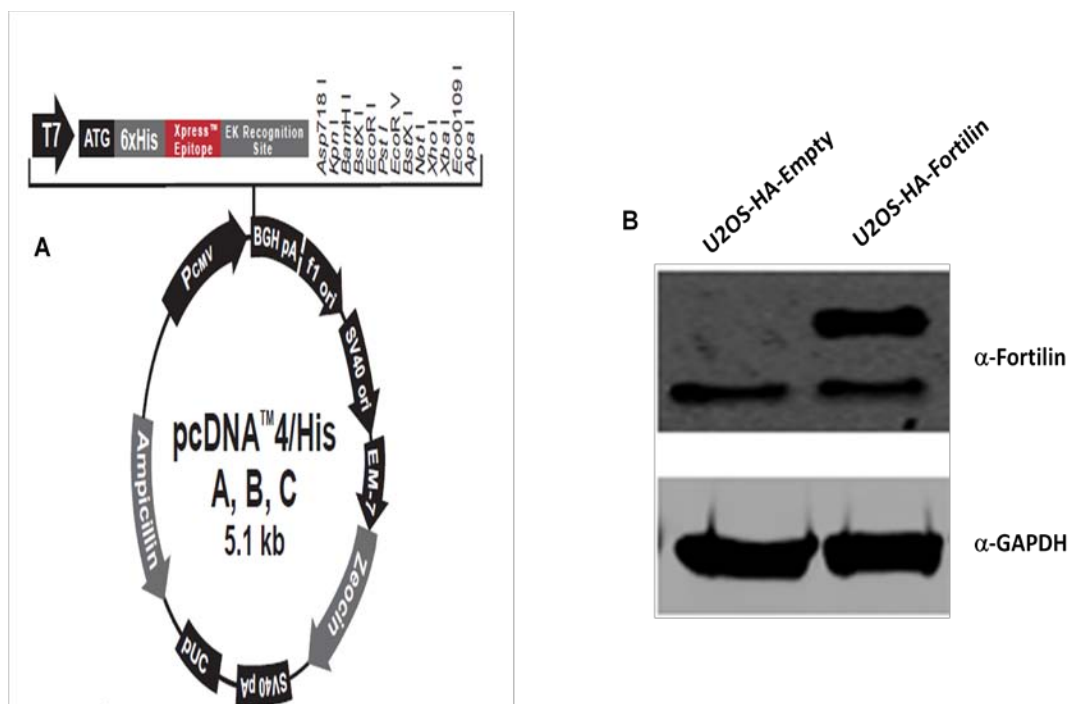
Figure 12: Cloning and overexpression of HA-Fortilin in U2OS cells. A. Human FT was directionally cloned into the pcDNA4 vector (HTTP://TOOLS.LIFETECHNOLOGIES.COM/CONTENT/SFS/VECTORS/PCDNA4HIS_MAP.PDF), with the N-terminus being in frame with the hemagglutinin epitope. **B.** U2OS cells were transfected with the empty vector and the HA-FT vector and grown in presence of the selective antibiotic zeocin (400μg/mL). Western blot analysis was performed on the lysate against anti-FT antibody; the lower FT band in both lanes corresponds to endogenous FT while the higher more robust band corresponds to the overexpressed HA-FT. Lysates were also stained for GAPDH as loading control.

in presence of 400μg/mL of zeocin as selective antibiotic till the cells stably overexpressed HA-FT. I used rat anti- HA agarose beads to perform the immunoprecipitation reaction (as described in section 2.7). I optimized both salt and detergent conditions in the IP wash buffer so as to minimize non-specific binding, finally deciding on using 20mM HEPES (pH = 7.4), 150mM NaCl and 0.01% NP-40 as wash buffer for all subsequent immunoprecipitation reactions. As shown in Fig. 13, HA-FT is successfully immunoprecipitated using the anti-HA agarose

beads and there is no IP using the HA-Empty cell lysate (negative control). The second lane in Fig. 13 contains the whole cell lysate from U2OS-HA-FT cells which shows two FT bands – the lower band corresponds to endogenous FT while the higher band corresponds to HA-FT. In the first lane, the whole cell lysate from U2OS-HA-Empty cells contains only the endogenous FT band. The western blot shown in Fig. 13 therefore, confirms the overexpression of HA-FT in U2OS cells and also successful immunoprecipitation of HA-FT using the anti-HA agarose beads.
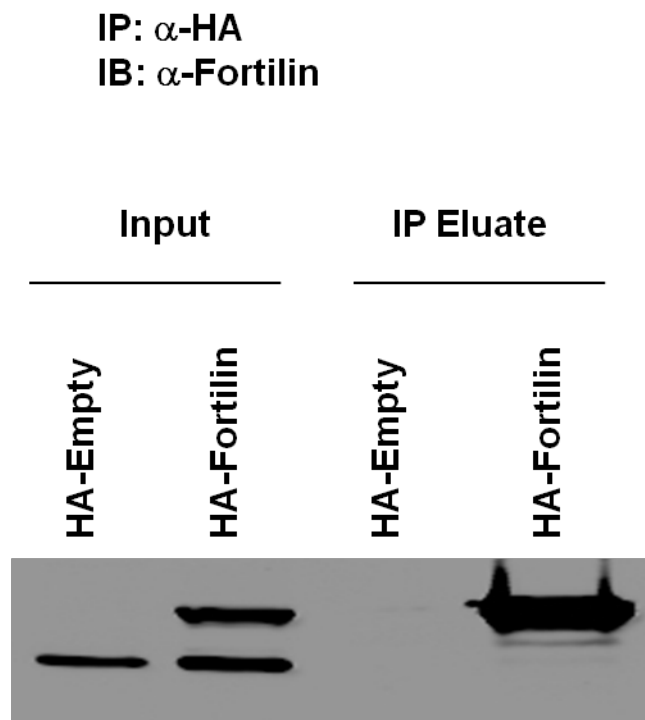
Figure 13: Immunoprecipitation of HA-FT from U2OS-HA-FT cells. HA-FT was successfully immunoprecipitated from U2OS-HA-FT cells using rat anti-agarose beads and confirmatory immunoblot was performed using anti-FT antibody, which showed specific immunoprecipitation of the HA-tagged FT but not endogenous FT.

3.2.2. CO-IMMUNOPRECIPITATION OF PUTATIVE FIPS AND PROTEOMIC ANALYSIS:
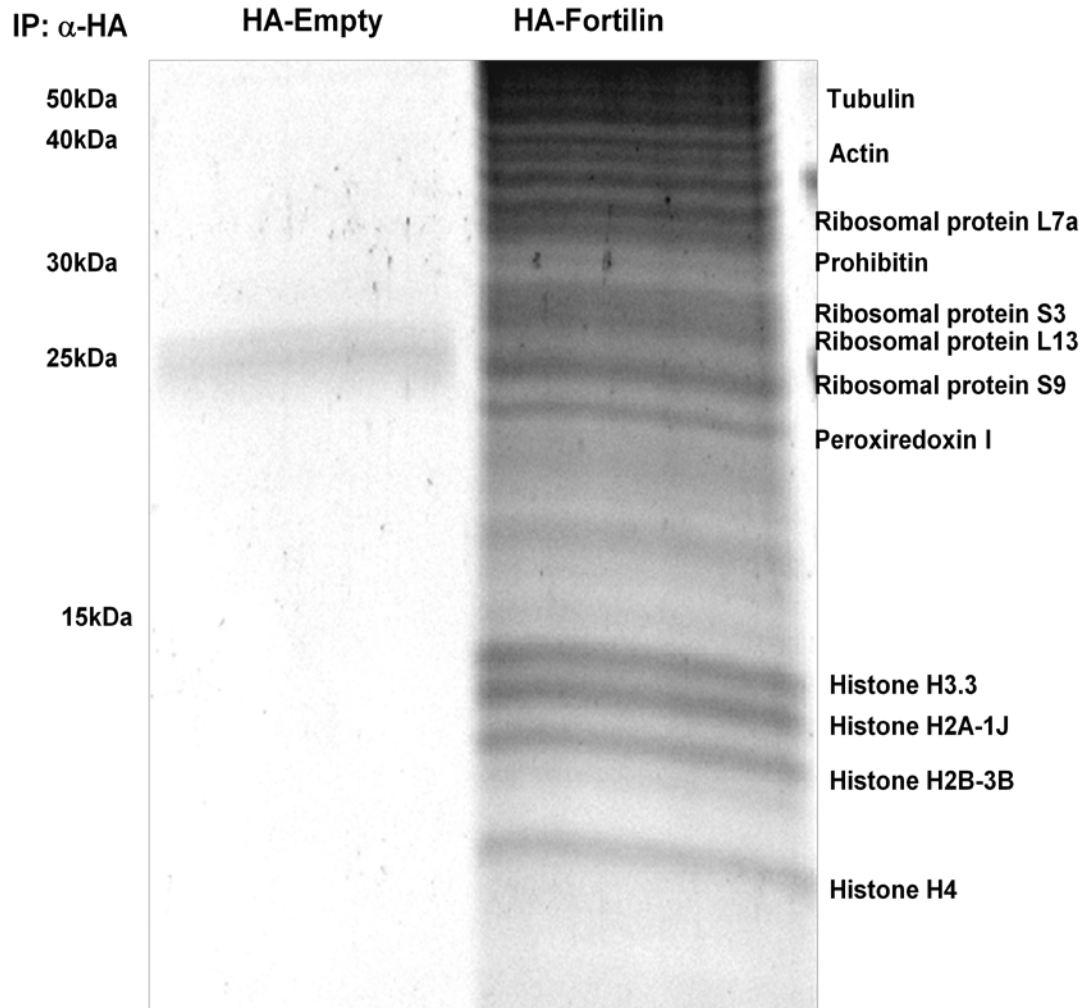
Figure 14: Detection of putative Fortilin Interacting Proteins. Anti-HA immunoprecipitation was performed in U2OS-HA-Empty and U2OS-HA-FT cell lysate using anti-HA agarose beads and the eluates were resolved on a large format SDS Polyacrylamide gel. The gel was then stained with the Sypro Ruby stain and protein bands were visualized under UV light. Protein bands which were present only in the U2OS-HA-FT IP lane were excised and identified via MALDI-TOF Mass Spectrometry.

In Fig. 13 I confirmed that using anti-HA agarose beads I had successfully immunoprecipitated HA-FT. In the next experiment I performed a large scale anti-HA immunoprecipitation in U2OS-HA-Empty and U2OS-HA-FT cell lysate with the anti-HA agarose beads, eluted the samples using 4X SDS loading buffer and resolved the eluates on a large format SDS Polyacrylamide gel. The gel was then stained with the Sypro Ruby stain and protein bands were visualized under UV light. Eluates from both U2OS-HA-Empty IP and U2OS-HA-FT IP were compared and protein bands present only in the U2OS-HA-FT IP lane were excised and submitted to the UTMB Biomolecular Resource Facility for identification via MALDI-TOF Mass Spectrometry. The Mascot Proteomics server was used to identify the bands. As shown in Fig. 14, a number of putative FIPs were identified, including the anti-oxidant, anti-apoptotic protein Peroxiredoxin I (Prx I). A complete list of all the putative FIPs is presented in Table 2. Previously characterized FIPs including actin, tubulin and histone H2B were also identified in this proteomic screen, leading credence the current data and strongly suggesting that the other proteins obtained in the screen were likely to be true FIPs.

3.2.3. CONFIRMATION OF PEROXIREDOXIN I AS A TRUE FORTILIN INTERACTING PROTEIN (FIP):

Prx I is one of six thioredoxin-dependent anti-oxidant enzymes [Chae *et al.* 1993; Chae *et al.* 1994; Chae *et al.* 1994] whose primary function is the scavenging

Table 2: Putative Fortilin Interacting Proteins:

Protein Name	Mol. Wt (kDa)	Peptide Count	Protein Score	
			% C.I	Expectation Score
Tubulin*	49.86	16	100	6.29E-26
Actin*	41.76	10	100	3.97E-29
60S Ribosomal protein L7a	29.97	9	100	3.15E-011
Prohibitin	29.79	11	100	5.00E-031
40S Ribosomal protein S3	26.67	7	100	3.15E-009
60S Ribosomal protein L13	24.25	8	100	1.99E-019
40S Ribosomal protein S9	22.6	13	100	2.50E-021
Peroxiredoxin I	22.1	9	100	5.00E-020
Histone H3.3	15.3	5	100	2.50E-008
Histone H2A*	13.9	7	100	1.99E-025
Histone H2B*	13.9	6	100	9.97E-019
Histone H4	11.4	6	100	9.97E-034

Table 2: Proteomic Screening and Identification of Fortilin Interacting Proteins. Putative Fortilin Interacting Proteins with predicted molecular weights, peptide counts and protein expectation scores. Previously reported FIPs including actin and tubulin were identified in this screen along with peroxiredoxin I and further studies were performed to confirm the interaction. (* indicates that these proteins have been already reported to be known fortilin interacting partners of FT.)

and reduction of reactive oxygen species (ROS), especially organic peroxides, hydroperoxides and peroxynitrites [Rhee *et al.* 1999; Hofmann *et al.* 2002; Wood *et al.* 2003]. Prx I and other peroxiredoxins have also been shown to have roles in promoting cell survival and in cell cycle regulation [Immenschuh and Baumgart-Vogt, 2005]. Prx I was identified in our proteomic screen as a putative FIP and I determined if Prx I was a true FIP using western blot analysis. I stably transfected U2OS cells with HA-Empty, HA-FT and HA-NQO2 vectors, where NQO2 or NAD(P)H dehydrogenase quinone 2 is another anti-oxidant protein which does not interact with FT (data not shown). Lysates from the three cell lines were subjected to immunoprecipitation using anti-HA agarose beads as described before and the eluates were resolved on an SDS Polyacrylamide gel. The immunoprecipitated protein complexes were subjected to WB analysis using an anti-Prx I antibody. As shown in Fig. 15A, peroxiredoxin was specifically immunoprecipitated from U2OS-HA-FT cells but not in U2OS-HA-Empty or U2OS-HA-NQO2 cells. This observation provided further evidence that Prx I is a real FIP. It also conclusively ruled out any non- specific interaction of FT with the HA-tag itself.

To rule out the possibility that there would be non-specific interaction of Prx I with the agarose beads, I performed IP using U2OS-HA-FT cell lysate and treated them with anti-HA agarose beads and anti-Protein C agarose beads. As shown in Fig. 15, Prx I was specifically co-immunoprecipitated only using the anti-HA agarose beads, which confirmed that there was no non-specific interaction between Prx and the agarose beads.
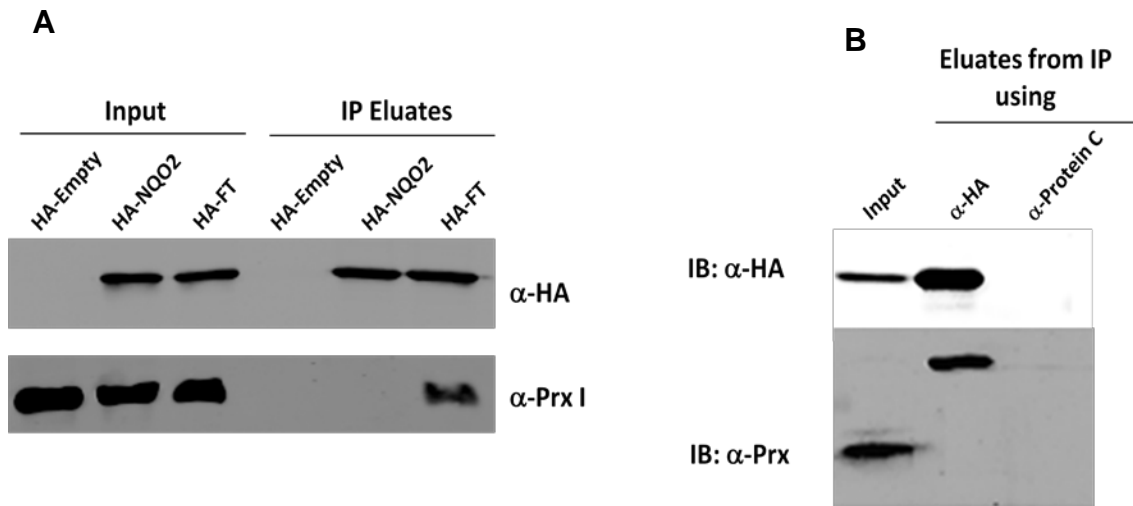
Figure 15: Confirmation of Peroxiredoxin as a true Fortilin Interacting Protein. A. U2OS cells stably transfected with HA-Empty, HA-FT and HA-NQO2 plasmids and the cell lysates were subjected to anti-HA immunoprecipitation. The samples were then analyzed by immunoblot using an anti-Prx antibody and Prx was shown to be specifically co-immunoprecipitated only with HA-FT, confirming that Prx Is a true FIP and ruling out the possibility of non-specific interaction between Prx and the HA-epitope. **B.** U2OS-HA-FT lysate was subjected to anti-HA immunoprecipitation using anti-HA and anti-Protein C agarose beads. Prx was specifically co-immunoprecipitated only with the anti-HA agarose bead and not the Protein C beads, ruling out non-specific interaction with the agarose beads.

3.2.4. VERIFICATION OF FORTILIN-PRX I INTERACTION USING RECIPROCAL CO-IMMUNOPRECIPITATION:

Prx I-VI were directionally cloned into the p3X-FLAG CMV 14 vector and the plasmids were transiently transfected into U2OS cells stably overexpressing HA-FT and the lysates from the cells were subjected to immunoprecipitation using anti-HA and anti-FLAG agarose beads. The eluates were subjected to immunoblotting using anti-HA and anti-FLAG antibodies. Sepharose beads were used as negative control to

rule out non-specific interaction with the beads. As shown in Fig. 16, FT co-immunoprecipitated Prx I, II, III and V but not IV and VI and was reversibly co-immunoprecipitated with Prx I, II, III and V but not with IV and VI, indicating that FT interacts specifically with Prx I, II, III and V but not with IV or VI under our immunoprecipitation conditions. The presence and absence of interaction between FT and the different Prx Isoforms are summarized in Table 3.
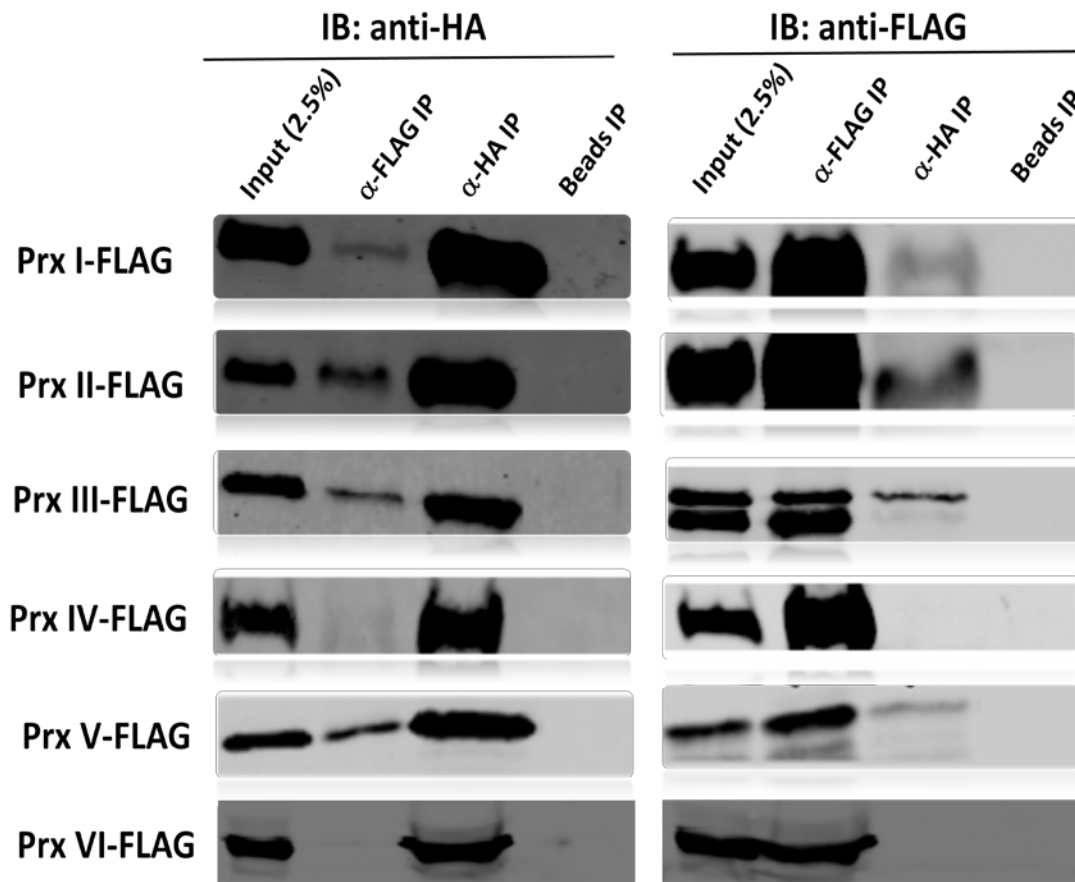
Figure 16: Reverse co-immunoprecipitation of FT with Peroxiredoxin isoforms. U2OS cells stably overexpressing HA-FT were transfected with Prx I-VI-FLAG plasmids and the lysates from the cells were subjected to immunoprecipitation using anti-HA and anti-FLAG agarose beads. The eluates were subjected to immunoblotting using anti-HA and anti-FLAG antibodies. FLAG-tagged Prx I, II, III and V were co-immunoprecipitated with HA-FT while HA-FT was reversibly co-immunoprecipitated with FLAG-tagged Prx I, II, III and V, but not with Prx IV and Prx VI, confirming that FT interacts *in vitro* with Prx I, II, III and V. The protein interactions are summarized in Table 3.

Table 3: Summary of Interactions between Fortilin and Peroxiredoxins I-VI

Plasmid transfected	FLAG co-IP in α–HA IP	HA co-IP in α–FLAG IP	FIP?
Prx I-FLAG	+	+	Yes
Prx II-FLAG	+	+	Yes
Prx III-FLAG	+	+	Yes
Prx IV-FLAG	-	-	No
Prx V-FLAG	+	+	Yes
Prx VI-FLAG	-	-	No

Table 3: Summary of Interactions between Fortilin and Peroxiredoxins I-VI. This table summarizes the presence or lack of interaction between FT and Prx I-VI. FT binds to Prx I, II, III and V but not to Prx IV and Prx VI under the experimental conditions used for these experiments. (+ and – indicate presence and absence of interaction between the proteins respectively)

3.2.5. IDENTIFICATION OF A FORTILIN MUTANT THAT FAILS TO INTERACT WITH PRX I:

I generated a series of FT point mutants based on the conserved residues present in FT from different species. All the mutants were cloned with an HA tag and

transiently expressed in U2OS cells along with the WT HA-FT and the empty-HA vector. The cell lysates were subjected to anti-HA IP using anti-HA agarose beads, the beads were washed with wash buffer and the immunoprecipitate was eluted using SDS loading dye. The samples along with the whole cell lysates were subjected to immunoblotting against anti-HA antibody to confirm successful IP of HA-tagged FT mutants and against Prx I antibody to determine whether Prx I was successfully co-immunoprecipitated with the mutants. As shown in the upper panel of Fig. 17,
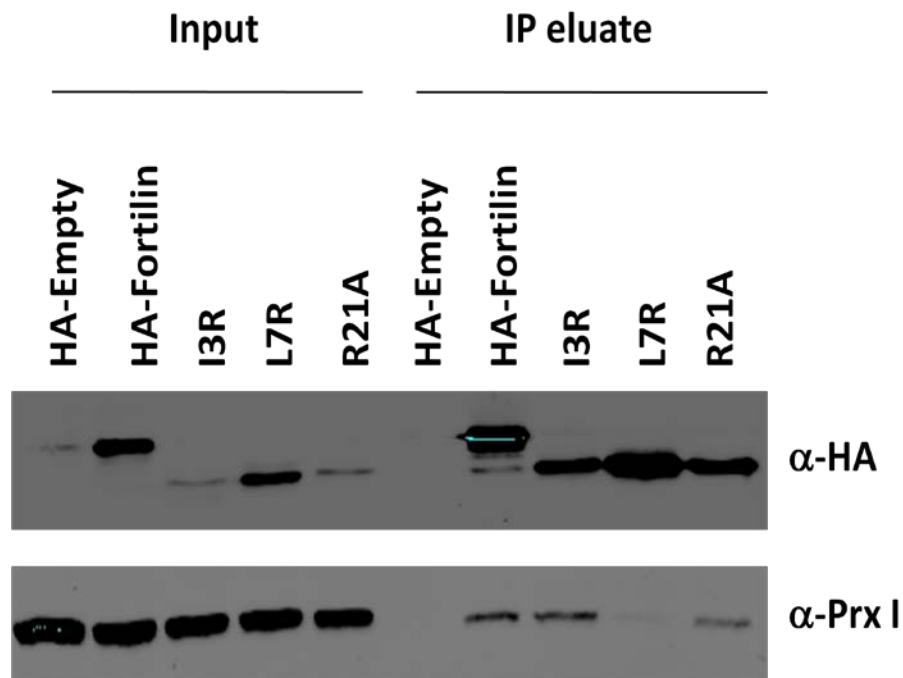
Figure 17: FT mutant L7R cannot co-immunoprecipitate Prx I. HA-tagged FT WT and mutants were transiently expressed in U2OS cells and subjected to anti-HA IP. HA was successfully immunoprecipitated in all cases. Prx I was successfully co-immunoprecipitated by WT, I3R and R21A but not by L7R, indicating that the Leu7 residue is crucial for the interaction of FT with Prx I.

HA-FT (WT or mutant) was successfully immunoprecipitated in all cases except for the U2OS-HA-empty cells used as negative control. Prx I was seen to be successfully co-immunoprecipitated with WT FT and the mutants I3R and R21A, but not with the mutant L7R. I was therefore able to successfully identify the residue, Leucine 7, of FT as being crucial for its interaction with Prx I. This construct would turn out to be a highly valuable tool to test the functional significance of the FT-Prx I interaction later in this project.

3.2.6. CO-IMMUNOPRECIPITATION OF FORTILIN WITH PRX I FROM MOUSE LIVER TISSUE:

In Figs. 16 and 17, I confirmed the interaction between FT and Prx I in U2OS cells overexpressing FT and/or Prx I via direct or reverse co-IP. I next wanted to determine if the interaction could be demonstrated in animal tissue. I sacrificed and harvested livers from 8-week old male C57BL/6J mice, lyzed the tissue in lysis buffer and performed an immunoprecipitation reaction using the lysate, mouse anti-Prx I antibody and sheep anti-mouse magnetic Dynabeads. Normal mouse IgG was used as negative control to ensure there was no non-specific binding. As shown in Fig. 18, Prx I is successfully immunoprecipitated from mouse liver tissue and there is a robust co-immunoprecipitation of FT with Prx I. The lack of any band in the IgG control confirmed that there was no non-specific binding. The data presented in Fig. 18 clearly demonstrates that the FT-Prx I interaction occurs not only in cultured

cells, but also in whole animal tissue, underscoring the physiological relevance of the FT-Prx I interaction.
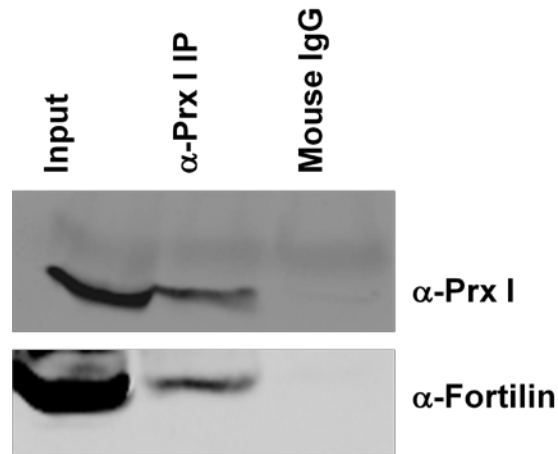
Figure 18: FT is co-immunoprecipitated with Prx I from mouse liver tissue. Mouse liver lysate was subjected to anti-Prx I immunoprecipitation. **Top panel.** There is successful immunoprecipitation of Prx I from mouse liver. **Bottom panel.** FT is successfully and specifically co-immunoprecipitated with Prx I in a robust manner. Lack of bands in the IgG control lane in both panels confirms lack of non-specific interaction.

3.2.7. SELECTION OF PRX I FOR FURTHER CHARACTERIZATION:

Having confirmed the interaction between FT and Prx I-III and V, I decided to further characterize the interaction between FT and Prx I. Both FT and Prx I have been known to be pro-survival as well as have a role in combating oxidative stress. Additionally, there have been reports of peroxiredoxin expression levels changing in FT-overexpressing transgenic mice hearts [Cheon *et al.* 2008] and of both Prx and

85

FT levels changing in neonatal rat cardiomyocytes exposed to H_2O_2 [Cullingford *et al.* 2006], which point to a possible interaction between Prx I and FT, as also indicated by our preliminary data. Prx I is thus, in all likelihood, a true FIP and the interaction between Prx I and FT merits further investigation.

3.2.8. DEMONSTRATION OF DIRECT FORTILIN-PRX I BINDING BY SURFACE PLASMON RESONANCE (SPR):

To determine whether FT and Prx I bind to each other directly, I cloned and purified pure recombinant FT from HEK293T cells and then biotinylated it. Following the biotinylation, FT was conjugated to streptavidin-tagged biosensors on the Blitz instrument (forteBio, Menlo Park, CA). As described in section 2.11.1, FT was loaded onto the biosensors, then titrated with increasing concentrations of pure recombinant Prx I to ascertain the binding ($k_{association}$) and then treated with a large excess of PBS to determine how quickly the interaction was abolished ($k_{dissociation}$) for each different concentration. A representative set of kinetic curves is shown in Fig. 19. The binding curves were normalized to that for 0μM Prx I concentration. From the results of three independent experiments, the average K_D value ($k_{dissociation}/ k_{association}$) was determined to be **124.79 ± 69.67nM**. For comparison, the published K_D of interaction between FT and p53 is 210nM [Amson *et al.* 2011]. K_D in the nanomolar range indicates very high affinity between FT and Prx I. I have, therefore conclusively demonstrated direct physical binding between FT and Prx I

and based on the value of the dissociation constant, the binding between the two

proteins appears to be very strong.
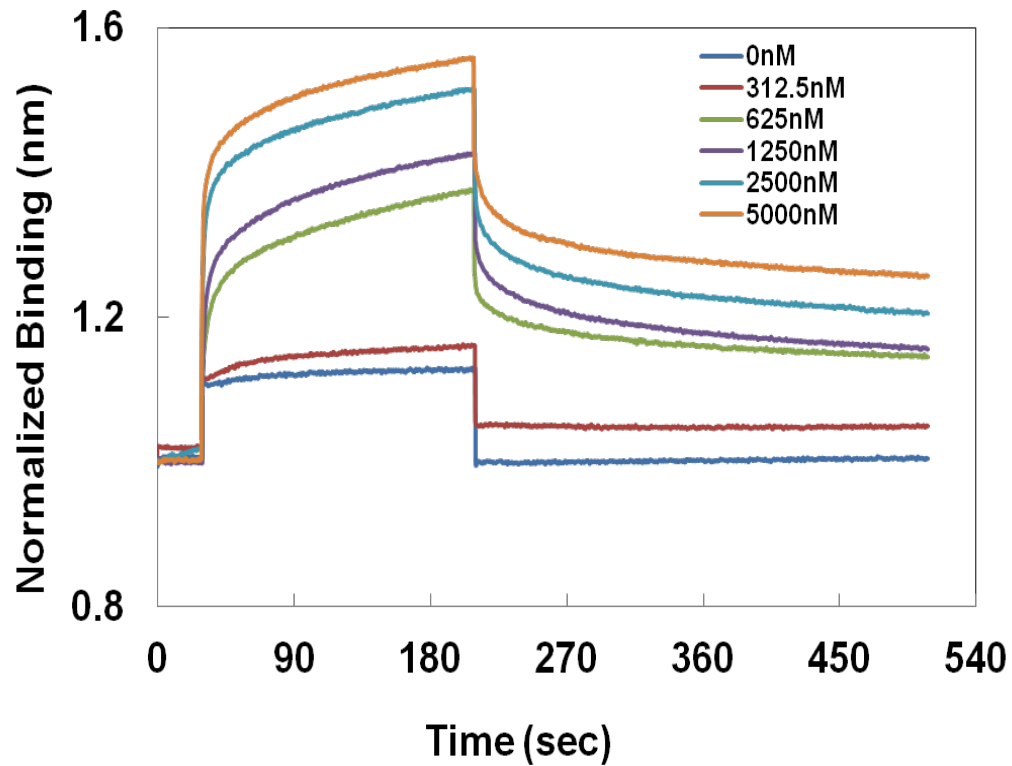
Figure 19: Direct binding between FT and Prx I. Biotinylated FT was conjugated to streptavidin-tagged biosensors and titrated with increasing concentrations of pure recombinant Prx I. Complex formation between the two proteins was monitored by measuring the increase in thickness of the protein layer on the biosensor as measured by a change in absorbance. Figure is representative of three independent experiments.

3.2.9. DEMONSTRATION OF FORTILIN-PRX I INTERACTION *IN VIVO* BY IMMUNOFLUORESCENCE:

Since I have already demonstrated that Prx I and FT interact specifically, I hypothesized that the two proteins should co-localize in the same subcellular site. In order to determine the site of interaction, U2OS cells were grown and fixed on glass
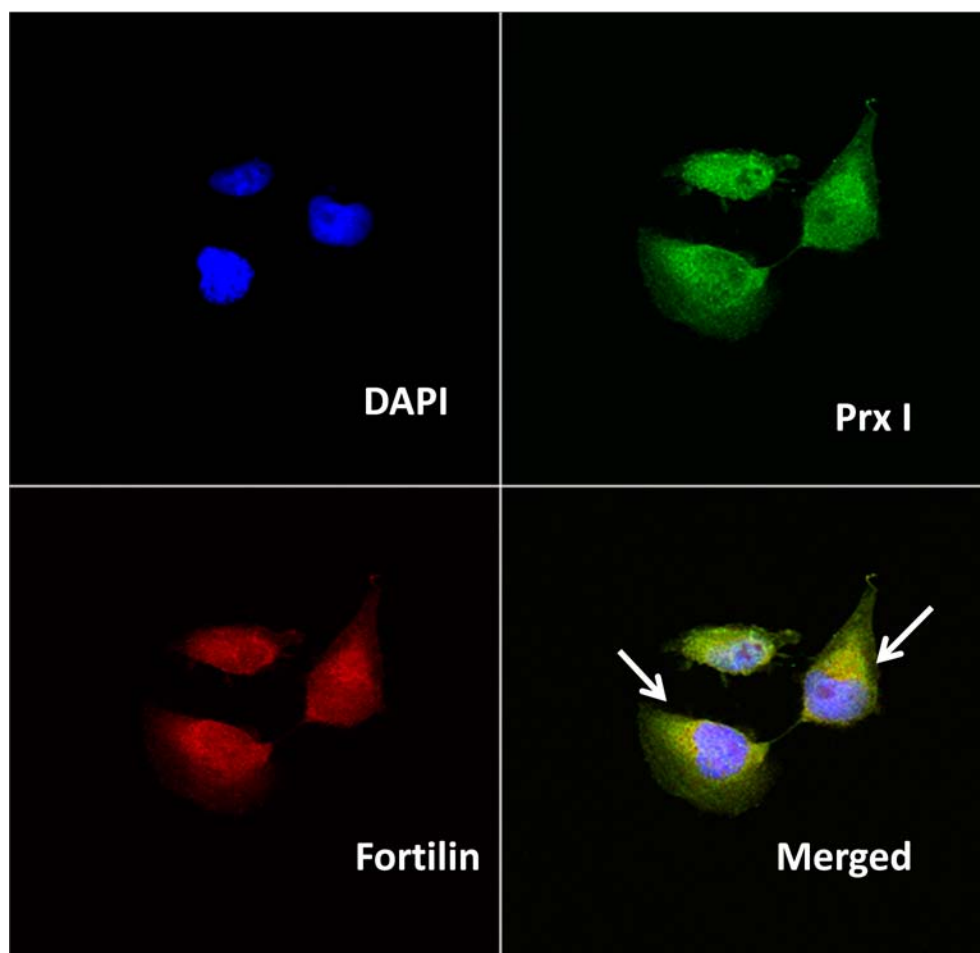
Figure 20: Demonstration of colocalization of Fortilin and Peroxiredoxin I using Immunofluorescence: U2OS cells were stained with antibodies against FT (red) and Prx I (green). White arrows indicate areas stained yellow, where FT and Prx I are seen to colocalize in the perinuclear region, possibly in the ER. Magnification – 60X.

cover slips and stained with primary antibodies against FT, Prx I and both and then visualized using a confocal microscope. The proteins were visualized using AlexaFluor 488 and AlexaFluor 568 tagged to secondary antibodies and the nuclei were stained with DAPI (blue). FT was stained in red while Prx I was stained in green and areas where FT and Prx I overlapped appeared yellow. As seen in Fig. 20, FT and Prx I appear to colocalize in the cytosolic and perinuclear region, possibly in the endoplasmic reticulum (ER), thereby providing a visual evidence of FT-Prx I interaction.

3.2.10. DEMONSTRATION OF FORTILIN-PRX I INTERACTION BY PROXIMITY LIGATION ASSAY:

In Fig. 20 I demonstrated that Prx I and FT colocalize in the perinuclear area inside the cell. To further verify that the two proteins are within close proximity to physically bind to each other, I performed a Proximity Ligation Assay. Briefly, U2OS cells were fixed and permeabilized on glass chamber slides, blocked, treated with primary antibodies against FT and Prx I or FT and Prx IV (negative control) and then treated with species-specific secondary antibodies or PLA probes each of which is conjugated to a unique short DNA sequence. If the FT and Prx I exist in close proximity inside the cells, the two DNA-tagged probes would consequently be in close proximity and the DNA strands can bind to each other when two other circle-forming DNA oligonucleotides are added to the cells and ligated using DNA ligase.
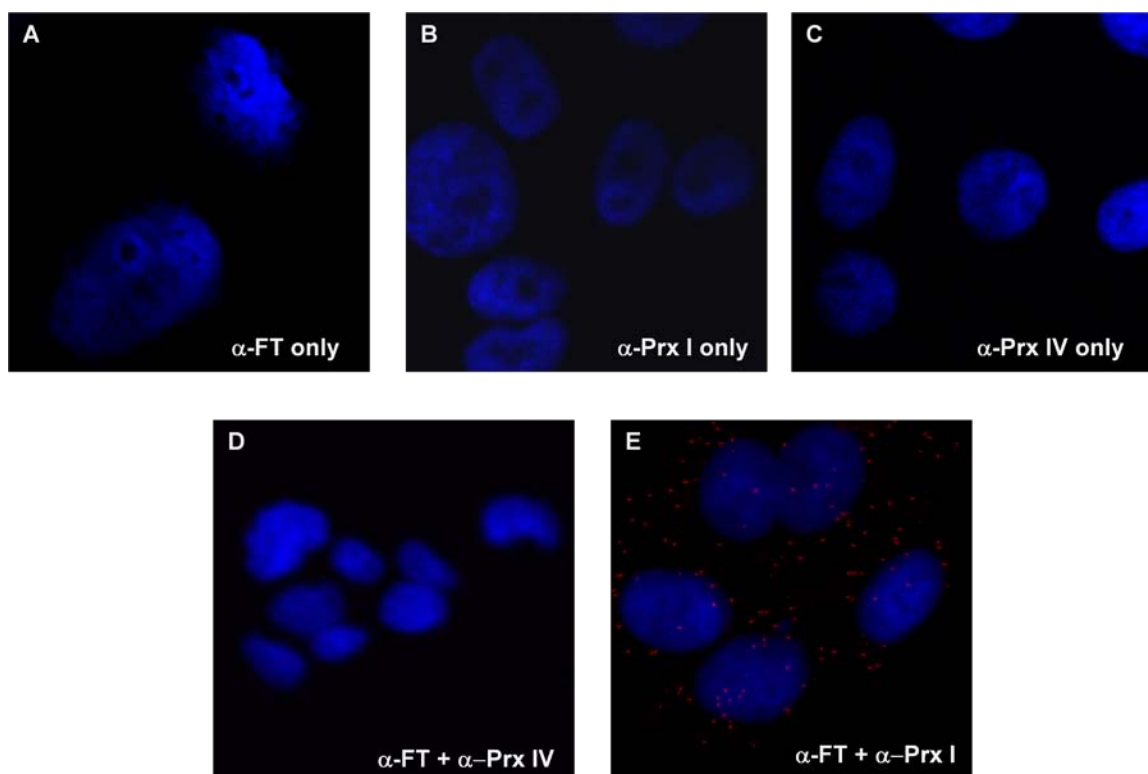
Figure 21: Demonstration of interaction between FT and Prx I by Proximity Ligation Assay (PLA): Proximity Ligation Assay (PLA) was performed on U2OS cells using primary antibodies against FT, Prx I and Prx IV. When the antibodies are used just by themselves **(A-C),** or when a combination of anti-FT and anti-Prx IV (negative control) antibodies is used **(D)** there are no red dots visible, indicating the lack of non-specific binding between FT and Prx IV. **E.** When a combination of anti-FT and anti-Prx I antibodies is used, red dots appear in the perinuclear area, indicating that FT and Prx I are in close physical proximity.

The circular DNA complex thus formed can be amplified several hundred folds through rolling circle amplification using a special DNA polymerase and the amplified product can be detected using fluorescently-labeled complementary oligonucleotide probes, as single discrete dots. As shown in Fig. 21A-C, when primary antibodies against FT, Prx I and Prx IV were used singly, there were no red dots, indicating that none of the antibodies on its own could produce a non-specific

signal. When a combination of FT and Prx IV was used, no positive signal was detected either (Fig. 21D), confirming our previous observation that Prx IV did not bind to FT (Fig. 17; Table 3). Using antibodies against FT and Prx I, I observed a large number of red dots in the perinuclear area (Fig. 21E), indicating that FT and Prx I are present in close physical proximity and are therefore highly likely to interact with one another. This data, therefore, represents a compelling visual evidence of the physical interaction between FT and Prx I.

3.2.11. DETERMINATION OF THE SUBCELLULAR SITE OF INTERACTION OF FT AND PRX I:

In Fig. 20 I demonstrated that FT and Prx I colocalized in the perinuclear region, indicating a possible ER and/or cytoplasmic site of interaction. To determine the subcellular site of interaction, I isolated nuclear, mitochondrial, ER and cytosolic protein fractions from U2OS cells using a combination of kits, as mentioned in section 2.3.9. The fractions were then resolved using SDS-PAGE and subjected to immunoblotting against marker proteins for each organelle to determine the purity of each fraction – topoisomerase IIβ (Topo IIβ) for nucleus, succinate dehydrogenase subunit A (SDHA) for the mitochondria, calnexin for the ER and GAPDH for the cytosol. As seen in Fig. 22, there is no cross contamination between the various organelles, as evident from the absence of a specific marker protein from all organelles except the one where it is known to be present. I further
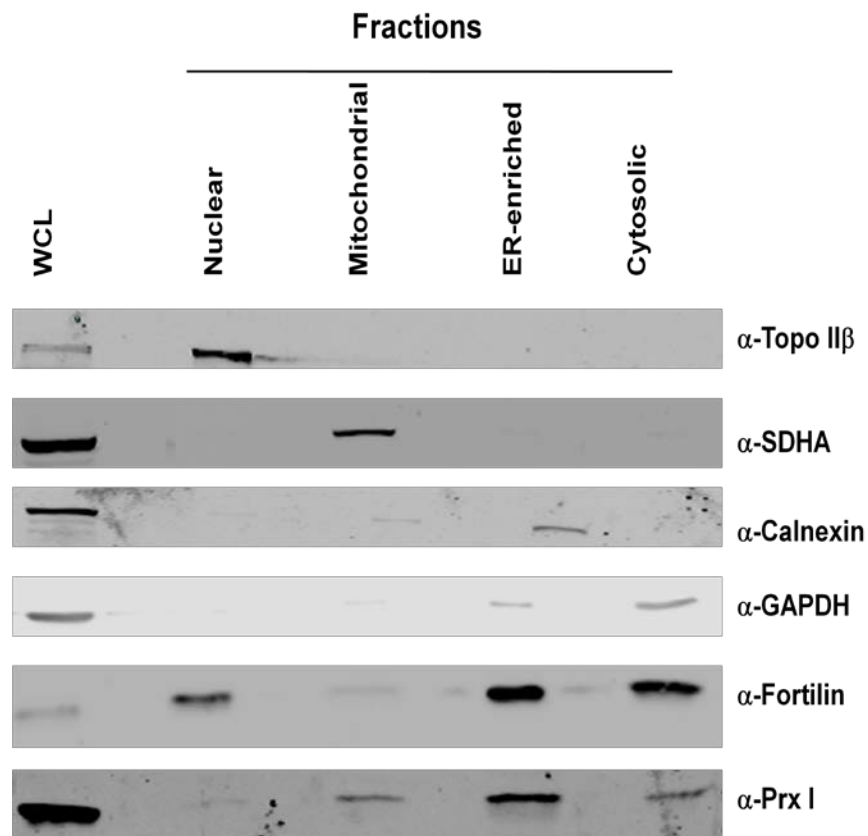
Figure 22: Colocalization of FT and Prx I in the cytosolic and ER-enriched fractions. Nuclear, mitochondrial, ER-enriched and cytosolic fractions were isolated from U2OS cells and immunoblotted for various organelle-specific markers to ascertain purity of the fractions. The fractions were also immunoblotted for FT and Prx I and the results indicated that the FT-Prx I interaction occurs in the cytosolic and ER compartments. WCL – whole cell lysate.

subjected them to immunoblotting against specific primary antibodies against FT and Prx I. Based on Fig. 22, FT is present in the nucleus, the ER-enriched fraction and the cytosol and also present at low concentration in the mitochondria. FT is primarily reported in literature to be a nucleus-cytoplasm shuttle protein and has never been detected in the mitochondria or the ER. Based on the distribution of the

two proteins in various organelles, I proposed that FT and Prx I interact in the cytoplasm and the ER – consistent with the staining pattern observed in the immunofluorescence experiment. Combining data from figures 20, 21 and 22 it can be reasonably argued that FT and Prx I interact specifically in the perinuclear region, predominantly in the cytosol and to some extent in the ER.

3.3. DISCUSSION:

Fortilin is a novel anti-apoptotic protein which has been shown previously to protect cells from etoposide [Li *et al.* 2001] and H_2O_2-induced cytotoxicity [Nagano-Ito *et al.* 2009; Lucibello *et al.* 2011]. However, the mechanism of this anti-apoptotic action is yet to be elucidated. The reported protein interactions of FT with anti-apoptotic molecules like MCL1 [Zhang *et al.* 2002] and Bcl-xL [Yang *et al.* 2005], and p53 [Rho *et al.* 2011; Chen *et al.* 2011; Amson *et a*, 2011] do not satisfactorily explain the anti-apoptotic action under oxidative stress. Combining a co-immunoprecipitation and Mass Spectrometry-based approach, I have identified a number of novel fortilin interacting proteins including the pro-survival anti-oxidant enzyme peroxiredoxin I (Prx I). The list of putative FIPs includes ribosomal proteins, histones, Prx I and the mitochondrial chaperone protein prohibitin. I also successfully detected interaction of FT with previously reported FIPs - Tubulin [Gachet *et al.* 1999; Bazile *et al.* 2009] actin [Tsarova *et al.* 2010] and γH2AX [Zhang *et al.* 2012].

I optimized salt and detergent conditions in the wash buffer to determine conditions at which non-specific binding would be minimized but FT and putative FIPs would remain bound to the beads. 150mM NaCl and 0.01% NP-40 were determined to be the optimal condition where FT and Prx I remain bound to the beads while non-specific binding with GAPDH was abolished (data not shown). The fact that Prx I remained bound to the beads after washing with 150mM salt and 0.01% detergent suggested that the FT-Prx I interaction was not electrostatic, an observation that was further confirmed by direct binding studies between the two purified proteins.

Peroxiredoxins (I-VI) are a class of six thioredoxin-dependent pro-survival anti-oxidant enzymes responsible for the catalytic degradation of hydrogen peroxide and other ROS. Overexpression of Prx I and II has been seen to have a protective role against oxidative stress-induced apoptosis. Interestingly, Prx expression levels are seen to increase in FT-overexpressing transgenic mice hearts [Cheon *et al.* 2008] and of both Prx I and FT levels change in neonatal rat cardiomyocytes exposed to H_2O_2 [Cullingford *et al.* 2006], which point to a possible interaction between Prx I and FT, as also indicated by the data presented in this chapter. I have detected a novel protein-protein interaction which would successfully explain the cytoprotective action of FT under conditions of oxidative stress. This is of immense clinical significance since resistance to oxidative stress has been identified as one of the ways cancer cells evade apoptosis [Lucibello *et al.* 2011]. The clinical significance is further underscored by the fact that exposure to

oxidative stress may be detrimental to cells, giving rise to disease phenotypes like heart failure and aging [Byrne *et al.* 2003; Ferrari *et al.* 2004]. For example, at the cellular level, heart failure is brought about by the death of cardiomyocytes, the likely primary cause of which is oxidative stress, produced by endogenous generation of ROS inside the cell especially in arterial diseases, atherosclerosis, myocardial infarction, ischemia-reperfusion injury and under elevated cytokine and chemokine levels. The FT-Prx I interaction, therefore, has potential application in research concerning these diseases.

Reciprocal co-immunoprecipitation studies identified Prx I-III and V as positive interacting partners of FT while Prx IV and VI showed no interaction with FT under the experimental conditions. Sequence alignment studies were performed using the MotifMaker motif generation program developed at UTMB (http://landau.utmb.edu:8080/pcpmer//Tools/SubmitFormMotifMaker.jsp) and they suggest that Prx I-V contain a conserved motif **FKGKKXVXFXVPXXFTXXCSXXH**. Based on sequence alignment of Prx I-III and V, the FIPs emerging from this project, the underlined X residue in the above residue is lysine, which is absent in Prx IV. It is therefore likely that Prx I-III and V bind to FT using this lysine residue. Similarly, Prx VI lacks the first eight residues (**--------FXXPXXFTXXC-----**) of the consensus sequence, which would explain its lack of binding to FT.

When I undertook the current study to characterize the interaction between FT and Prx I, our working hypothesis was that the anti-apoptotic action of FT is dependent on its interaction with Prx I. Therefore, a definitive test of that hypothesis would be achieved if I could identify a point mutant of FT which fails to bind to Prx I and determine whether it had a different effect on the enzyme activity of Prx I as compared to wild type FT. To this end, I generated point mutants of FT by site-directed mutagenesis and cloned the mutants into the HA-vector. Anti-HA IP demonstrated that the FT mutant L7R was unable to co-immunoprecipitate Prx I, indicating that the Leu^7 residue is crucial for the interaction between FT and Prx I. The fact that mutating a hydrophobic residue (Leucine) to a charged residue (Arginine) abrogates the binding suggests that the two proteins may bind each other via hydrophobic interaction, an observation which is supported by previous reports and suggestions that FT may act as a chaperone.

Direct binding between pure, recombinant FT and Prx I was confirmed by SPR experiments. A nanomolar K_D indicated strong binding between the two proteins and this was also the most definitive proof so far of the binding between FT and Prx I. A comparison with published data on FT-p53 binding [Amson *et al.* 2011] indicates that FT has nearly identical K_D of interaction with both proteins and that the FT-Prx I interaction is as strong as, if not stronger, than the FT-p53 interaction.

Immunofluorescence imaging in U2OS cells by confocal microscopy and subcellular fractionation by differential centrifugation point to perinuclear i.e.

cytosolic and/or ER localization for both proteins. FT has so far been reported to localize predominantly in the cytosol and the nucleus [Li *et al.* 2001]. I have, however, detected FT in the mitochondrial and ER-enriched fractions. Further studies, including electron microscopy, are needed to confirm this result. Prx I on the other hand has so far been detected in the nucleus, mitochondria, peroxisomes and the cytosol [Immenschuh *et al.* 2003]. Combining the results from Figs. 20-22, I have enough evidence to propose that the FT-Prx I interaction occurs in the perinuclear region, predominantly in the cytosol.

In summary, using a combination of co-immunoprecipitation and Mass Spectrometry, I identified a list of novel FIPs, including the pro-survival anti-oxidant enzyme peroxiredoxin I. By performing reverse co-immunoprecipitation studies, I conclusively demonstrated that FT interacts specifically with Prx I-III and V –an observation which has not been reported in FT or Prx literature. Additionally, I demonstrated through direct binding studies, immunofluorescence and proximity ligation assay that FT and Prx I bind to each other with a strong K_D of interaction and that they colocalize in the perinuclear area, predominantly in the cytosolic compartment and this observation was further corroborated by our subcellular fractionation studies. The data presented in this chapter, therefore, demonstrates a novel interaction between FT and Prx I and provides a solid foundation for testing the functional significance of this novel interaction, as described in the subsequent chapters.

CHAPTER IV: EFFECT OF FORTILIN ON THE STABILITY AND ENZYMATIC FUNCTION OF PEROXIREDOXIN I AND THE EFFECT OF PEROXIREDOXIN I ON THE ANTI-APOPTOTIC ACTIVITY OF FORTILIN

4.1. INTRODUCTION:

FT is a small anti-apoptotic protein which protects cells from oxidative stress-induced cell death and has been shown in Chapter III to interact with the anti-oxidant enzyme Prx I. FT has previously been shown also act like a molecular chaperone similar to a heat shock protein. In fact, Gnanasekar *et al* in 2009 have demonstrated that FT indeed acts as a heat shock protein by preventing thermal denaturation of proteins in *E. coli*. Furthermore, overexpression of FT protects bacterial cells from heat-induced cell death. Based on this evidence I hypothesized that FT may bind to and stabilize Prx I. Our initial goal was to test whether FT acts as a chaperone for Prx I.

Prx I is a dimeric anti-oxidant enzyme, the primary function of which is the catalytic degradation of H_2O_2, organic hydroperoxides and peroxynitrites - sources of reactive oxygen species (ROS) that cause oxidative damage to proteins and DNA [Chae *et al.* 1993; Chae *et al.* 1994; Chae *et al.* 1994]. The ability of Prx I to reduce ROS depends on the thioredoxin-thioredoxin reductase (Trx-TrxR) system which

supplies NADPH as reducing equivalents and allows the oxidized enzyme to be reduced back to its native state, as shown in Fig. 23. In a 2-cysteine peroxidase like Prx I, there are two conserved Cys residues in the active site of the enzyme – the so-called "resolving" cysteine (S_R) and the so-called "peroxidative" cysteine (S_R). In the first step of the reaction, the S_R of one subunit of the enzyme (Cys–S_PH) reduces the peroxide moiety (R-O-O-H) to produce the oxidized sulphenic acid derivative of the enzyme (Cys–S_POH). In the second step of the reaction, the Cys–S_POH form of one subunit of the dimer condenses with the redox cysteine-containing subunit of the dimer (Cys–S_RH) to produce an intermediate - Cys–S_P--S_R-Cys. The system utilizes NADPH as reducing equivalents and the oxidized cysteine in the enzyme is reduced back to its active thiol state via the Trx-TrxR (RSH) system, thereby completing the enzymatic cycle [Kim *et al.* 2005; Woo *et al.* 2006]. This reaction can be utilized in a very elegant *in vitro* assay [Kim *et al.* 2005] using pure recombinant Prx I, Trx, TrxR and NADPH to determine the enzymatic activity of Prx I, by following the oxidation of NADPH spectrophotometrically upon initiation of the reaction by the addition of H_2O_2. Since FT has been shown to enhance the anti-apoptotic activity of Mcl-1 upon binding to it, I wanted to investigate whether the addition of pure recombinant FT had any amplifying effect on the anti-oxidant ability of Prx I. The second part of this chapter is therefore dedicated to studying the effects of addition of exogenous FT on the enzymatic ability of Prx I. Taken together, the results from these studies will provide crucial information regarding the functional consequence of the FT-Prx I interaction and may provide valuable clues towards the model of apoptosis prevention by FT.

1. $Cys\text{–}S_PH + R\text{-}O\text{-}O\text{-}H \xrightarrow{[O]} Cys\text{–}S_POH + R\text{-}O\text{-}H$

2. $Cys\text{–}S_POH + Cys\text{–}S_RH$ — One subunit of dimer — Other subunit of dimer — Condensation → $Cys\text{-}S_P\text{-}\text{-}S_R\text{-}Cys$ (H_2O, $[H]$, NADPH, Reactivated Prx enzyme, Thioredoxin (2RSH), Thioredoxin reductase, R-S-S-R)
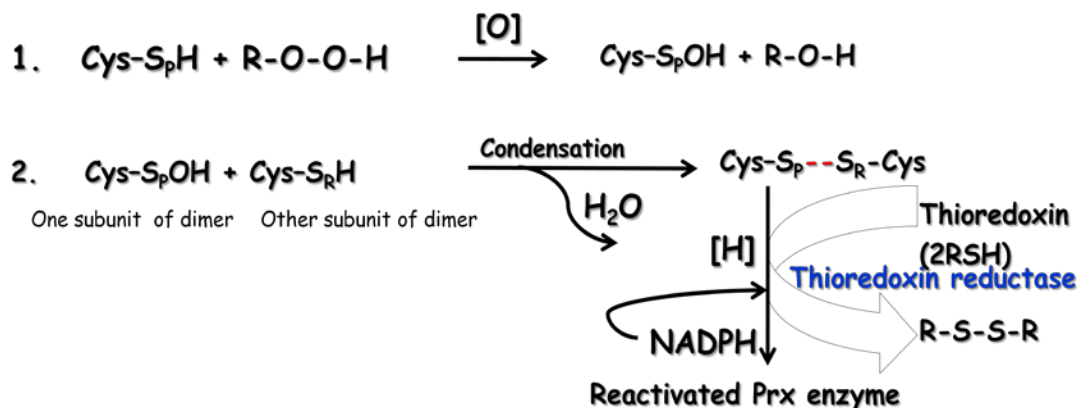
Figure 23: Schematic representation of the Prx I enzymatic cycle. In the first step of the reaction, the S_R of one subunit of the enzyme ($Cys\text{–}S_PH$) reduces the peroxide moiety ($R\text{-}O\text{-}O\text{-}H$) to produce the oxidized sulphinic acid derivative of the enzyme ($Cys\text{–}S_POH$). In the second step of the reaction, the $Cys\text{–}S_POH$ form of one subunit of the dimer condenses with the redox cysteine-containing subunit of the dimer ($Cys\text{–}S_RH$) to produce an intermediate - $Cys\text{–}S_P\text{-}\text{-}S_R\text{-}Cys$. The system utilizes NADPH as reducing equivalents and the oxidized cysteine in the enzyme is reduced back to its active thiol state via the Trx-TrxR (RSH) system, thereby completing the enzymatic cycle.

4.2. RESULTS

4.2.1. FORTILIN PREVENTS PROTEOSOMAL DEGRADATION OF PRX I:

After constructing a stable cells line with downregulated FT, our first step was to ensure via western blot that FT was indeed downregulated in the U2OS-sh-FT cells. As shown in Fig. 24A, there was a clear downregulation of FT in the U2OS-sh-FT cells. After ensuring that FT was indeed knocked down, U2OS-sh-Control and U2OS-

sh-FT cells were plated on 6-well plates and allowed to grow overnight at 37⁰C. The cells were then washed with PBS and incubated with culture medium containing 100μg/mL CHX to stop cellular protein synthesis and harvested at different time points – 0, 2, 4, 8, 12 and 24 hours post-CHX treatment. Harvested cells were lyzed and immunoblotted with primary antibodies against FT, Prx I and GAPDH as loading control. Protein band densities were determined using the LI-COR imaging system software. Prx I expression index was determined as the ratio of band intensities of Prx I and GAPDH at each time point. As shown in Fig. 24B (upper panels), Prx I protein levels decreased faster in FT-deficient cells as compared to control cells. In U2OS-sh-Control cells, the Prx I band intensity remained virtually constant for 24 hours; in stark contrast, the Prx I band intensity started decreasing in U2OS-sh-FT cells from 4 hours post-CHX treatment and was virtually undetectable beyond 12 hours, indicating that the absence of FT enhances the degradation of the protein. In other words, the presence of FT is essential to maintain Prx I homeostasis, thus pointing to a clear role of FT in stabilizing Prx I. I calculated the expression index of Prx I relative to loading control GAPDH and fitted the data using linear regression method. When the relative Prx I expression indices were plotted at various time points, as shown in Fig, 24C, I observed a dramatic decrease in the extrapolated half life of Prx I from **9.35 ± 0.25 hours** in U2OS-sh-Control cells to **5.52 ± 0.89 hours** in U2OS-sh-FT cells. The nearly 40% decrease in Prx I half life gives a semi-quantitative measure of the striking decrease in stability of Prx I upon downregulation of FT.
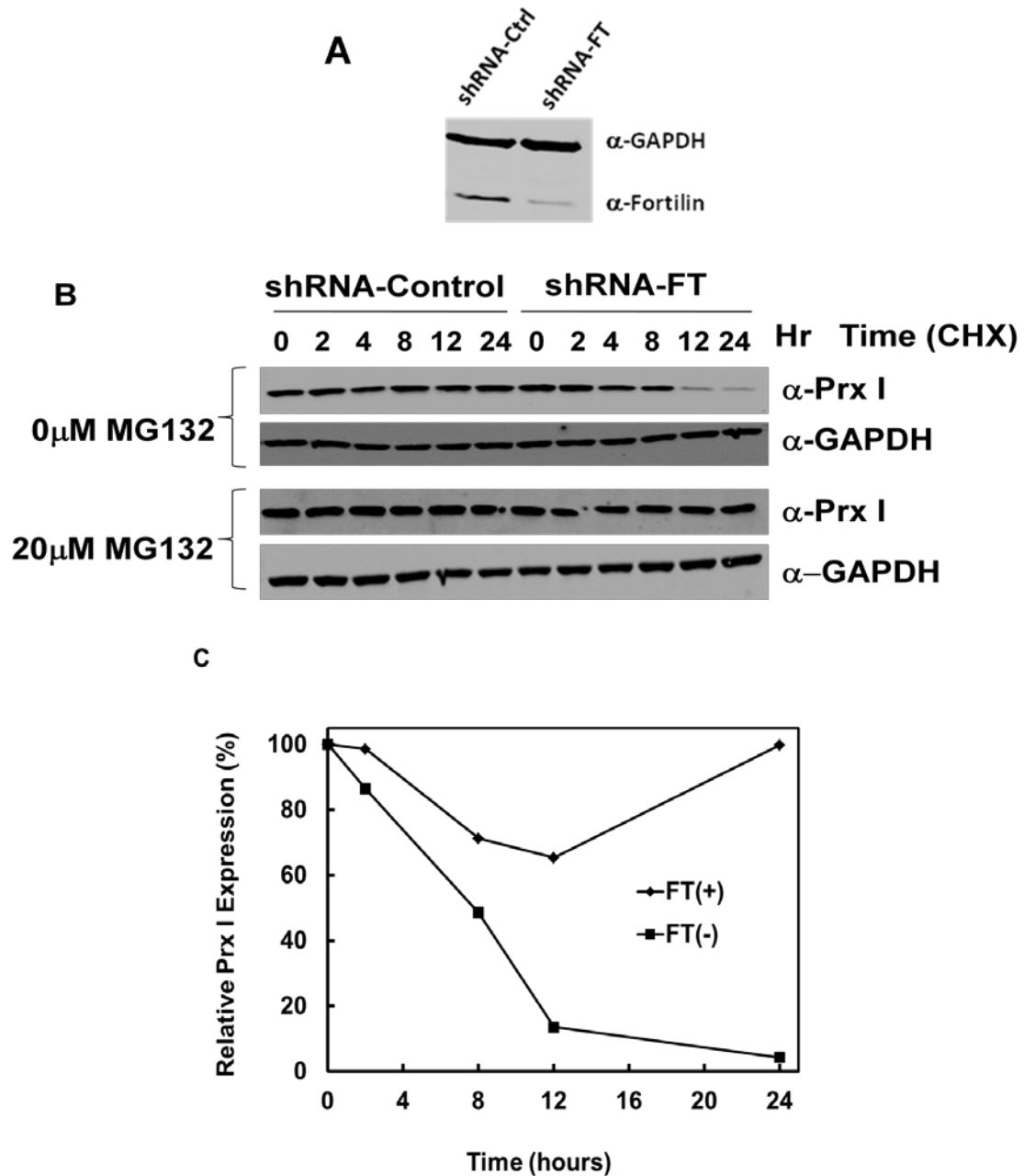
Figure 24: Fortilin prevents the proteosomal degradation of Prx I. **A**. FT downregulation in U2OS-sh-FT cells was confirmed by blotting against FT antibody, GAPDH was used as loading control. **B**. **Upper panel-** Prx I and GAPDH bands at various time points indicate that Prx I levels decrease faster in FT-deficient cells as compared to the control. **Lower panels-** Proteasome inhibitor MG132 abolishes the decrease in Prx I levels in FT-deficient cells, indicating that FT prevents the proteosomal degradation of Prx I. **C.** Graphical representation of Prx I expression index at various time points. Half life of Prx I was calculated by linear regression method in control and sh-FT cells and there was ~40% reduction in Prx I half life in FT-deficient cells.

Having observed a decrease in Prx I protein levels in FT-deficient cells, I hypothesized that in the absence of FT, Prx I protein underwent rapid proteasomal degradation. To test this hypothesis, I first pre-treated U2OS-sh-control and U2OS-sh-FT cells with 20μM MG132, a proteasome inhibitor, followed by treatment with 100μg/mL CHX. Cells were harvested at regular intervals and the cell lysates were immunoblotted against anti-Prx I and anti-GAPDH antibodies. In contrast to our previous observation, pre-treatment with the proteasome inhibitor MG132 completely prevented the decrease in Prx I levels in FT-deficient cells (Fig. 24B, lower panels), indicating that FT stabilized Prx I by preventing its proteosomal degradation.

4.2.2. THE EFFECT OF ADDITION OF EXOGENOUS FORTILIN ON THE ENZYMATIC ACTIVITY OF PRXI:

I performed an *in vitro* peroxidase assay using pure recombinant Prx I, Trx and TrxR with NAPDH and H_2O_2, in presence or absence of pure recombinant FT. The decrease in NAPDH absorbance was monitored at 340nm for 30 minutes at 30^0C. As shown in Fig. 25, in the absence of both FT and Prx I, there was a very slight decrease in NADPH absorbance, since NAPDH undergoes slow spontaneous degradation. Almost a similar trend was noticed when the assay was performed in presence of only FT, with Prx I being absent from the system, indicating that FT itself did not have any peroxidase activity. In presence of Prx I but not FT, there is a
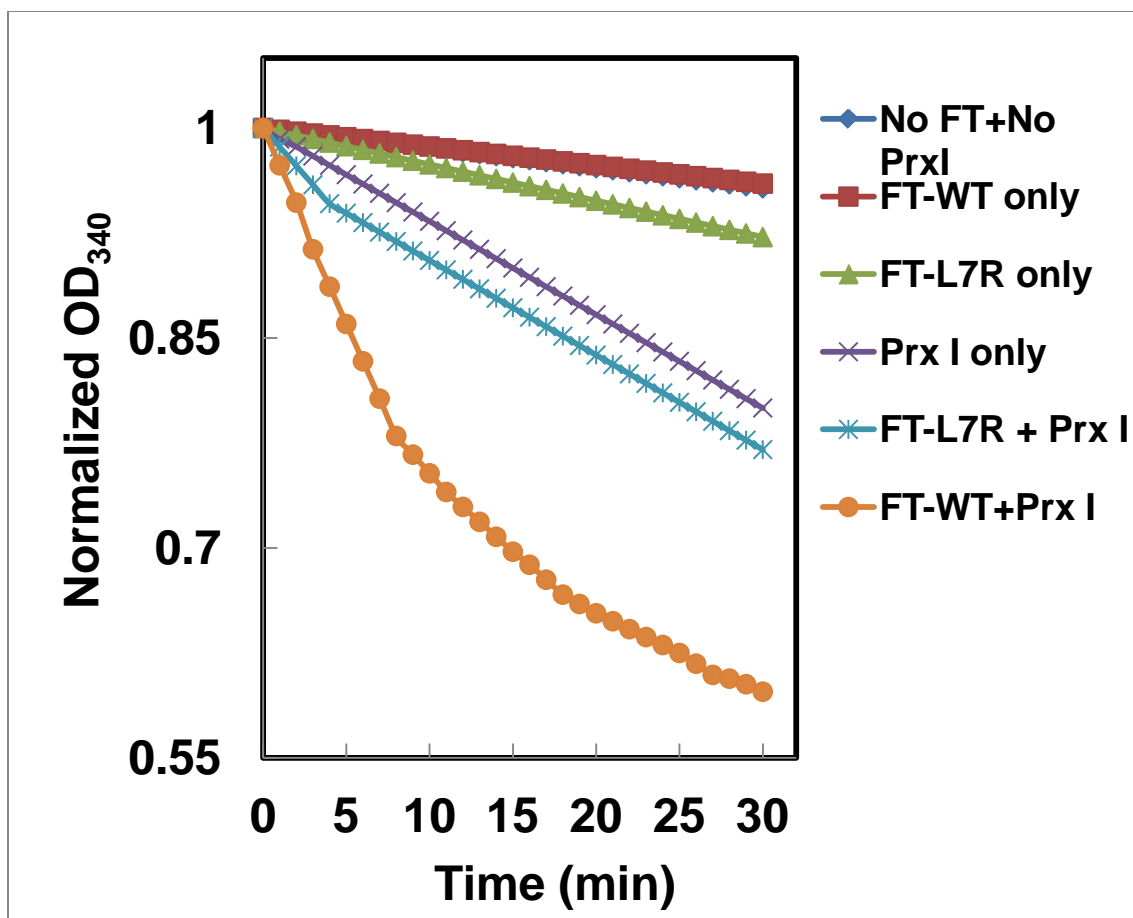
Figure 25: Wild type Fortilin increases the enzyme activity of Prx I. Peroxidase assay was performed using pure recombinant Prx I, Trx and TrxR with NAPDH and H_2O_2, in presence or absence of pure recombinant wild type and mutant FT and the decrease in NAPDH absorbance was monitored at 340nm for 30 minutes at 30^0C. Using none of the proteins or using FT-WT or FT-L7R mutant, there was very slight decrease in the absorbance over 30 minutes. In presence of only Prx I, NADPH was oxidized and the same effect was observed using the buffer used to purify FT. When pure FT was added exogenously in presence of Prx I, there was a dramatic increase in the reaction rate but not in presence of mutant FT, indicating that addition of FT enhanced the peroxidase activity of Prx I.

steady decrease in NAPDH absorbance confirming that the recombinant Prx I was able to reduce hydrogen peroxide. When the same assay was performed using equimolar amounts of Prx I and FT, there was a dramatic increase in the oxidation of NADPH, indicating that the addition of exogenous FT enhances the peroxidase

activity of Prx I. When the same assay was performed using Prx I and pure recombinant FT-L7R mutant, which does not bind to Prx I, there was no change in the peroxidase activity of Prx I, confirming that the striking increase in peroxidase activity upon addition of FT was due to the binding of FT to Prx I and not a non-specific effect. The initial rates of the reaction under different conditions were calculated using the first 10 time points up to which point the curve is mostly linear, using Michaelis-Menten kinetics. Prx I activity was increased about 2.3-2.5 folds in presence of wild type FT but remained virtually unchanged in presence of FT-L7R mutant.

4.2.3. FORTILIN INHIBITS THE MST1-INDUCED PHOSPHORYLATION OF PRX I:

Following the demonstration in Fig. 25 that fortilin increases the enzymatic activity of Prx I, I proceeded to investigate the mechanism by which FT increases the activity of Prx I. In 2013, Rawat, reported that Prx I is deactivated by phosphorylation of its Thr^{90} and Thr^{183} residues by the serine/threonine kinase Mst1 [Rawat *et al.* 2013]. I hypothesized that FT may increase the activity of Prx I by inhibiting its phosphorylation-induced inactivation. I incubated Prx I and Mst1 in kinase buffer in presence of increasing quantities of pure recombinant wild type and

Prx I	+	+	+	+	+	+	+	+	+	+	+
Mst1	-	-	+	+	+	+	-	+	+	+	+
FT-WT (µg)	0	2	0	1	2	4	-	-	-	-	-
FT-L7R (µg)	0	0	-	-	-	-	2	0	1	2	4

α-Prx I

α-p-Thr
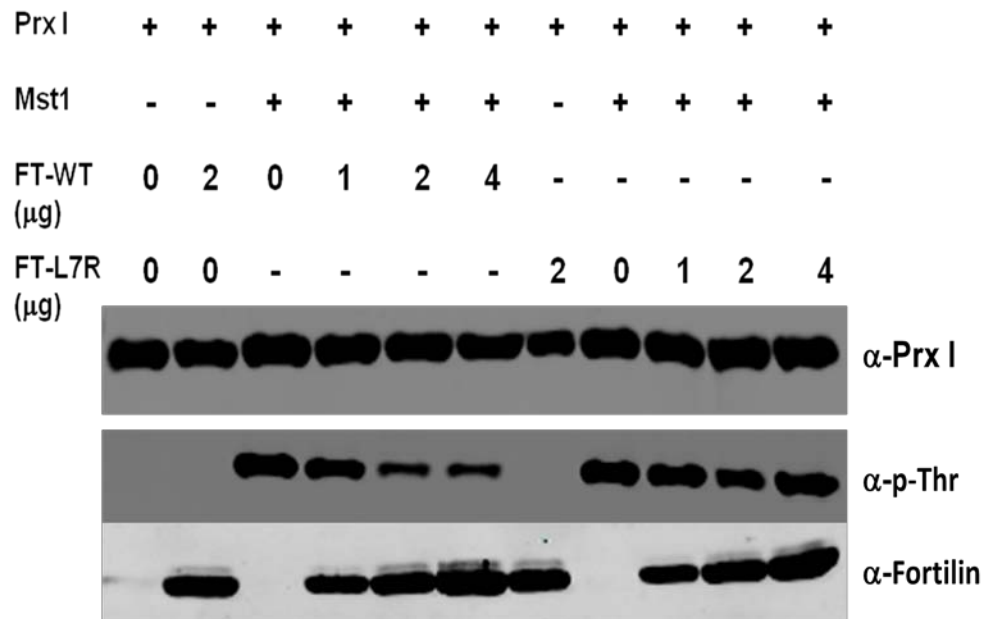
α-Fortilin

Figure 26: Fortilin prevents the Mst1-induced phosphorylation of Prx I. Prx I was incubated with Mst1 kinase in presence of increasing amounts of wild type FT, which caused a dose-dependent decrease of threonine phosphorylation. But the inhibitory effect on phosphorylation was not observed with mutant FT, indicating that FT specifically inhibits the phosphorylation of Prx I.

mutant FT (L7R) at 30^0C for 30 minutes and then detected the level of Prx I phosphorylation by performing western blot against phosphothreonine antibody. As shown in Fig. 26, in presence of increasing amounts of wild type FT, there was a dose-dependent decrease in Prx I phosphorylation which was completely abrogated in presence of mutant FT, indicating that wild type FT specifically binds to Prx I and prevents its deactivating phosphorylation. However, in the presence of pure recombinant FT-L7R mutant, the phosphorylation status of Prx I remained virtually constant, thus indicating that FT specifically binds to Prx I and prevents its Mst1-

induced phosphorylation. This observation is the first of its kind and may explain the effect of FT on the enzyme activity of Prx I. The band intensities of the phosphothreonine and Prx I bands were measured and the ratio of phosphothreonine to Prx I was calculated for the different concentrations of FT – wild type and mutant - and normalized that for the ratio with no FT and represented graphically (Fig. 27).
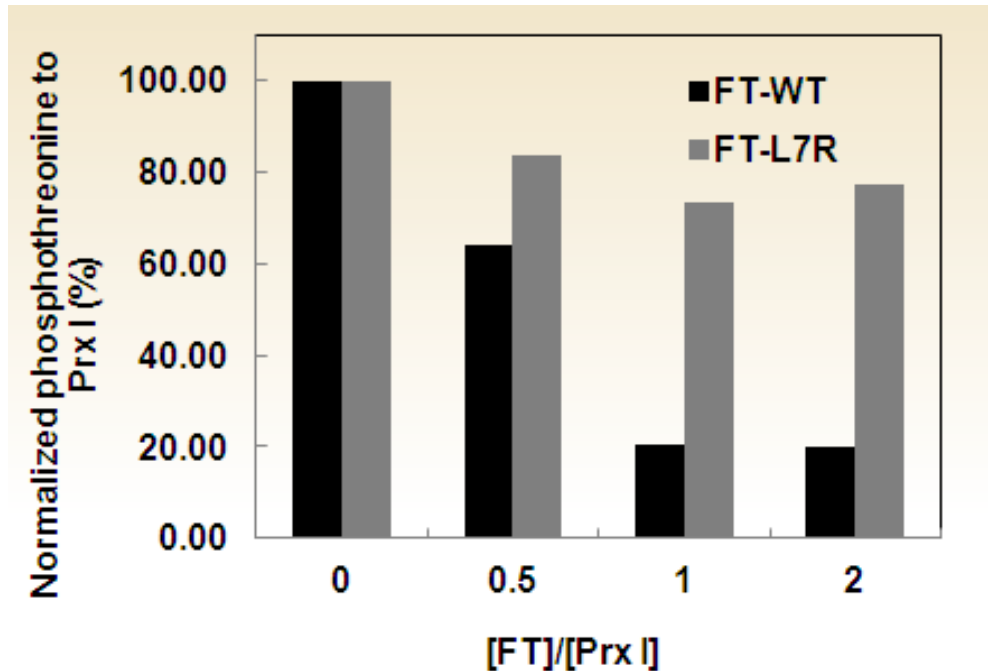
Figure 27: Graphical representation of the effect of wild type and mutant fortilin on the Mst1-induced phosphorylation of Prx I. Ratios of Phosphothreonine and Prx I band intensities at different [FT]: [Prx I] ratios were normalized to that at zero [FT]: [Prx I]. In presence of wild type FT there is a dose dependent decrease in phosphorylation while in presence of mutant FT, the phosphorylation status remains virtually constant.

4.2.4. FORTILIN CAN PROTECT U2OS CELLS FROM HYDROGEN PEROXIDE-INDUCED CELL DEATH

Researchers have previously demonstrated that FT overexpression is protective against H_2O_2-induced apoptosis in CHO-K1 cells [Nagano-Ito *et al.* 2009]. Since I have performed all our previous studies in U2OS cells, I decided to first ensure that FT was indeed able to protect U2OS cells from ROS-induced cell death. I exposed U2OS-HA-Empty and U2OS-HA-FT cells to increasing concentrations of H_2O_2 for 4 hours at 37^0C, harvested the cells performed and DNA fragmentation ELISA on the cells. FT appeared to protect U2OS cells in a dose-dependent manner and I confirmed that FT can protect U2OS cells against H_2O_2-induced cell death (Fig. 28). I chose the 150μM concentration of H_2O_2 for further studies.

4.2.5. ANTI-APOPTOTIC ABILITY OF FORTILIN IS DEPENDENT ON ITS INTERACTION WITH Prx I

To further test our hypothesis that the anti-apoptotic ability of FT is dependent on its interaction with Prx I, I stably overexpressed HA-Empty, HA-FT (WT) and HA-FT-L7R mutant, which was shown in chapter III to be unable to interact with Prx I, in U2OS cells. The cells were then exposed to 150μM H_2O_2 for 4 hours at 37^0C, harvested and subjected to DNA fragmentation ELISA. As shown in
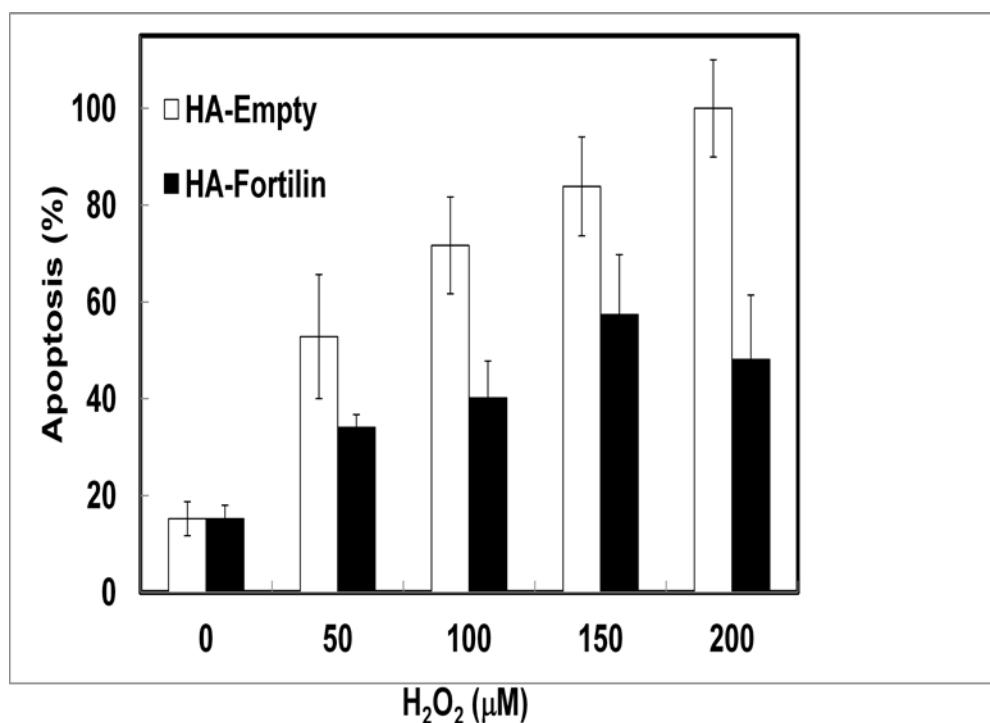
Figure 28: Fortilin protects U2OS cells against H₂O₂-induced cell death. DNA fragmentation ELISA confirms that FT protects U2OS cells against H_2O_2 in a dose-dependent manner; with increasing concentrations of H_2O_2, the protective ability decreases.

Fig. 29, the ability of HA-FT-L7R to protect U2OS cells from oxidative stress-induced cell death was significantly lower than that of HA-FT (WT). In fact there was ~50% more cell death in HA-FT-L7R than HA-FT (WT), which indicates that interaction with Prx I is extremely important for the anti-apoptotic ability of FT under oxidative stress.
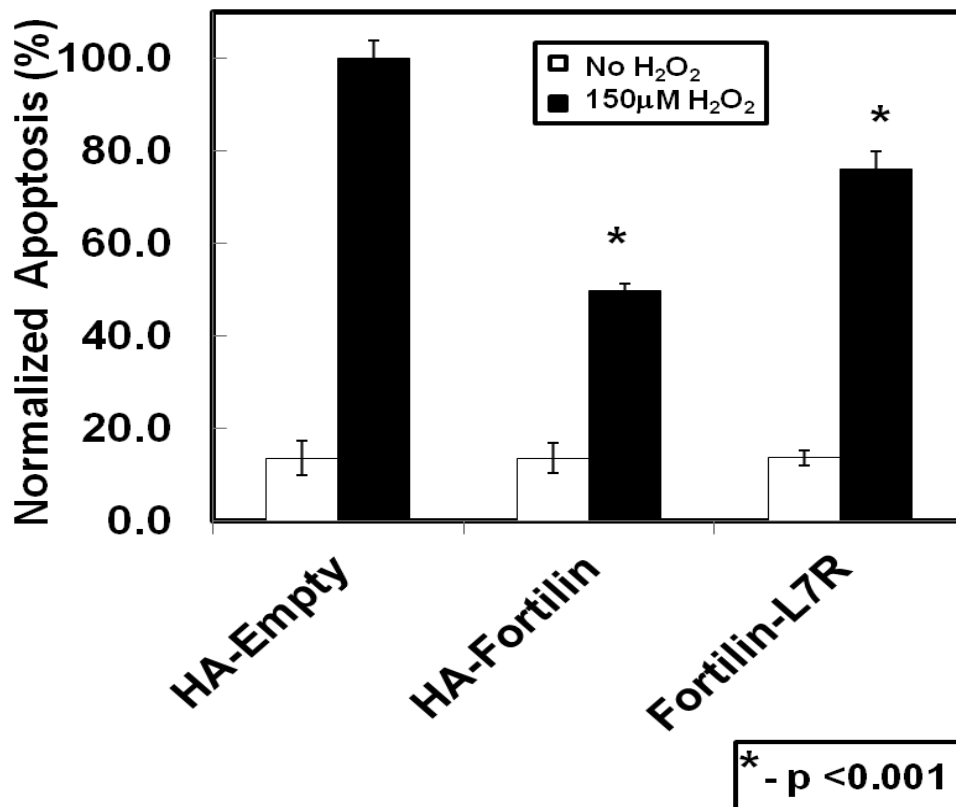
Figure 29: Anti-apoptotic ability of FT-L7R mutant is lower than that of WT FT. FT-L7R mutant that fails to interact with Prx I has lower anti-apoptotic ability against oxidative stress as compared to wild type FT.

4.3. DISCUSSION:

Fortilin is a 23kDa polypeptide which acts as an inhibitor of apoptosis by binding to and inhibiting the function of the tumor suppressor protein p53. One of the other functions of FT, as reported by Gnanasekar *et al.* is its ability to act as a

heat shock protein with chaperone-like activity. Heat shock proteins (HSPs) are proteins which are involved in stabilizing other proteins when the cell encounters different kinds of stress – thermal, chemical, toxic, hypoxia etc. Chaperones are proteins that are involved in non-covalent folding or unfolding of other proteins and macromolecular structures, by preventing the aggregation of newly-synthesized polypeptides and assembled subunits of a macromolecular assembly into non-functional aggregates. Gnanasekar and colleagues identified FT as a novel heat shock protein that can bind to a variety of client proteins even under steady state and protect them from elevated temperature-induced damage. Based on this observation, I explored the possibility that FT may have a chaperone-like protective function on Prx I. I examined the effect of FT knockdown on the expression of Prx I over a period of 24 hours and observed that in the absence of FT, Prx I protein levels decreased steadily from about 4 hours post-cycloheximide treatment and were barely detectable beyond 12 hours, in stark contrast to normal cells with steady-state levels of FT. In-depth investigation into the molecular mechanism of the stabilization of Prx I by FT, I demonstrated that when the cells are pre-treated with the 26S proteasome inhibitor MG132, Prx I protein levels in FT-deficient cells remain virtually constant. This indicated that FT was preventing the proteosomal degradation of Prx I, possibly by binding to Prx I and sequestering it from the protein degradation machinery of the cell. The prevention of Prx I degradation by FT thus represents a novel mechanism of regulation of Prx I. As touched upon in the introduction section, FT is seen to be upregulated in tumors of epithelial origin [Li *et al.* 2001] and Prx I gene expression is upregulated in Ras-transformed epithelial

cells [Prosperi *et al.* 1993]; our observation that FT is essential to maintain steady state Prx I levels in a cell may be able to explain this possible correlation between elevated FT and Prx I levels in epithelial cancers.

Prx I enzymatic activity is reported to be regulated by its phosphorylation, the redox environment and the protein sulfiredoxin (Srx) which is able to reverse the hyperoxidation of the protein. Prx I is phosphorylated by the cyclin-dependent kinase (CDK) Cdc2 at its Thr^{90} residue and this leads to around 80% decrease in its enzymatic activity [Chang *et al.* 2002]. An identical effect is brought about by the phosphorylation of Prx I at Thr^{90} and Thr^{183} by the serine/threonine kinase Mst1 [Rawat *et al.* 2013]. The conserved Cys^{52} residue at the active site of Prx I is stabilized by the positively charged environment around it. The Thr^{90} residue is close to the active site Cys^{52} and its phosphorylation possibly introduces a negative charge in the environment, thereby destabilizing it and leading to inactivation of the enzyme [Immenschuh and Baumgart-Vogt, 2005]. Srx can reduce hyperoxidized Prx I back to the active state and thus regulate its activity. However, it was recently demonstrated by Bae, [Bae *et al.* 2011] that Srx is not sufficient to revert hyperoxidized Prx I to its active state. Here I have demonstrated that exogenous addition of pure, recombinant FT increases the enzymatic activity of Prx I in an *in vitro* peroxidase assay. I conclusively showed that FT itself has no peroxidase activity since it is unable to cause degradation of NADPH in the assay. Our finding was further strengthened by the observation that FT-L7R mutant, which fails to bind to Prx I, was unable to increase the enzymatic activity of Prx I. I, therefore,

demonstrated unambiguously that binding to FT increases the anti-oxidant activity of Prx I by greater than 2 fold. This observation represents a novel mechanism of regulation of Prx I at the functional level.

When I performed an *in vitro* peroxidase assay with the FT-L7R mutant, I observed that exogenous addition of the mutant to Prx I does not cause an enhancement in the enzymatic activity of Prx I as in case of the wild type. The initial velocity of the reaction was almost identical to that when Prx I alone was used. I have therefore conclusively demonstrated that it is only the direct interaction between Prx I and FT that brings about the observed increase in peroxidase activity of Prx I. This data thus establishes FT as a novel and specific regulator of Prx I activity and that the activity of Prx I is dependent on its direct interaction with FT. The current observation is another crucial piece of evidence in support of our hypothesis that FT exerts its anti-apoptotic influence in a Prx I-mediated manner.

I next chose to investigate the possible mechanism by which FT may regulate the activity of Prx I. As mentioned above, Prx I is regulated by phosphorylation of its Thr^{90} and Thr^{183} residues. This deactivating phosphorylation is mediated by the cyclin-dependent kinase Cdc2 and also by the tumor suppressor kinase Mst1. I hypothesized that FT would regulate the activity of Prx I by preventing its phosphorylation-induced inactivation. When an *in vitro* phosphorylation assay was performed using pure recombinant Prx I, Mst1 and increasing amounts of wild type FT, there was a clear, dose-dependent decrease in Prx I phosphorylation. This effect

was, however, completely abrogated when the same assay was performed using increasing amounts of pure mutant FT-L7R which showed a virtually constant level of Prx I phosphorylation. FT, therefore, binds to Prx I to prevent its phosphorylation and this observation can explain how FT increases the enzymatic activity of Prx I. I have thus demonstrated a novel pathway of positive regulation of Prx I activity by FT, which may offer mechanistic insight into the phenomenon of cellular protection under oxidative stress by both FT and Prx I.

At the outset of the current dissertation project, our working hypothesis was that the anti-apoptotic activity of FT is dependent on its interaction with Prx I. To test this hypothesis definitively, I compared the anti-apoptotic actions of wild type FT and FT-L7R mutant under oxidative stress induced by H_2O_2 in U2OS cells. Our results indicated a ~50% decrease in the protective action of the FT mutant that fails to bind to Prx I. This indicates that the anti-apoptotic action of Prx I is dependent on its interaction with Prx I, at least partially. It should be noted here that the anti-apoptotic action of FT is not completely abrogated in the absence of binding to Prx I; this phenomenon can, however, be rationalized by the observation that FT binds to three other Prx Isoforms (II, III and V) all of which have the similar protective effect on cells as that of Prx I and therefore, FT may still continue to exert its protective effect on the cell under oxidative stress, despite not being able to bind to Prx I.

In summary, in this chapter I investigated the effect of FT on the stability and enzymatic function of Prx I. Our data indicate that FT stabilizes Prx I by preventing its proteosomal degradation and that addition of pure recombinant wild type FT, but not a mutant of FT that fails to bind to Prx I, enhances the peroxidase activity of Prx I *in vitro.* Digging deeper into the possible mechanism of how FT increases the enzymatic action of Prx I, I demonstrated that wild type FT increases the enzymatic activity of Prx I by preventing its inactivating phosphorylation by the serine/threonine kinase Mst1, while mutant FT cannot. Finally, I showed that the anti-apoptotic activity of FT under oxidative stress is dependent on its interaction with Prx I. Taken together these data establish the FT-Prx I interaction as an important regulatory mechanism for the functions of both proteins.

CHAPTER V: PROTECTIVE EFFECT OF FORTILIN-PEROXIREDOXIN I INTERACTION ON ALCOHOL-INDUCED DAMAGE IN MOUSE LIVER

5.1. INTRODUCTION:

Reactive oxygen species (ROS) are major contributors to protein and DNA damage, eventually leading to cell death and disease conditions like cancer, atherosclerosis, myocardial infarction, neurodegenerative diseases and alcoholic liver disease, to name a few. Alcoholic liver disease (ALD), which encompasses fatty liver, acute alcoholic hepatitis and cirrhosis, accounts for 2.1 in every 1000 alcohol-related deaths in the United States [Chen *et al.* 2006], and it is estimated that 10 to 15 percent of alcoholics will develop cirrhosis [Mann *et al.* 2004] The pathogenesis of alcohol-induced liver damage is attributed to the production of a variety of ROS in the liver, including superoxide anions or radicals, hydrogen peroxide, organic hydroperoxides, lipid peroxides and peroxynitrite, resulting from heavy alcohol consumption [Dey and Cederbaum, 2006; Arteel *et al.* 2003; Koch *et al.* 2004; Cederbaum *et al.* 2009]. ROS are scavenged within a cell by antioxidant enzymes like superoxide dismutases, catalase, glutathione peroxidases and peroxiredoxins. Peroxiredoxin I (Prx I) is a crucial anti-oxidant enzyme, the deletion of which exacerbates ethanol-induced oxidative injury in mouse livers [Bae *et al.* 2011], characterized by high levels of protein oxidation. In chapter IV, I demonstrated that

the enzymatic activity of Prx I is increased in presence of FT, which inhibits the inactivating phosphorylation of Prx I. In the current chapter, I tested the hypothesis that the absence of FT and thereby the lack of the protective effects of the FT-Prx I interaction would result in higher ethanol-induced oxidative liver damage. Using the Cre recombinase-LoxP system, I knocked out FT specifically from the liver of male C57BL/6J mice and developed acute oxidative liver damage in these mice, along with control mice, by treating them with high doses of ethanol over a short period of time. I then tested the animals for oxidative liver damage by sacrificing them and examining tissue architecture by H&E staining, liver function, measurement of malondialdehyde (MDA) and total cellular glutathione depletion and formation 4-hydroxynonenal (4-HNE) adduct by immunostaining. All these biochemical and histopathological parameters conclusively demonstrated that FT liver-specific knockout (FT-KO) mice had significantly higher ethanol-induced oxidative liver damage as compared to control mice, thus indicating that the FT-Prx I interaction is a novel protective mechanism against oxidative tissue damage in the liver.

5.2. RESULTS:

5.2.1. GENERATION OF LIVER-SPECIFIC FORTILIN KNOCKOUT MICE:

5.2.1.1. GENOTYPING:

In the current study, I crossed mice overexpressing Alb-Cre ($Cre^{+/+}$) with mice overexpressing floxed fortilin alleles – the FT sequence flanked by two identical LoxP sites – designated as LFL ($LFL^{+/+}$) (Fig. 15). In the F1 generation, crossing $Cre^{+/+}LFL^{-/-}$ mice with $Cre^{-/-}LFL^{+/+}$ mice gave rise to $Cre^{+/-}LFL^{+/-}$ mice. When these mice were self-crossed, in the F2 generation, I obtained mice with the following three genotypes: $Cre^{+/-}LFL^{-/-}$, $Cre^{+/-}LFL^{+/-}$ and $Cre^{+/-}LFL^{+/+}$. Mice with two copies of Cre - $Cre^{+/+}$- were not obtained, irrespective of the LFL status of the pups. The genetic backgrounds of the mice were confirmed via PCR (Fig. 30) and summarized in Table 4. 8-week old male mice with the genotype $Cre^{+/-}LFL^{+/+}$ were further tested for FT expression in the liver, tissue and kidney by quantitative real time PCR (qRT-PCR) and western blot, with 8-week old male mice with the genotype $Cre^{-/-}LFL^{+/+}$ as controls.
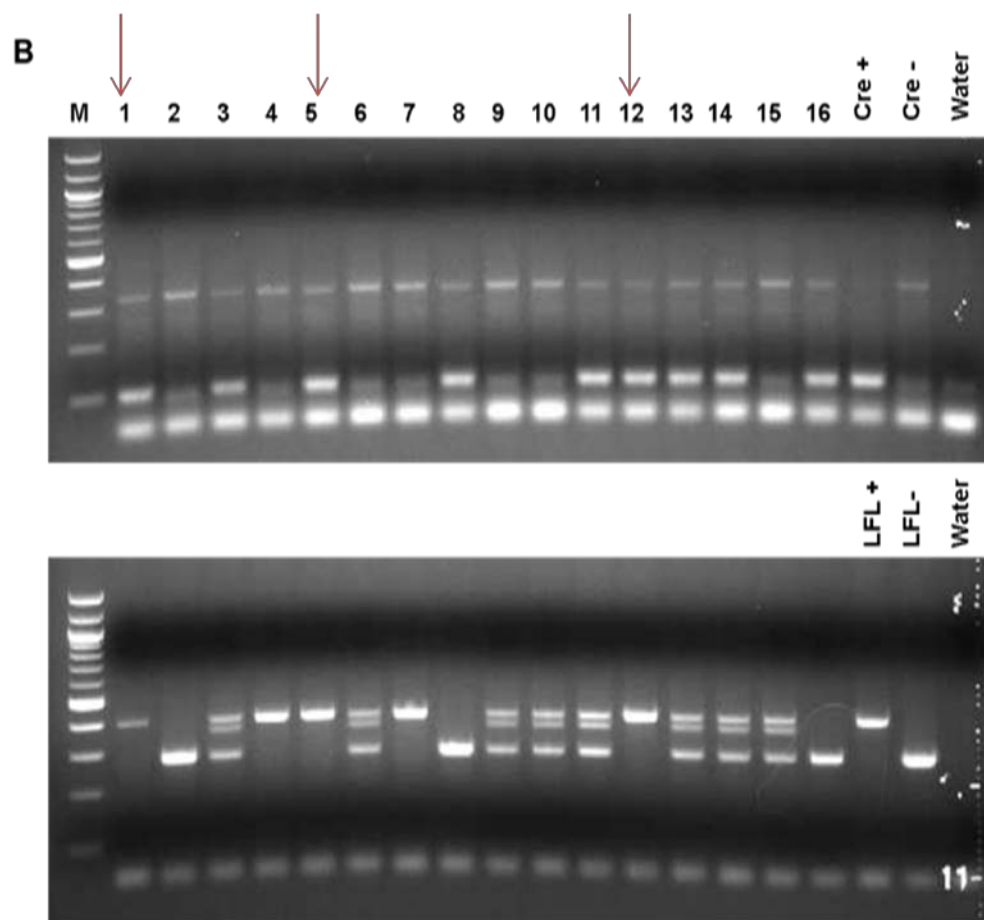
Figure 30: Representative Genotyping of F2 generation mice using primers specific to *Cre* and *LFL* genes. 100ng of DNA collected from the tail snips of 3-week old mice was subjected to PCR using primers specific for the Cre transgene **(top panel)** and the LFL transgene **(bottom panel)**. Positive and negative controls were used for both the transgenes. Using primers specific for Cre, samples 1, 3, 5, 8, 11-14 and 16 were found to contain at least one copy of the Cre transgene. Samples 1, 4, 5, 7 and 12 contained two copies of the LFL transgene. Combining the two panels, samples 1, 5 and 12 were found to contain the genotype $Cre^{+/-}LFL^{+/+}$.

Table 4: Genotyping of F2 generation Mice

Mouse	Cre genotype	LFL genotype	Overall genotype
1	+/-	+/+	$Cre^{+/-}LFL^{+/+}$
2	-/-	-/-	$Cre^{-/-}LFL^{-/-}$
3	+/-	+/-	$Cre^{+/-}LFL^{+/-}$
4	-/-	+/+	$Cre^{-/-}LFL^{+/+}$
5	+/-	+/+	$Cre^{+/-}LFL^{+/+}$
6	-/-	+/-	$Cre^{-/-}LFL^{+/-}$
7	-/-	+/+	$Cre^{-/-}LFL^{+/+}$
8	+/-	-/-	$Cre^{+/-}LFL^{-/-}$
9	-/-	+/-	$Cre^{-/-}LFL^{+/-}$
10	-/-	+/-	$Cre^{-/-}LFL^{+/-}$
11	+/-	+/-	$Cre^{+/-}LFL^{+/-}$
12	+/-	+/+	$Cre^{+/-}LFL^{+/+}$
13	+/-	+/-	$Cre^{+/-}LFL^{+/-}$
14	+/-	+/-	$Cre^{+/-}LFL^{+/-}$
15	-/-	+/-	$Cre^{-/-}LFL^{+/-}$
16	+/-	-/-	$Cre^{+/-}LFL^{-/-}$

Table 4: Genotyping of F2 generation Mice. The genotypes of the mice on which PCR reactions were performed using primers specific to Cre and LFL are summarized in the table above.

5.2.1.2. CONFIRMATION OF FORTILIN KNOCKOUT IN THE LIVER OF $Cre^{+/-}LFL^{+/+}$ MICE BY REAL-TIME QUANTITATIVE PCR:

I performed real-time quantitative PCR using RNA collected from the livers of three 8-week old male $Cre^{+/-}LFL^{+/+}$ mice and three 8-week old male $Cre^{-/-}LFL^{+/+}$ mice, using primers and probe specific for fortilin. Absolute quantification of FT mRNA relative to total RNA used for the reaction was performed and the results showed that in the livers of $Cre^{+/-}LFL^{+/+}$ mice, the amount of FT mRNA was at least 10^3-fold decreased as compared to that of $Cre^{-/-}LFL^{+/+}$ mice, as demonstrated in Fig 31.

5.2.1.3. CONFIRMATION OF FORTILIN KNOCKOUT IN THE LIVER OF $Cre^{+/-}LFL^{+/+}$ MICE BY WESTERN BLOT:

Three 8-week old male $Cre^{-/-}LFL^{+/+}$ mice and three 8-week old male $Cre^{+/-}LFL^{+/+}$ mice were sacrificed and their hearts, livers and kidneys were harvested. The organs were homogenized in RIPA buffer and subjected to immunoblotting against anti-FT and anti-GAPDH antibodies. As shown in Fig. 32, there was no difference in the FT levels in the hearts and kidneys of $Cre^{-/-}LFL^{+/+}$ and $Cre^{+/-}LFL^{+/+}$ mice. However, there was a drastic difference in FT expression in the livers of the two groups of mice with FT levels being undetectable in the liver of $Cre^{+/-}LFL^{+/+}$ mice, but present in normal amounts in the livers of $Cre^{-/-}LFL^{+/+}$ mice. GAPDH was used as a loading control. The results indicated that a single copy of the Cre transgene was

sufficient to delete FT completely or at least decrease its expression to levels undetectable using western blot. I had, therefore, successfully generated liver-specific FT knockout mice.
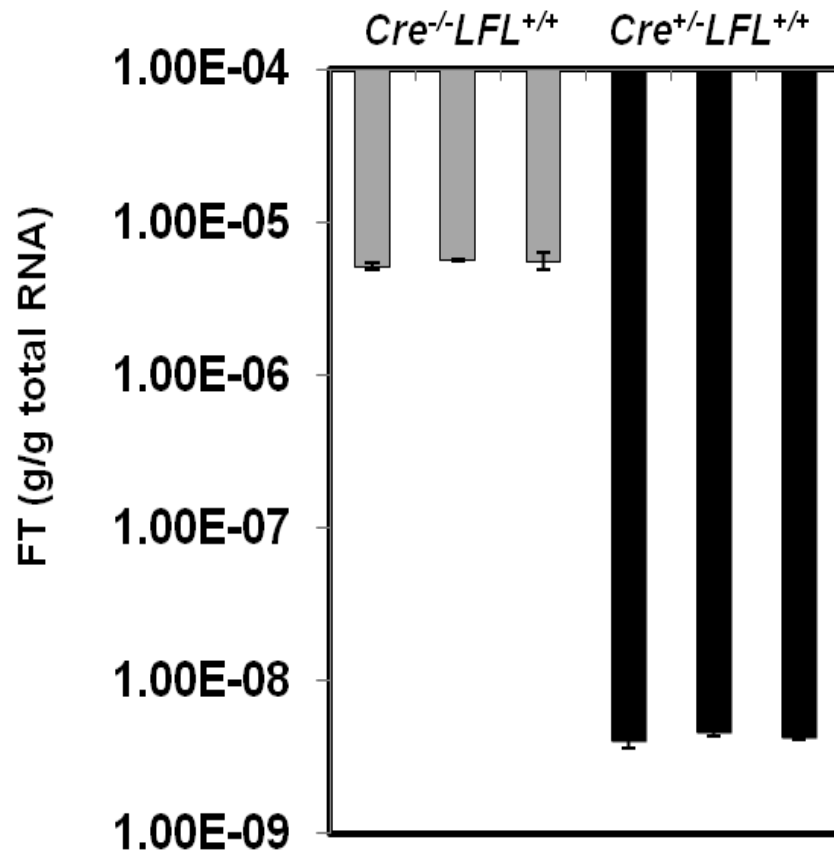
Figure 31: Absolute Quantification of FT mRNA in the liver of *Cre$^{-/-}$LFL$^{+/+}$* and *Cre$^{+/-}$LFL$^{+/+}$* mice. RNA collected from the livers of 8-week old male *Cre$^{-/-}$LFL$^{+/+}$* and *Cre$^{+/-}$LFL$^{+/+}$* mice was subjected to qRT-PCR using primers and probe specific for FT. Absolute quantification of FT mRNA was performed using a standard curve constructed using known concentrations of FT mRNA. *Cre$^{-/-}$LFL$^{+/+}$* mice were found to contain around 10μg of FT mRNA per gram of total RNA while *Cre$^{-/-}$LFL$^{+/+}$* mice were found to contain around 10ng of FT mRNA per gram of total RNA, indicating that *Cre$^{+/-}$LFL$^{+/+}$* mice contained a 10^3-fold lower amount of FT mRNA as compared to *Cre$^{-/-}$LFL$^{+/+}$* mice.

These mice would be used in the subsequent experiments to test the effect of alcohol-induced oxidative damage and determine the role of FT in protecting the animals from such damage.
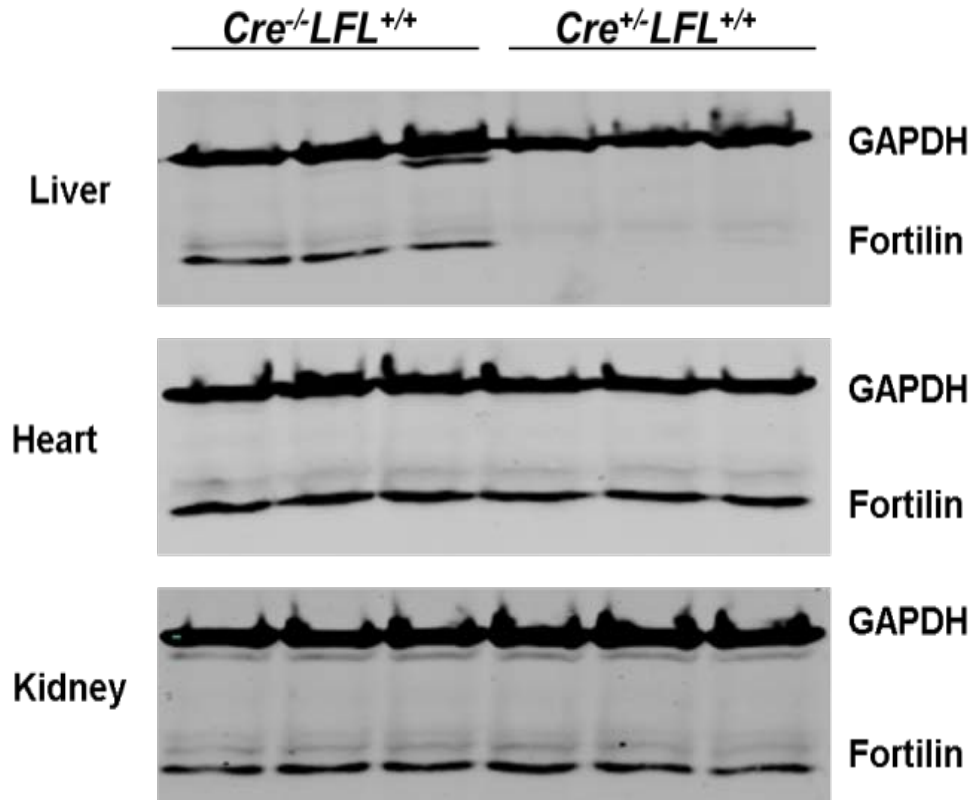
Figure 32: Verification of FT knockout in the liver of *Cre⁻ᐟ⁻LFL⁺ᐟ⁺* and *Cre⁺ᐟ⁻LFL⁺ᐟ⁺* mice. Heart, liver and kidneys were harvested from 8-week old male *Cre⁻ᐟ⁻LFL⁺ᐟ⁺* and *Cre⁺ᐟ⁻LFL⁺ᐟ⁺* mice and the respective tissue lysates were subjected to immunoblotting using anti-FT antibody. GAPDH was used as loading control. FT levels were identical in the hearts and kidneys of *Cre⁻ᐟ⁻LFL⁺ᐟ⁺* and *Cre⁺ᐟ⁻LFL⁺ᐟ⁺* mice; however, FT was undetectable in the livers of *Cre⁺ᐟ⁻LFL⁺ᐟ⁺* mice while the livers of *Cre⁻ᐟ⁻LFL⁺ᐟ⁺* mice were found to contain normal levels of FT, confirming the successful generation of liver-specific FT knockout mice.

5.2.2. INDUCTION OF ETHANOL-INDUCED LIVER DAMAGE IN *Cre^{-/-}* *LFL^{+/+}* AND *Cre^{+/-}LFL^{+/+}* MICE

5.2.2.1. DETERMINATION OF ETHANOL DOSE TO INDUCE ACUTE ALCOHOLIC LIVER DAMAGE:

In 2011, Kumar and colleagues induced alcoholic liver damage in mice by feeding them ethanol (5g/kg body weight) via oral gavage, dividing the entire amount of ethanol into three doses administered every 12 hours [Kumar *et al.* 2011]. To determine whether the same dose would be effective in our mice, I planned to feed 8-week old male *Cre^{-/-}LFL^{+/+}* mice with the same dose, using a stock solution of 20% ethanol diluted in PBS, under general anesthesia, in three doses administered every 12 hours. However, all the mice that were used to perform this dosage study, died during the procedure possibly due to alcohol poisoning, usually after the administration of the third dose. The animals appeared to be in discomfort and exhibited labored breathing. The cause of death was ascertained to be alcohol poisoning and not asphyxiation or mechanical injury during oral gavage by analyzing the liver profile of the dead animals.

I therefore chose to test other conditions of ethanol treatment, varying both the volume and concentration of the ethanol dose as well as the time between successive doses. After testing different conditions, the dosage that was found to be

most appropriate was 2.5g/kg body weight, using a stock solution of 20% ethanol diluted in PBS, under general anesthesia, divided into 6 doses administered every 6 hours. The animals were sacrificed 12 hours after the administration of the last dose and blood was collected in heparin-treated tubes for analysis of liver function parameters using VetScan mammalian liver profile disc (Abaxis, Union City, CA) on a VetScan VS2 instrument.

5.2.2.2. ANALYSIS OF LIVER PROFILE OF *Cre$^{-/-}$LFL$^{+/+}$* AND *Cre$^{+/-}$LFL$^{+/+}$* MICE TREATED WITH ETHANOL

Six 8-week old male *Cre$^{-/-}$LFL$^{+/+}$* (control) mice and six 8-week old male *Cre$^{+/-}$LFL$^{+/+}$* (FT-KO) mice were fed with 2.5g/kg body weight of ethanol in six doses administered every 6 hours. The animals were sacrificed 12 hours after the final dose by CO_2 overdose and blood was analyzed for liver profile parameters. The heart, liver and kidneys of the animals were also harvested for further analysis. The following parameters were determined: body weight, alkaline phosphatase (ALP), alanine aminotransferase (ALT), bile acids (BA), total bilirubin (TBIL), albumin (Alb), blood urea nitrogen (BUN) and cholesterol (Chol).

5.2.2.2.1. ALKALINE PHOSPHATASE (ALP):

The enzyme alkaline phosphatase (ALP) is responsible for hydrolyzing and removing phosphate groups from proteins and nucleotides. ALP is ubiquitously present in all mammalian tissues with higher concentration in the liver, bile duct, kidney, bone and the placenta. Diagnostically as far as the liver is concerned, higher ALP levels indicate obstruction of the bile duct [Pruessner *et al.* 1998], cholestasis, cholecystitis, cholangitis, cirrhosis of the liver, primary biliary cirrhosis, hepatitis, fatty liver disease, sarcoidosis and liver cancer, as well as drug overdose. As shown in Fig. 33, there was a slight elevation in the ALP levels in *Cre-/-LFL+/+* and *Cre+/- LFL+/+* mice after alcohol treatment (p =0.003).
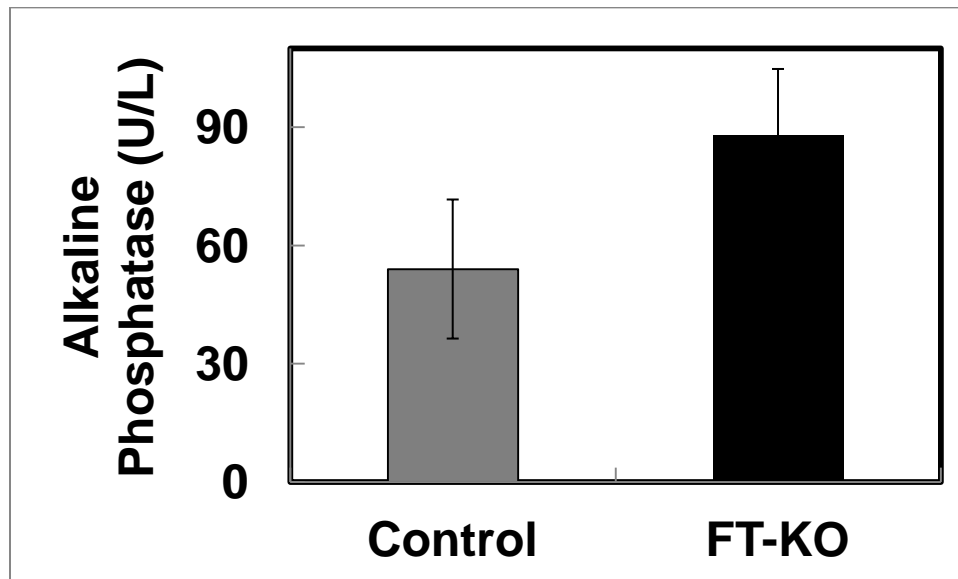
Figure 33: Alkaline Phosphatase (ALP) levels in the serum of control and FT-KO mice fed with ethanol. Blood was harvested from 8-week old male control and FT-KO mice after ethanol treatment and analyzed by VetScan mammalian liver profile discs. Post-ethanol treatment there was a slight increase in the ALP of FT-KO mice, but this increase was found to be statistically insignificant.

5.2.2.2.2. ALANINE AMINOTRANSFERASE (ALT):

The enzyme ALT catalyzes the transamination of alanine where the amino group of alanine is transferred to α-ketoglutarate, leading to the formation of pyruvate and glutamate. It is also referred to as serum glutamic pyruvic-
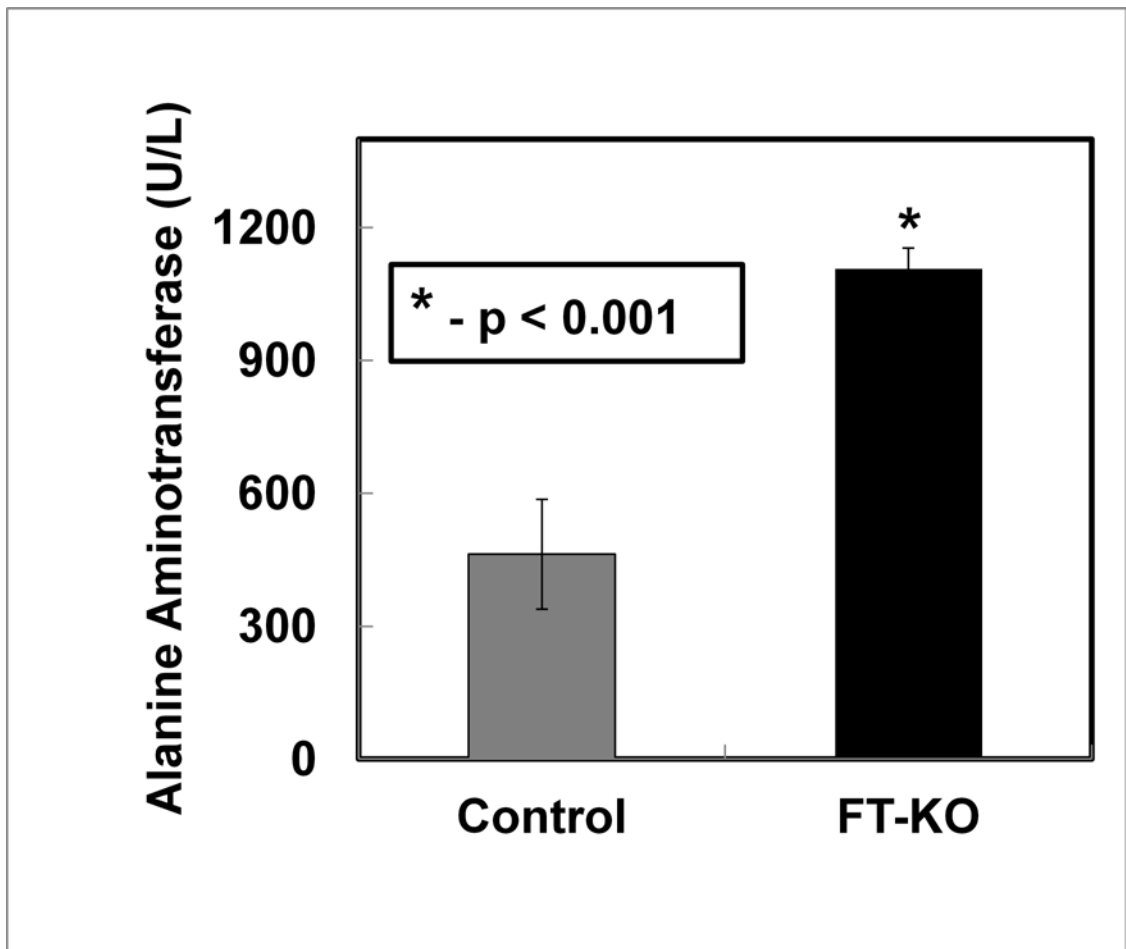
Figure 34: Alanine aminotransferase (ALT) levels in the serum of control and FT-KO mice fed with ethanol. Blood was harvested from 8-week old male *Cre⁻/⁻LFL⁺/⁺* and *Cre⁺/⁻LFL⁺/⁺* mice after ethanol treatment and analyzed by VetScan mammalian liver profile discs. Post-ethanol treatment there was a significant increase in the ALT of *Cre⁺/⁻LFL⁺/⁺*, as compared to *Cre⁻/⁻LFL⁺/⁺* mice, indicating extensive liver damage in FT-KO mice fed with ethanol.

transaminase (SGPT). Clinically, ALT is commonly used as a marker for liver health, with ALT levels under 50U/L being considered to be normal [Lenaerts *et al.* 2005]. Elevation of ALT is indicative of liver damage and therefore is commonly used to grade liver damage in humans and other animals. In the current project, as described earlier, six 8-week old male *Cre^{-/-}LFL^{+/+}* mice and six 8-week old male *Cre^{+/-}LFL^{+/+}* mice were fed with 2.5g/kg body weight of ethanol in six doses administered every 6 hours. Blood was collected after sacrifice and the ALT levels were analyzed using mammalian liver profile discs. As shown in Fig. 34, there was a significant elevation of ALT in *Cre^{+/-}LFL^{+/+}* mice as compared to *Cre^{-/-}LFL^{+/+}* mice at the baseline level, indicating that the deletion of FT from the liver causes significant liver damage even without alcohol challenge. Post ethanol treatment, the average ALT of *Cre^{-/-}LFL^{+/+}* mice was found to be **422 ± 82.85 U/L** while that of *Cre^{+/-}LFL^{+/+}* mice was found to be **1107.97 ± 47.17 U/L**. The difference in average ALT values was statistically significant between *Cre^{-/-}LFL^{+/+}* mice and *Cre^{+/-}LFL^{+/+}* mice challenged with ethanol (p = 8.46E-10). These results clearly indicate that FT protects the liver from damage and that ethanol-induced liver damage is exacerbated in FT liver knockout mice. In other words, the lack of FT makes the liver susceptible to ethanol-induced liver damage.

5.2.2.2.3. BILE ACIDS (BA):

Cholesterol-derived cholic acid and chenodeoxycholic acid (primary bile acids) and deoxycholic acid and lithocholic acid (secondary bile acids) and their

conjugated forms with glycine and taurine represent a total of 8 bile acids present in the bile of mammals, with taurocholic acid and glycocholic acid being the predominant components of human bile salts. The major function of these bile acids and their resultant salts is to help in the emulsification of dietary lipids. Clinically, bile acids are used as diagnostic parameters in cholestasis, portosystematic shunt and hepatic microvascular dysplasia. In the current project, there was a huge variation of bile acid levels in the blood of $Cre^{-/-}LFL^{+/+}$ and $Cre^{+/-}LFL^{+/+}$ mice (Fig. 35), preventing me from concluding anything concrete based on these results.

Figure 35: Bile salts (BA) levels in the serum of control and FT-KO mice fed with ethanol. Blood was harvested from 8-week old male $Cre^{-/-}LFL^{+/+}$ and $Cre^{+/-}LFL^{+/+}$ mice after ethanol treatment and analyzed by VetScan mammalian liver profile discs. Bile acid levels showed wild variations in the blood of $Cre^{-/-}LFL^{+/+}$ and $Cre^{+/-}LFL^{+/+}$ mice and thus remained inconclusive.

5.2.2.2.4. TOTAL BILIRUBIN (TBIL):

The yellow pigment bilirubin is an end-product of metabolic breakdown of heme that is excreted through bile and urine. Clinically, high levels of bilirubin are caused by increased breakdown of erythrocytes, hepatitis, jaundice and liver damage in general. In the blood of $Cre^{-/-}LFL^{+/+}$ and $Cre^{+/-}LFL^{+/+}$ mice, (Fig. 36) post-ethanol treatment, there was no statistically significant difference between the total bilirubin levels of the two genetic groups (p=0.047).

Figure 36: Total bilirubin (TBIL) levels in the serum of control and FT-KO mice fed with ethanol. Blood was harvested from 8-week old male $Cre^{-/-}LFL^{+/+}$ and $Cre^{+/-}LFL^{+/+}$ mice after ethanol treatment and analyzed by VetScan mammalian liver profile discs. Post-ethanol treatment there was no statistically significant difference between the bilirubin levels of the two groups of mice.

5.2.2.2.5. ALBUMIN:

Albumin is the most highly abundant protein present in the plasma and is responsible for the maintenance of osmotic pressure in the blood [Farruqia *et al.* 2010]. In average adult humans, the normal level of albumin ranges from 3.5 to 5.0g/dL. Clinically, variation in albumin levels is typically caused by conditions like liver disease, nephritic syndrome, malignancies (hypoalbuminemia or lowering of serum albumin) and dehydration and vitamin A-deficiency (hyperalbuminemia or elevation of serum albumin).
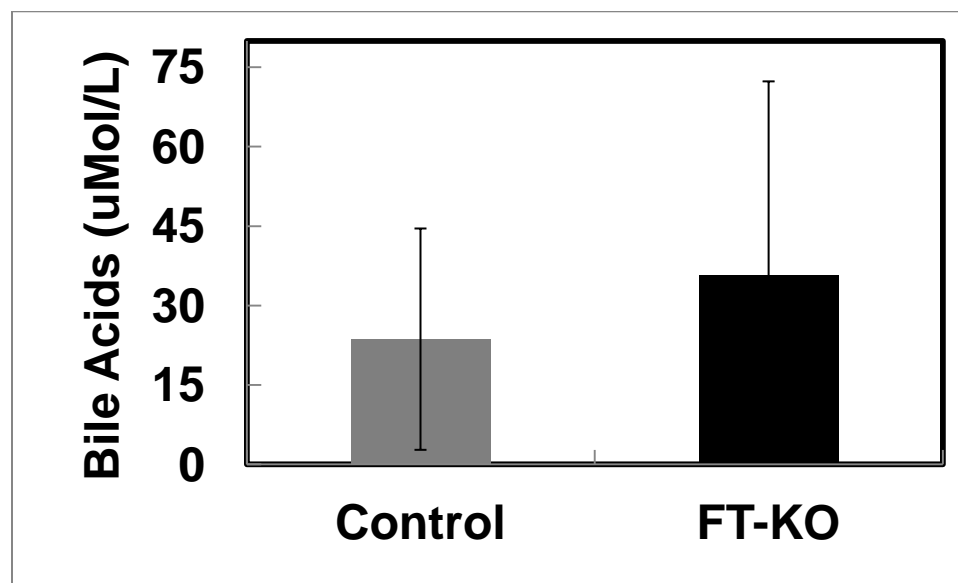

Figure 37: Albumin (Alb) levels in the serum of control and FT-KO mice fed with ethanol. Blood was harvested from 8-week old male $Cre^{-/-}LFL^{+/+}$ and $Cre^{+/-}LFL^{+/+}$ mice after ethanol treatment and analyzed by VetScan mammalian liver profile discs. Albumin levels were nearly identical in the blood of $Cre^{-/-}LFL^{+/+}$ and $Cre^{+/-}LFL^{+/+}$ mice fed with ethanol.

When the blood of *Cre$^{-/-}$LFL$^{+/+}$* and *Cre$^{+/-}$LFL$^{+/+}$* mice, (Fig. 37) was analyzed, there was virtually no difference in the albumin content in the blood of the two groups of mice (p=0.676), indicating that the lack of FT had no effect on the albumin status of the liver.

5.2.2.2.6. BLOOD UREA NITROGEN (BUN):

Blood urea nitrogen (BUN) is a parameter that measures the amount of urea-derived nitrogen in the blood as a result of protein digestion. Clinically, the normal

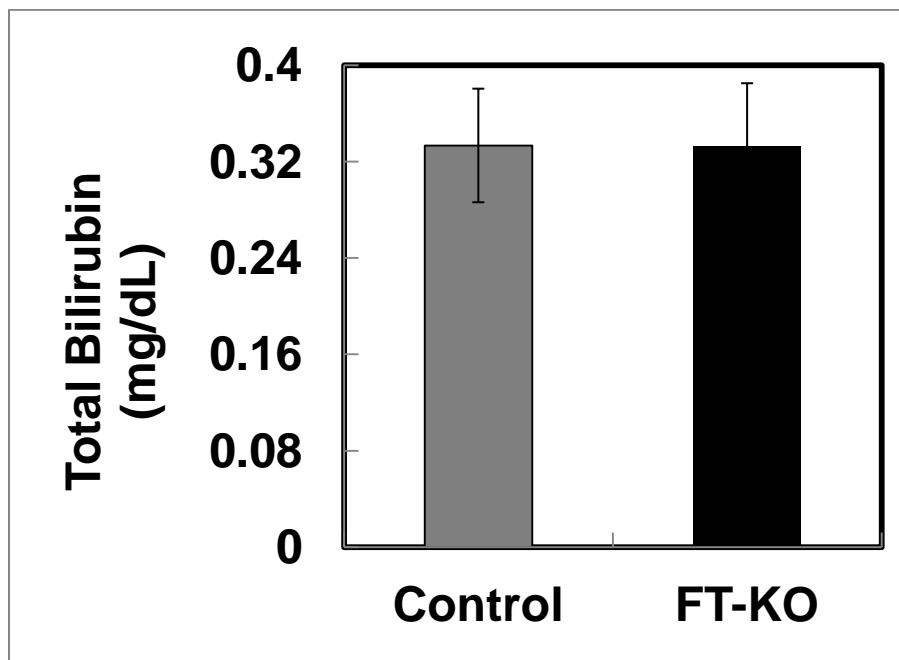**Figure 38: Blood urea nitrogen (BUN) levels in the serum of control and FT-KO mice fed with ethanol.** Blood was harvested from 8-week old male *Cre$^{-/-}$LFL$^{+/+}$* and *Cre$^{+/-}$LFL$^{+/+}$* mice after ethanol treatment and analyzed by VetScan mammalian liver profile discs. Post-ethanol treatment there was no statistically significant difference between the BUN levels of the mice of the two genetic backgrounds.

range of BUN in a normal adult human is 7-21mg/dL and is an indication of general nutrition as well as renal function. In the current study, as shown in Fig. 38, when fed with ethanol, the difference between BUN levels of ethanol-treated control and FT-KO levels was statistically insignificant (p =0.28).

5.2.2.2.7. CHOLESTEROL:

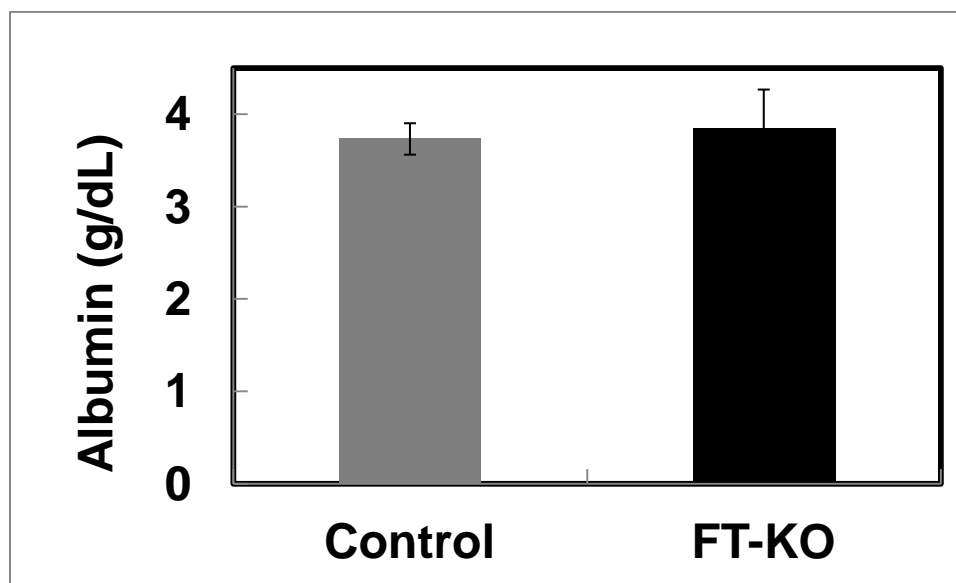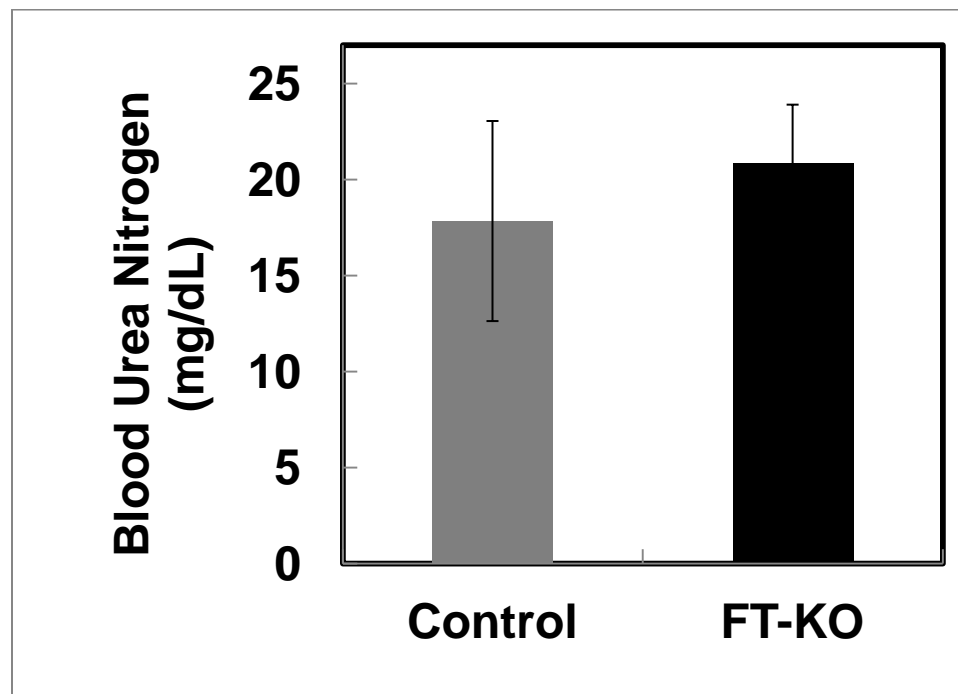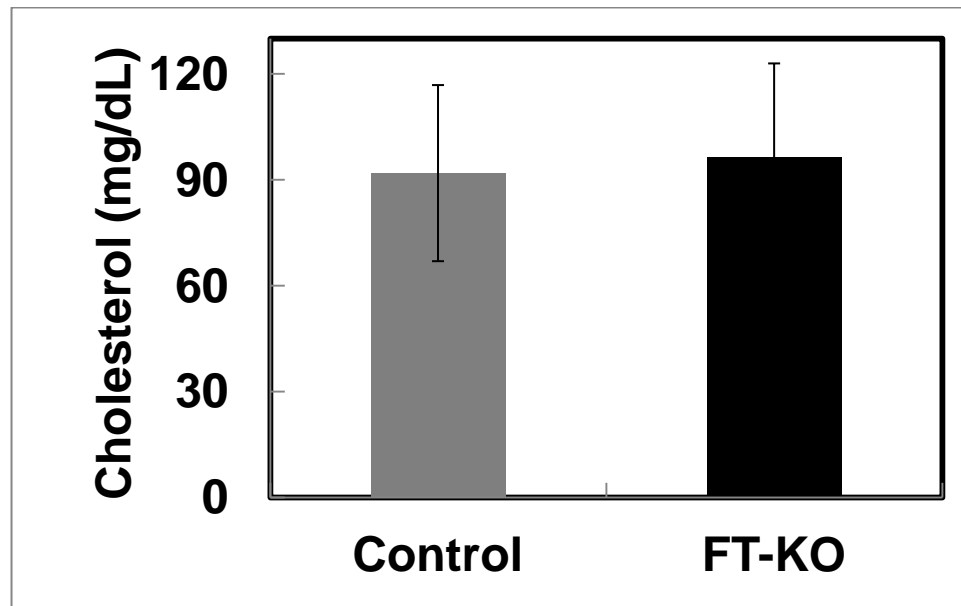**Figure 39: Cholesterol levels in the serum of control and FT-KO mice fed with ethanol.** Blood was harvested from 8-week old male *Cre^-/-LFL^+/+* and *Cre^+/-LFL^+/+* mice after ethanol treatment and analyzed by VetScan mammalian liver profile discs. Post-ethanol treatment there was no statistically significant difference between the cholesterol levels of the mice of the two genetic backgrounds.

The liver serves as the major site of cholesterol synthesis in the body, producing 20-25% of the total daily quota and also serves as the major site of cholesterol metabolism and breakdown in the body. Total cholesterol in the blood is therefore considered a marker for assessing liver function. Cholesterol concentration in the blood below 200mg/dL is considered normal for a normal adult human. As shown in Fig. 39, when I analyzed the blood of $Cre^{-/-}LFL^{+/+}$ mice and $Cre^{+/-}LFL^{+/+}$ mice fed with ethanol, the difference between the cholesterol levels of the two groups of mice was statistically insignificant (p =0.778).

5.2.3. INCREASED TISSUE DAMAGE IN THE LIVERS OF FT-KO MICE FED WITH ETHANOL:

The livers of six 8-week old male $Cre^{-/-}LFL^{+/+}$ and $Cre^{+/-}LFL^{+/+}$ mice, fed with ethanol, were fixed and perfused with neutral-buffered formalin, embedded in paraffin, cut into 5μm sections and stained with hematoxylin and eosin (H&E) to visualize the tissue architecture. Upon treatment with ethanol, both $Cre^{-/-}LFL^{+/+}$ and $Cre^{+/-}LFL^{+/+}$ mice exhibit liver damage. H&E stained livers of ethanol-fed $Cre^{-/-}LFL^{+/+}$ mice (Fig. 40) show some damage by way of some hepatocytes containing nuclei that appear to be starting to disintegrate. Analysis of the stained livers of ethanol-fed $Cre^{+/-}LFL^{+/+}$ mice shows dramatic liver damage with a large number of ballooned

and/or swollen hepatocytes with pyknotic nuclei i.e. nuclei undergoing disintegration.
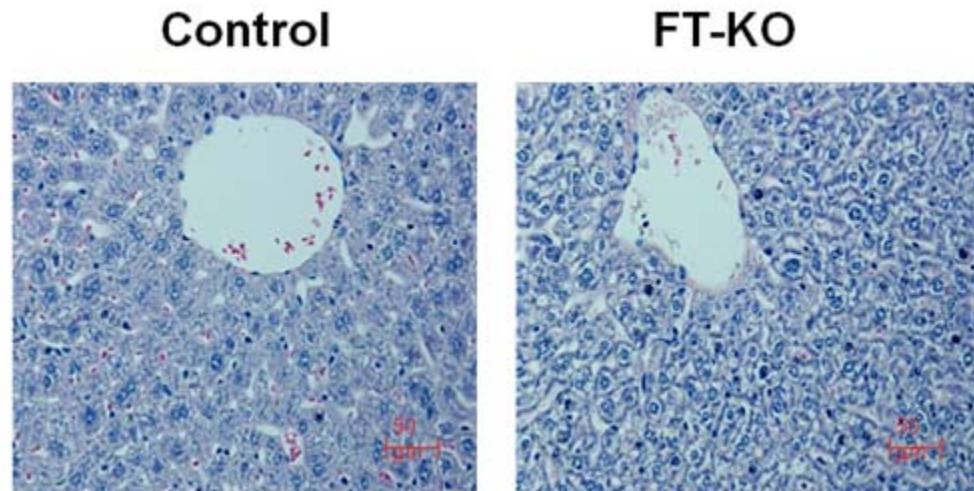
Figure 40: H&E staining of the liver of control and FT-KO mice fed with ethanol. Livers were harvested from 8-week old male *Cre^{-/-}LFL^{+/+}* and *Cre^{+/-}LFL^{+/+}* mice fed with ethanol and stained with hematoxylin and eosin. When fed with ethanol, FT-KO livers are characterized by drastic liver damage, evident from the increase in number of ballooned cells and pyknotic nuclei and general disruption of tissue architecture.

The drastic damage seen in these livers correlates perfectly with the nearly lethal ALT levels of 1107.97 ± 47.17 U/L. Taken together with the ALT values, these results conclusively demonstrate that the absence of FT in the liver exacerbates ethanol-induced liver damage.

5.2.4. INCREASED ALCOHOL-INDUCED OXIDATIVE LIVER DAMAGE

IN FT-KO MICE: MDA PRODUCTION

In Figs. 34 and 40, I have conclusively demonstrated that ethanol-induced liver damage is exacerbated by the deletion of FT from the liver. In chapter IV, I had demonstrated that FT protects cells from oxidative stress-induced cell death. Combining the two observations, I investigated whether the liver damage observed in Figs. 34 and 40 was indeed because of oxidative stress caused by ethanol consumption. A characteristic feature of ethanol-induced oxidative damage is lipid peroxidation in the liver, which can be monitored by measuring the amount of malondialdehyde (MDA) produced as a result of lipid peroxidation. As shown in Fig. 41, there is significantly higher MDA production in the livers of $Cre^{+/-}LFL^{+/+}$ mice as compared to the livers of $Cre^{-/-}LFL^{+/-}$ mice, but no such difference was observed in the kidneys of the treated animals, indicating that ethanol specifically causes higher oxidative damage to the livers of FT-KO livers.

5.2.5. INCREASED ALCOHOL-INDUCED OXIDATIVE LIVER DAMAGE

IN FT-KO MICE: GSH DEPLETION

An important characteristic indicator of oxidative liver damage is the depletion of cellular glutathione (GSH) [Lu *et al.* 2007]. When livers of ethanol-
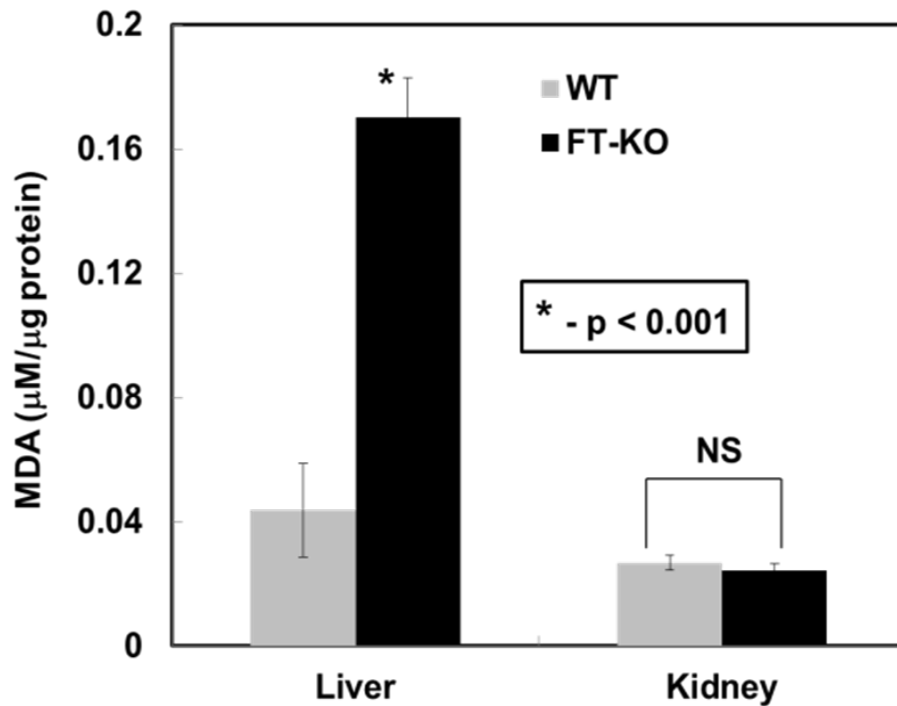
Figure 41: Increased MDA production in the liver of *Cre⁺/⁻LFL⁺/⁺* mice. Liver and kidneys were harvested from 8-week old male *Cre⁻/⁻LFL⁺/⁺* and *Cre⁺/⁻LFL⁺/⁺* mice fed with ethanol and the tissues were tested for MDA production. The livers of *Cre⁺/⁻LFL⁺/⁺* mice showed significantly higher lipid peroxidation evidenced by increased MDA production as compared to *Cre⁻/⁻LFL⁺/⁺* mice. No such difference was observed in the kidneys of these mice.

-treated *Cre⁺/⁻LFL⁺/⁺* mice were tested for total glutathione, it was observed that *Cre⁺/⁻LFL⁺/⁺* mice had a small but significant depletion of cellular GSH (Fig. 42), indicating higher oxidative damage in these mice as compared to *Cre⁻/⁻LFL⁺/⁻* mice.
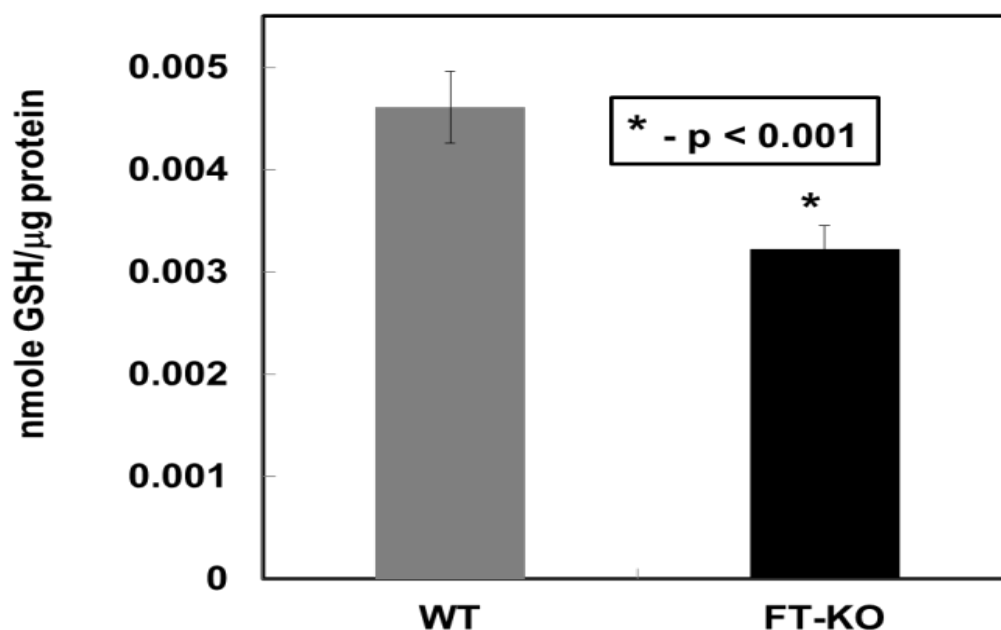
Figure 42: Increased GSH depletion in the liver of *Cre$^{+/-}$LFL$^{+/+}$* mice. Livers were harvested from 8-week old male *Cre$^{-/-}$LFL$^{+/+}$* and *Cre$^{+/-}$LFL$^{+/+}$* mice fed with ethanol and the tissues were tested for GSH levels. The livers of *Cre$^{+/-}$LFL$^{+/+}$* mice showed significantly lower GSH levels, resulting from higher GSH depletion as compared to *Cre$^{-/-}$LFL$^{+/+}$* mice.

5.2.6. INCREASED ALCOHOL-INDUCED OXIDATIVE LIVER DAMAGE

IN FT-KO MICE: 4-HNE PRODUCTION

4-hydroxynonenal (4-HNE) is a doubly unsaturated hydroxyalkenal produced as a result of lipid peroxidation and a marker of oxidative tissue damage. The livers of *Cre$^{-/-}$LFL$^{+/+}$* and *Cre$^{+/-}$LFL$^{+/-}$* mice after ethanol treatment were immunostained using an anti-4-HNE antibody. As shown in Fig. 43, 4-HNE staining
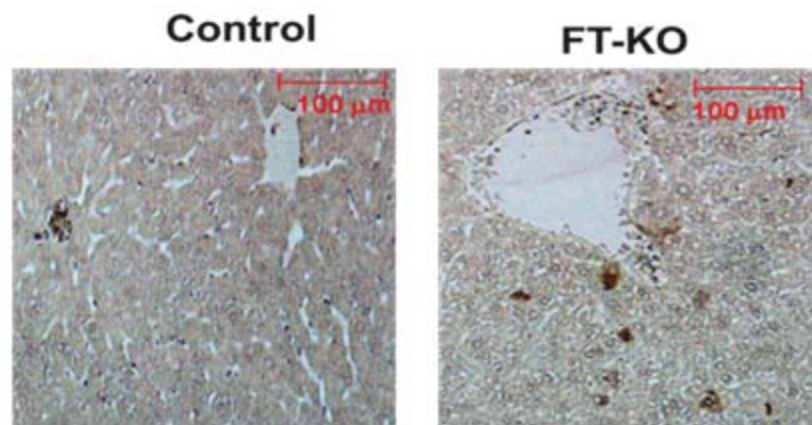
Figure 43: 4-HNE staining in the liver of *Cre^-/-LFL^+/+* and *Cre^+/-LFL^+/+* mice with ethanol treatment. Livers were harvested from 8-week old male *Cre^-/-LFL^+/+* and *Cre^+/-LFL^+/+* mice fed with ethanol and stained for 4-HNE (Dark brown coloration was considered to be positive staining). FT-KO livers showed significantly higher 4-HNE adduct formation as compared to very little staining in the control livers.

in the livers of *Cre^+/-LFL^+/-* mice was increased significantly upon ethanol treatment, as compared to control mice fed with ethanol. This confirms that the lack of FT causes a high degree of oxidative liver damage induced by acute ethanol consumption. The staining was quantified and expressed graphically in Fig. 44.

5.3. DISCUSSION:

Fortilin has been previously demonstrated to protect cells against H_2O_2 and As_2O_3 induced oxidative damage. In the current project, I have demonstrated that FT

can protect cells from H_2O_2-induced oxidative damage in U2OS cells. To translate our
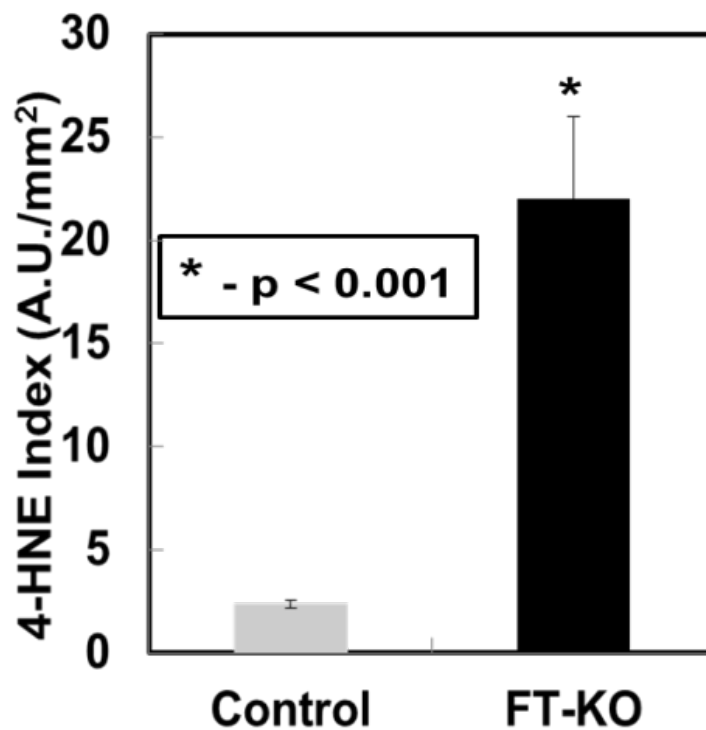
Figure 44: Quantification of 4-HNE staining in the livers of *Cre$^{-/-}$LFL$^{+/+}$* and *Cre$^{+/-}$LFL$^{+/+}$* mice post-ethanol treatment. Post-ethanol treatment there was a significant increase in the 4-HNE adduct formation in the livers of *Cre$^{+/-}$LFL$^{+/+}$* mice as compared to *Cre$^{-/-}$LFL$^{+/+}$* mice.

findings to a whole animal model, I generated a FT-liver specific knockout mouse strain and induced acute ethanol-induced oxidative liver damage in these mice. The choice of ethanol as the agent to induce oxidative damage in the liver was inspired by the fact that ethanol is much more widely consumed all over the world as

compared to acetaminophen, antimycin A or cisplatin – other agents that induce oxidative damage to the body and are responsible for a large number of health and social problems. Our hypothesis was that acute ethanol consumption would lead to significant liver damage in FT-KO mice.

Table 5: Summary of liver parameters of ethanol-treated control and FT-KO mice

Parameters	Control	FT-KO	Inference
ALP (U/L)	54	88	No significant difference
ALT (U/L)	422	1107.17	Highly significant difference, indicative of acute liver damage
Bile Acids (μMol/L)	23.67	35.67	No significant difference
TBIL (mg/dL)	0.33	0.33	No significant difference
Albumin (g/dL)	3.73	3.85	No significant difference
BUN (mg/dL)	17.83	20.83	No significant difference
Cholesterol (mg/dL)	91.83	96.33	No significant difference
MDA (μM/μg protein)	0.04	0.17	Significant difference, indicative of oxidative liver damage
GSH(nmole/μg protein)	0.0046	0.0032	Small but significant difference, indicative of oxidative liver damage
Tissue damage	+	++++	Acute liver damage in FT-KO mice
4-HNE production	+	++++	High oxidative damage in FT-KO mice

Table 5: Summary of liver parameters of ethanol-treated control and FT-KO mice. The liver parameters of control and FT-KO mice are summarized in the table above.

When fed with ethanol, there was a significantly higher degree of oxidative liver damage in FT-KO mice as compared to control mice, indicating that the absence of FT exacerbates acute ethanol-induced liver damage. A comparison of the liver profiles of the two groups of mice (summarized in Table 5) reveals that FT-KO mice have significantly higher lipid peroxidation (as reflected in higher MDA production; Fig. 41), GSH depletion (Fig. 42) and protein oxidation (4-HNE production; Fig. 43). All these parameters are markers of oxidative damage. The liver damage caused by ethanol-induced oxidative stress is reflected in the damaged tissue architecture (Fig. 40) as well as the elevation of ALT to nearly lethal levels in FT-KO mice (Fig. 34). It must be mentioned here that the ALT values of control mice are also significantly elevated, but this elevation is much lower than that in FT-KO mice. The data presented in this chapter clearly suggests that the lack of FT in the level predisposes mice towards alcohol-induced damage. A potential clinical application of this observation in future would be to use the FT status of a person to predict his/her susceptibility to ethanol-induced liver damage.

In conclusion, in this chapter I described the generation of FT liver-specific knockout mice and demonstrated that these mice have significantly higher ethanol-induced oxidative liver damage as compared to their control littermates. It has not escaped our notice that the FT-KO mice already exhibit significant liver damage even without ethanol challenge, indicating that FT plays a significant role in

maintaining normal liver homeostasis. The total extent of damage that is caused by the deletion of FT from the liver will be investigated in depth in the future. However, based on the liver profile data presented above, it has been conclusively demonstrated that the deletion of FT from the liver makes the mice highly susceptible to ethanol-induced oxidative liver damage and in future, the FT levels in the serum of a person would be used as a preventive screening tool to determine the predisposition of an individual towards alcoholic liver damage.

CHAPTER VI: GENERAL CONCLUSIONS AND FUTURE DIRECTIONS

6.1. GENERAL CONCLUSIONS:

FT is a highly conserved, ubiquitously expressed, multi-functional protein. Discovered in Ehrlich ascites tumor cells [Yenofsky *et al.* 1983] as a protein whose mRNA is rapidly translated into protein upon stimulation with growth factors, the protein has subsequently been demonstrated to be a histamine releasing factor [MacDonald *et al.* 1995], a microtubule stabilizing protein [Gachet *et al.* 1999] that binds to α- and β-tubulin and actin [Bazile *et al.* 2009; Langdon *et al.* 2004; Tuynder *et al.* 2002; Tsarova *et al.* 2010] and a novel heat shock protein with chaperone-like activity [Zhang *et al.* 2002; Liu *et al.* 2005; Gnanasekar *et al.* 2009]. In the last decade, various groups have demonstrated that FT is a potent anti-apoptotic protein under etoposide-induced cytotoxic stress [Li *et al* 2001], calcium ion-induced stress [Graidist *et al.* 2007], UV stress [Bommer *et al.* 2010; Gnanasekar and Ramaswamy, 2007; Chen *et al.* 2011] and oxidative stress [Nagano-Ito *et al.* 2009; Lucibello *et al.* 2011]. Despite being a potent anti-apoptotic protein, FT lacks sequence or structural homology with known families of anti-apoptotic proteins. It has been recently

144

demonstrated that FT protects cells from apoptosis by inhibiting p53-mediated upregulation of the pro-apoptotic protein Bax [Chen *et al.* 2011]. Taken together, this data suggests that FT may be crucially implicated in a variety of conditions like cancer, neurodegeneration, aging and cardiovascular diseases.

In the current project, I performed a systemic immunoprecipitation and mass spectrometry-based proteomic screen to identify novel fortilin interacting proteins (FIPs) that would potentially explain the mechanism of the anti-apoptotic action of FT under oxidative stress. I detected a novel interaction between FT and the anti-oxidant enzyme Prx I, which was further verified by reverse co-immunoprecipitation studies wherein I demonstrated that FT specifically interacts with four members of the peroxiredoxin family – Prx I-III and V but not with the other two – Prx IV and VI. Non-specific interactions with the HA-epitope tag and agarose beads were ruled out after it was observed that another HA-tagged protein and non-specific agarose beads were unable to co-immunoprecipitate Prx I. I additionally identified a FT point mutant – FT-L7R- which fails to bind to Prx I in an immunoprecipitation reaction. The mutant would prove to be an important tool for the functional experiments performed in the subsequent chapters. This novel protein-protein interaction represents a potential mechanism by which FT protects cells from ROS-induced apoptosis. Direct binding studies using recombinant proteins indicated a K_D in the nanomolar range, suggesting a rather strong interaction between the two proteins. Immunofluorescence and proximity ligation assay (PLA) indicated physical colocalization of FT and Prx I in the cytosolic and

perinuclear regions. Currently available literature evidence points to a cytosolic localization of FT, with oxidative stress and DNA damage response pathways reported to cause translocation of FT to the nucleus. Our data, therefore, corroborate findings by previously published works. Given that FT and Prx I both are pro-survival proteins under oxidative stress and that our preliminary data indicated a physical interaction between them, I hypothesized that the anti-apoptotic action of FT under oxidative stress was dependent on its interaction with Prx I.

As I characterized the FT-Prx I interaction further, I demonstrated that FT stabilizes Prx I by inhibiting its proteasomal degradation and in fact, the deletion of FT appeared to reduce the half life of Prx I by over 40% in U2OS cells under our experimental conditions. This observation is in agreement with previous evidence demonstrating that FT has chaperone-like activity. When I investigated the effect of FT on the function of Prx I, using pure recombinant wild type FT and pure recombinant mutant FT-L7R, I observed that addition of pure wild type FT to Prx I strikingly increased its peroxidase activity by about 2.5 fold, while addition of the mutant did not cause any detectable change in the enzyme's activity, which indicates that the biological effect of FT on Prx I is a specific consequence of binding to each other. Having established the effect of FT on the biological activity of Prx I, I sought to investigate the mechanism by which FT may increase the said activity. I demonstrated that FT prevents the deactivating phosphorylation of Prx I by the serine/threonine kinase Mst1 on its Thr^{90} and Thr^{183} residues, possibly by denying

Mst1 access to these sites, thus exhibiting a novel mechanism for control of Prx I function.

FT has been shown to be protective against H_2O_2-induced cell death in normal (CHO-K1) cells [Nagano-Ito *et al.* 2009] and As_2O_3-induced death in breast cancer cells. In the current project, I demonstrated that FT protected U2OS cells from H_2O_2-induced apoptosis. This is an important observation pertaining to the anti-apoptotic action of FT, since Lucibello *et al* have proposed FT as a protein that renders cancer cells resistant to oxidative stress-induced death. Since resistance to oxidative death is one of the proposed mechanisms of cancer cell survival, the ability of FT to protect cancer cells from ROS does reinforce the role of FT as a pro-survival factor. The fact that FT has now been shown to be anti-apoptotic against ROS in multiple malignant and non-malignant cell types underscores the importance of FT as a so-called "stress response" protein.

I further assessed the role of Prx I in the anti-apoptotic action of FT by overexpressing wild type FT and FT-L7R mutant in U2OS cells and exposing the cells to H_2O_2. I observed that the L7R mutant that fails to bind to Prx I has significantly lowered (~50%) anti-apoptotic action under oxidative stress as compared to wild type FT. This conclusively demonstrates that the anti-apoptotic activity of FT under oxidative stress is mediated via Prx I. The fact that the lack of interaction with Prx I does not completely abrogate the anti-apoptotic action of FT indicates that binding to Prx I is not the only mechanism by which FT exerts its protective effect. I have shown in our preliminary data in Chapter III that FT interacts specifically with other

Prx isoforms like Prx II, III and V. These interactions may explain the persistence of the anti-apoptotic activity of FT despite lack of interaction with Prx I.

Finally, to evaluate the role of the FT-Prx I interaction in protecting cells and tissues from oxidative damage in a live animal, I generated a liver-specific FT knockout mouse strain and fed the mice with very high doses of ethanol, leading to acute liver damage. Comparative assessment of the liver profiles of these mice with control mice fed with the same amount of ethanol indicates that FT-KO mice suffer from significantly higher tissue damage by way of protein oxidation and lipid peroxidation, resulting in physical destruction of liver architecture as well as a near-lethal elevation in the liver enzyme alanine-aminotransferase. In other words, the deletion of FT from the liver appears to exacerbate acute ethanol-induced liver damage.

In summary, the data presented in the current study demonstrate a specific and novel interaction between FT and Prx I that results in a mutual positive regulation of the two proteins at the level of biological function. Based on our preliminary data, I propose a working model of our observations. As shown in Fig. 45, FT prevents the Mst1-induced deactivating phosphorylation of Prx I and this sustains the protective anti-oxidant effect of Prx I, thus inhibiting oxidative stress-induced apoptosis.
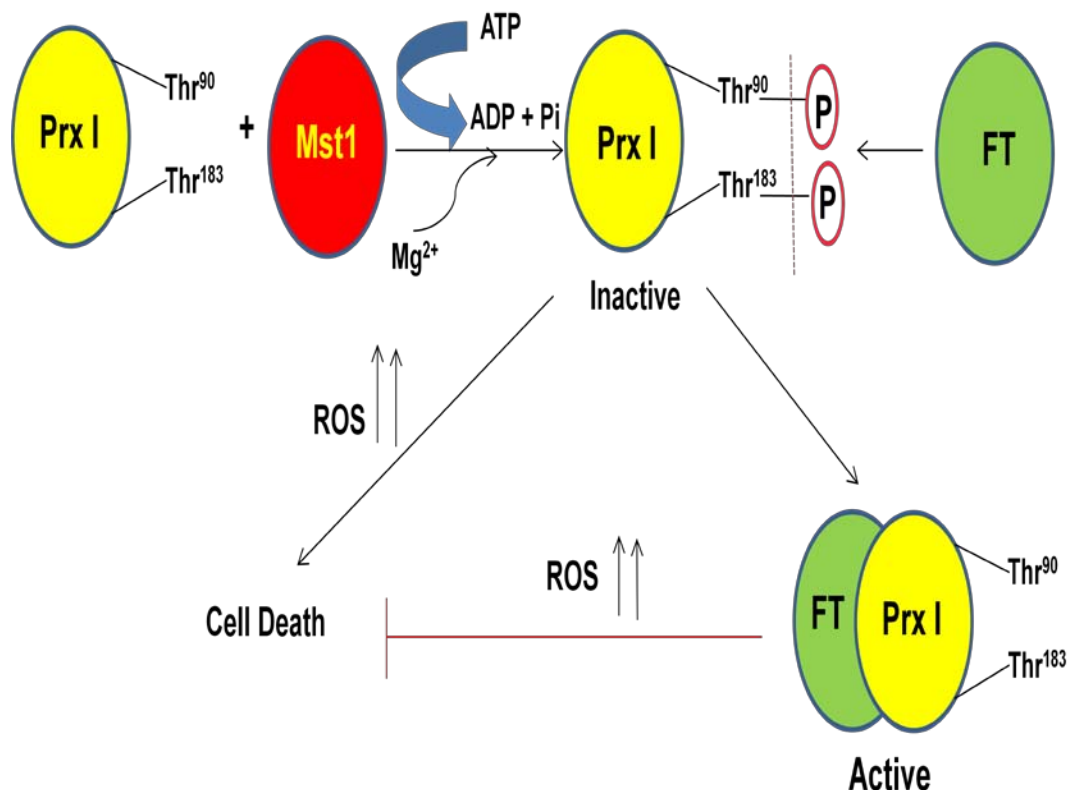
Figure 45: Working model. Upon stimulation with oxidative stress, FT is translocated into the nucleus from the cytosol, where it upregulates the transcription of Prx I and also increases its enzymatic activity in the cytosol. Prx I reciprocally increases the transcription of FT which in turn inhibits p53 and subsequent activation of the pro-apoptotic protein Bax, thereby constituting a positive feedback loop that results in protection of the cell from ROS-induced apoptosis.

6.2. FUTURE DIRECTIONS:

The current project, apart from proposing a novel mechanism of prevention of ROS-induced apoptosis by FT, also raises a number of interesting questions. The first important question that needs to be answered is how FT prevents the Mst1-induced phosphorylation of Prx I. It may be speculated that by binding to Prx I, FT

provides steric hindrance and denies Mst1 access to the phosphorylation sites Thr^{90} and Thr^{183}. This hypothesis may be tested using pure recombinant proteins to determine if increasing amounts of FT decreases the physical binding between Prx I and Mst1 and also via virtual docking studies.

The second question that follows directly from the results of this project is to investigate whether FT has the similar effect on the stability and function of Prx II, III and V as on Prx I, since FT has been shown to bind to all of these proteins. Given that the Prx Isoforms are fairly homologous in terms of sequence and function, the effect of FT on these proteins is likely to be similar to its effect on Prx I.

As demonstrated in this project, FT appears to block the access of Mst1 to the phosphorylation sites on Prx I, it will be very crucial to determine if the binding of FT to Prx I brings about any change in the structure of either protein. While the structures of both proteins have already been determined individually, the structure of the FT-Prx I complex will be an important tool in further understanding the biology of both proteins.

In order to test the significance of the FT-Prx I interaction, I generated FT liver-specific knockout mice and induced acute ethanol-mediated oxidative damage in their livers. However, even without ethanol challenge, the mice appeared to have some level of baseline liver damage and this needs to be investigated thoroughly. It will be very interesting to elucidate the exact function of FT in the liver and

determine whether the damage caused by the lack of FT in the liver resembles any known human disease. Furthermore, since our data indicates that the lack of FT predisposes mice towards ethanol-induced liver damage, a very important follow-up study stemming from the current one would be to determine if the FT status of an individual can be correlated to their susceptibility to oxidative liver damage, not only via ethanol, but also via other agents known to cause oxidative damage to the liver. Finally, since the deletion of FT exacerbates alcoholic liver damage, it is not unreasonable to expect that the overexpression of FT in the liver would be protective against ethanol stress. This would also help in determining whether the FT level in the body is indeed an appropriate marker for the ability of an individual to combat liver damage.

REFERENCES:

Amson, R., Pece, S., Lespagnol, A., Vyas, R., Mazzarol, G., Tosoni, D., Colaluca, I., Viale, G., Rodrigues-Ferreira, S., Wynendaele, J., Chaloin, O., Hoebeke, J., Marine, J.C., Di Fiore, P.P., Telerman, A. (2011) Reciprocal Repression between P53 and TCTP. *Nat. Med.* 18(1), 91-99.

Arteel, G.E. (2003) Oxidants and antioxidants in alcohol-induced liver disease. *Gastroenterology.* 124, 778-970.

Ashkenazi, A. (2002) Targeting death and decoy receptors of the tumor-necrosis factor superfamily. *Nat. Rev. Cancer.* 2, 420–430.

Bae, S.H., Sung, S.H., Cho, E.J., Lee, S.K., Lee, H.E., Woo, H.A., Yu, D.Y., Kil, I.S., Rhee, S.G. (2011) Concerted action of sulfiredoxin and peroxiredoxin I protects against alcohol-induced oxidative injury in mouse liver. *Hepatology.* 53(3), 945-953.

Bazile F., Pascal, A., Arnal, I., Le Clainche, C., Chesnel, F., Kubiak, J.Z. (2009) Complex relationship between TCTP, microtubules and actin microfilaments regulates cell shape in normal and cancer cells. *Carcinogenesis.* 30(4), 555-565.

Belch, J.J., Bridges, A.B., Scott, N., Chopra, M. (1991) Oxygen free radicals and congestive heart failure. *Br. Heart J.* 65, 245-248.

Bommer, U-A., Thiele, B.J. (2004) The translationally controlled tumour protein (TCTP) *Intl. J. Biochem. Cell. Biol.* 36, 379-385.

Byrne, J.A., Grieve, D.J., Cave, A.C., Shah, A.M. (2003) Oxidative stress and heart failure. *Arch. Mal. Coeur. Vaiss.* 96, 214-221.

Cans, C., Passer, B.J., Shalak, V., Nancy-Portebois, V., Crible, V., Amzallag, N., Allanic, D., Tufino, R., Argentini, M., Moras, D., Fiucci, G., Goud, B., Mirande, M., Amson, R., Telerman, A. (2003) Translationally controlled tumor protein acts as a guanine nucleotide dissociation inhibitor on the translation elongation factor eEF1A. *Proc. Natl. Acad. Sci. USA.* 100(24), 13892-13897.

Cederbaum, A.I., Lu, Y., Wu, D. (2009) Role of oxidative stress in alcohol-induced liver injury. *Arch. Toxicol.* 83, 519-548.

Chae, H.Z., Kim, I.H., Kim, K., Rhee, S.G. (1993) Cloning, sequencing, and mutation of thiol-specific antioxidant gene of *Saccharomyces cerevisiae*. *J. Biol. Chem.* 268, 16815-16821.

Chae, H.Z., Robison, K., Poole, L.B., Church, G., Storz, G., Rhee, S.G. (1994) Cloning and sequencing of thiol-specific antioxidant from mammalian brain: alkyl hydroperoxide reductase and thiol-specific antioxidant define a large family of antioxidant enzymes. *Proc. Natl. Acad. Sci. USA.* 91, 7017-7021.

Chae, H.Z., Uhm, T.B., Rhee, S, G. (1994) Dimerization of thiolspecific antioxidant and the essential role of cysteine 47. *Proc. Natl. Acad. Sci. USA.* 91, 7022-7026.

Chen, S.H., Wu, P.S., Chou, C.H., Yan, Y.T., Liu, H., Weng, S.Y., Yang-Yen, H.F. (2007) A knockout mouse approach reveals that TCTP functions as an essential factor for cell proliferation and survival in a tissue- or cell type-specific manner. *Mol. Biol. Cell.* 18(7), 2525-2532.

Chang, T-S., Jeong, W., Choi, S.Y., Yu, S., Kang, S.W., Rhee, S.G. (2002) Regulation of Peroxiredoxin I by Cdc2-mediated Phosphorylation. *J. Biol. Chem.* 277(28), 25370-25376.

Chen, C.M., Yi, H., Falk D.E., Stinson, F.S., Dawson, D.A., Grant, B.F. (2006) Alcohol Use and Alcohol Use Disorder in the United States: Main Findings from the 2001–2002 National Epidemiologic Survey on Alcohol and Related Conditions (NESARC). U.S. Alcohol Epidemiologic Data Reference Manual, Vol. 8, Number 1. Bethesda, MD: National Institute on Alcohol Abuse and Alcoholism.

Chen Y., Fujita, T., Zhang, D., Doan, H., Pinkaew, D., Liu, Z., Wu, J., Koide, Y., Chiu, A., Lin, C.C., Chang, J.Y., Ruan, K-H, Fujise, K. (2011) Physical and functional antagonism between tumor suppressor protein p53 and fortilin, an anti-apoptotic protein. *J. Biol. Chem.* 286(37), 32575-32585.

Cheon, S.C., Suh, J-K., Kim, M-J., Kim, S.W., Lee, K. (2008) Identification of differentially expressed proteins in the heart of translationally controlled tumor protein over-expressing transgenic mice. *Biomed. Chromatrogr.* 22, 1091-1099.

Chitpatima, S.T., Makrides, S., Bandyopadhyay, R., Brawerman, G. (1988) Nucleotide sequence of a major messenger RNA for a 21 kilodalton polypeptide that is under translational control in mouse tumor cells. *Nucleic Acids Res.* 25, 2350.

Chu, S.H., Lee-Kang, J., Lee, K.H., and Lee, K. (2003) Roles of reactive oxygen species, NF-kappaB, and peroxiredoxins in glycochenodeoxycholic acid-induced rat hepatocytes death. *Pharmacology.* 69, 12–19.

Clarke, M., Bennett, M., Littlewood, T. (2007) Cell death in the cardiovascular system. *Heart.* 93, 659-664.

Cullingford, T.E., Wait, R., Clerk, A., Sugden, P.H. (2006) Effects of oxidative stress on the cardiac myocyte proteome: modifications to peroxiredoxins and small heat shock proteins. *J. Mol. Cell. Cardiol.* 40, 157-172.

Dey, A., Cederbaum, A.I. (2006) Alcohol and oxidative liver injury. *Hepatology.* 43, S63-S74.

Diraison, F., Hayward, K., Sanders, K.L., Brozzi, F., Lajus, S., Hancock, J., Francis, J.E., Ainscow, E., Bummer, U-A., Molnar, E., Avent, N.D., Varadi, A. (2011) Translationally controlled tumor protein (TCTP) is a novel glucose-regulated protein that is important for survival of pancreatic beta cells. *Diabetologia.* 54, 368-379.

Farruqia A. (2010) Albumin usage in clinical medicine: tradition or therapeutic? *Transfus. Med. Rev*. 24(1), 53-63.

Feng, B., Yao, P.M., Li, Y., Devlin, C.M., Zhang, D., Harding, H.P., Sweeney, M., Rong, J.X., Kuriakose, G., Fisher, E.A. (2003). The endoplasmic reticulum is the site of cholesterol-induced cytotoxicity in macrophages. *Nat. Cell Biol.* 5, 781-792.

Feng, Y., Liu, D., Yao, H., Wang, J., (2007) Solution structure and mapping of a very weak calcium-binding site of human translationally controlled tumor protein by NMR. *Arch. Biochem. Biophys.* 467(1), 48-57.

Ferrari, R., Guardigli, G., Mele, D., Peroco. G.F., Ceconi, C., Curello, S. (2004) Oxidative stress during myocardial ischaemia and heart failure. *Curr. Pharm. Des.* 10, 1699-1711.

Gachet, Y., Tournier, S., Lee, M., Lazaris-Karatzas, A., Poulton, T., Bommer, U-A. (1999) The growth-related, translationally controlled protein P23 has properties of a tubulin binding protein and associates transiently with microtubules during the cell cycle. *J. Cell Sci.* 112, 1257-1271.

Gnanasekar, M., Gajalakshmi, D., Ramaswamy, K. (2009) Translationally controlled tumor protein is a novel heat shock protein with chaperone-like activity. *Biochem. Biophys. Res. Comm*. 386, 333-337.

Gnanasekar, M., Thirugnanam, S., Zheng, G., Chen, A., Ramaswamy, K. (2009) Gene silencing of translationally controlled tumor protein (TCTP) by siRNA inhibits cell growth and induces apoptosis of human prostate cancer cells. *Intl. Journ. Oncol.* 34, 1241-1246.

Graidist, P., Phongdara, A., Fujise, K. (2004) Antiapoptotic Protein Partners Fortilin and MCL1 Independently Protect Cells from 5-Fluorouracil-induced Cytotoxicity. *J. Biol. Chem.* 279(39), 40868-40875.

Graidist, P., Yazawa, M., Tongnunt, M., Nakatomi, A., Lin, C.C., Chang, J.Y., Phongdara, A., Fujise, K. (2007) Fortilin binds Ca2+ and blocks Ca2+-dependent apoptosis in vivo. *Biochem. J.* 408(2), 181-191.

Gu, H., Marth, J.D., Orban, P.C., Mossman, H., Rajewsky, K. (1994) "Deletion of the DNA polymerase beta gene in T cells using tissue-specific gene targeting. *Science.* 265, 103-106.

Hanahan, D, Weinberg, R.A. (2000) The hallmarks of cancer. *Cell.* 100, 57–70.

Hanahan, D, Weinberg, R.A. (2011) Hallmarks of cancer: the next generation. *Cell.* 144(5), 646-674.

Hinojosa-Moya, J., Xoconostle-Cazares, B., Piedra-Ibarra, E., Mendez-Tenorio, A., Lucas, W.J., Ruiz-Medrano, R. (2008) Phylogenetic and Structural Analysis of Translationally Controlled Tumor Proteins. *J. Mol. Evol*. 66, 472-483.

Hofmann, B., Hecht, H-J., Flohe, L. (2002) Peroxiredoxins. *Biol. Chem.* 383: 347–3364.

Hsu, Y.C., Chern, J.J., Cai, Y., Liu, M., Choi, K.W. (2008) Drosophila TCTP is essential for growth and proliferation through dRheb GTPase. *Nature.* 445 (7129), 785-788.

Immenschuh, S., Baumgart-Vogt, E. (2005) Peroxiredoxins, Oxidative Stress, and Cell Proliferation. *Antioxid. Redox Sig.* 7(5&6), 768-777.

Immenschuh, S., Baumgart-Vogt, E., Tan, M., Iwahara, S., Ramadori, G, Fahimi, H.D. (2003) Differential cellular and subcellular localization of heme-binding protein 23/peroxiredoxin I and heme oxygenase-1 in rat liver. *J. Histochem. Cytochem.* 51, 1621-1631.

Johansson, H., Dzeneta, V-H., Simonsson, T., Simonsson, S. (2010) Translationally controlled tumor protein interacts with nucleophosmin during mitosis in ES cells. *Cell Cycle.* 9(11), 2160-2169.

Jonsson, T.J., Johnson, L.C., Lowther, W.T. (2008) Structure of the sulphiredoxin-peroxiredoxin complex reveals an essential repair embrace. *Nature.* 451, 98-101.

Johansson, H., Svensson, F., Runnberg, R., Simonsson, T., Simonsson, S. (2010) Phosphorylated Nucleolin Interacts with Translationally Controlled Tumor Protein during Mitosis and with Oct4 during Interphase in ES cells. *PLoS One.* 5(10), e13678.

Jung, J., Kim, H.Y., Kim, M., Sohn, K., Kim, M., Lee, K. (2011) Translationally controlled tumor protein induced human breast epithelial cell transformation through the activation of Src. (2011) *Oncogene.* 1-11.

Kamitani, T., Kito, K., Nguyen, H. P., Yeh, E. T. (1997) Characterization of NEDD8, a developmentally down-regulated ubiquitin-like protein. *J. Biol. Chem.* 272, 28557–28562.

Kim, M., Min, H.J., Won, H.Y., Park, H., Lee, J-C., Park, H-W., Chung, J., Hwang, E.S., Lee, K. (2009) Dimerization of Translationally Controlled Tumor Protein Is Essential For Its Cytokine-Like Activity. *PLoS One*, 4(7), e6464.

Kim, J-A., Park, S., Kim, K., Rhee, S.G., Kang, S.W. (2005) Activity assay of mammalian 2-Cys peroxiredoxins using yeast thioredoxin reductase system. *Anal. Biochem.* 338, 216-223.

Kim, M-J., Lyu, J., Sohn, K-B., Kim, M., Cho, M-C., Joo, C-K., Lee. K. (2009) Over-expression of translationally controlled tumor protein in lens epithelial cells seems to be associated with cataract development. *Transgenic Res.* 18, 953-960.

Kim, M-J., Kwon, J-S., Suh, S.H., Suh, J-K., Jung, J., Lee, S-N., Kim, Y-H., Cho, M-C., Oh, G.T., Lee. K. (2008) Transgenic overexpression of translationally controlled tumor protein induces systemic hypertension via repression of Na$^+$, K$^+$ -ATPase. *J Mol. Cell. Cardiol.* 44, 151-159.

Koch, O.R., Pani, G., Borrello, S., Colavitti, R., Cravero, A, Farre, S., Galeotti, T. (2004). Oxidative stress and antioxidant defenses in ethanol-induced cell injury. *Mol Aspects Med.* 25, 191-198.

Koide, Y., Kiyota, T., Tonganunt, M., Pinkaew, D., Liu, Z., Hutadilok-Towatana. N., Phongdara, A., and Fujise, K. (2009) Embryonic lethality of fortilin-null mutant mice by BMP-pathway overactivation. *Biochim. Biophys. Acta.* 1790(5), 326-338.

Kumar, K.J.S., Chu, F-H., Hsieh, H-W., Liao, J-W., Li, W-H., Lin, J. C-C., Shaw, J-F., Wang, S-Y. (2011) Antroquinonol from ethanolic extract of mycelium of *Antrodia cinnamomea* protects hepatic cells from ethanol-induced oxidative stress through Nrf-2 activation. *J. Ethnopharmacol.* 136(1), 168-177.

Lenaerts, A.J., Johnson, C.M., Marrieta, K.S., Gruppo, V., Orme, I.M. (2005) Significant increases in the levels of liver enzymes in mice treated with anti-tuberculosis drugs. *Int. J. Antimicrobial Agents.* 26(2), 152-158.

Langdon, J.M., Vonakis, B.M., MacDonald, S.M. (2004) Identification of the interaction between the human recombinant histamine releasing factor/translationally controlled tumor protein and elongation factor-1 delta (also known as eElongation factor-1B beta). *Biochim. Biophys. Acta.* 1688, 232-236.

Lee, J.H., Rho, S.B., Park, S.Y., Chun, T. (2008) Interaction between fortilin and transforming growth factor-beta stimulated clone-22 (TSC-22) prevents apoptosis via the destabilization of TSC-22. *FEBS Lett.* 582(8), 1210-1218.

Li, F., Zhang, D., Fujise K. (2001) Characterization of fortilin, a novel antiapoptotic protein. *J. Biol. Chem*. 276(50), 47542-47549.

Li, S., Chen, X., Ding, Y., Liu, X., Wang, Y., He, J. (2011) Expression of translationally controlled tumor protein (TCTP) in the uterus of mice of early pregnancy and its possible significance during embryo implantation. *Human Reprod.* 0(0), 1-9.

Lin, J.H., Li, H., Yasumura, D., Cohen, H.R., Zhang, C., Panning, B., Shokat, K.M., Lavail, M.M., and Walter, P. (2007). IRE1 signaling affects cell fate during the unfolded protein response. *Science.* 318, 944-949.

Liu, H., Peng, H-W., Cheng, Y-S., Yuan, H.S., Yang-Yen, H-F. (2005) Stabilization an Enhancement of the Antiapoptotic Activity of Mcl-1 by TCTP. *Mol. Cell. Biol.* 25(8), 3117-3126.

Liu, M.C., Proud, D., Lichtenstein, L.M., MacGlashan, D.W., Jr, Schleimer, R.P., Adkinson, N.F. Jr, Kagey-Sobotka, A., Schulman, E.S., Plaut, M. (1986) Human lung macrophage-derived histamine-releasing activity is due to IgE-dependent factors. *J. Immunol.* 136, 2588–2595.

Lu, Z.M., Tao, W.Y., Zou, X.L., Fu, H.Z., Ao, Z.H., (2007) Protective effects of mycelia of *Antrodia camphorata* and *Armillariella tabescens* in submerged culture against ethanol-induced hepatic toxicity in rats. *J. Ethnopharmacology.* 110,160–164.

Lucibello M., Gambacurta, A., Zonfrillo, M., Pierimarchi, P., Serafino, A., Rasi, G., Rubartelli, A., Garaci, E. (2011) TCTP is a critical survival factor that protects cancer cells from oxidative stress-induced cell-death. *Exp. Cell. Res*. 317(17), 2479-2489.

Ma, Q., Geng, Y., Xu, W., Wu, Y., He, F., Shu, W., Huang, M., Du, H., Li, M. (2010) The Role of Translationally Controlled Tumor Protein in Tumor Growth and Metastasis of Colon Adenocarcinoma Cells. *J. Proteome Res.* 9(1), 40-49.

MacDonald, S.M., Lichtenstein, L.M., Proud, D., Plaut, M., Naclerio, R.M., MacGlashan, D.W., Kagey-Sobotka, A. (1987) Studies of IgE-dependent histamine releasing factors: heterogeneity of IgE. *J. Immunol.* 139, 506–512.

MacDonald, S.M., Rafnar, T., Langdon, J., Lichtenstein, L.M. (1995) Molecular identification of an IgE-dependent histamine-releasing factor. *Science.* 269, 688-690.

Mak, C.H., Su, K.W., Ko, R.C. (2001) Identification of some heat-induced genes of *Trichinella spiralis*, *Parasitology.* 123, 293–300.

Mallat, Z., Philip, I., Lebret, M., Chatel, D., maclouf, J., Tedgui, A. (1998) Elevated levels of 8-iso-prostaglandin F2☐ in pericardial fluid of patients with heart failure: A potential role for in vivo oxidant stress in ventricular dilatation and progression to heart failure. *Circulation.* 97, 1536-1539.

Mann, R.E., Smart, R.G., Govoni, R. (2004) National Institute on Alcohol Abuse and Alcoholism.

Munirathnam, G., Ramaswamy, K. (2012) Sumoylation of human translationally controlled tumor protein is important for its nuclear transport. *Biochem. Res. Int.* 831940.

Nagano-Ito, M., Banba, A., Ichikawa, S. (2009) Functional cloning of genes that suppress oxidative stress-induced cell death: TCTP prevents hydrogen peroxide-induced cell death. *FEBS Lett.* 583(8), 1363-1367.

Nguyen T., Sherratt P.J., Pickett, C.B. (2003) Regulatory mechanisms controlling gene expression mediated by the antioxidant response element. *Annu. Rev. Pharmacol. Toxicol.* 43, 233-260.

Norbeck J., Blomberg, A. (1997) Two-dimensional electrophoretic separation of yeast proteins using a non-linear wide range (pH 3-10) immobilized pH gradient in the first dimension; reproducibility and evidence for isoelectric focusing of alkaline (pI 4-7) proteins. *Yeast.* 13, 1519-1534.

Neumann, C.A., Krause, D.S., Carman, C.V., Das, S., Dubey, D.P., Abraham, J.L., Bronson, R.T., Fujiwara, Y., Orkin, S.H., and Van Etten, R.A. (2003) Essential

role for the peroxiredoxin Prdx1 in erythrocyte antioxidant defence and tumor suppression. *Nature.* 424, 561–565.

Pasmans, S.G., Witteman, A.M., Aalbers, M., Boonstra, J.G., Mul, E.P., van der Zee, J.S., Knol, E.F., Jansen, H.M., Aalberse, R.C. (1994) Variability of IgE-dependent histamine-releasing activity in supernatants of human mononuclear cells. *Int Arch Allergy Immunol.* 103(1), 44-52.

Prosperi, M.T., Ferbus, D., Karczinski, I., Goubin, G. (1993) A human cDNA corresponding to a gene overexpressed during cell proliferation encodes a product sharing homology with amoebic and bacterial proteins. *J. Biol. Chem.* 268, 11050–11056.

Pruessner, H.T. (1998) Detecting celiac disease in your patients. *Am. Farm. Physician.* 57(5), 1023-34, 1039-1041.

Rawat, S.J., Creasy, C.L., Peterson, J.R., and Chernoff, J. (2013) The Tumor Suppressor Mst1 Promotes Changes in the Cellular Redox State by Phosphorylation and Inactivation of Peroxiredoxin-1 Protein. *J. Biol. Chem.* 288, 8762–8771.

Rehmann, H., Bruning, M., Berghaus, C., Schwarten, M., Kohler, K., Stocker, H., Stoll, R., Zwartkruis, F.J., Wittinghofer, A. (2008) Biochemical characterisation of TCTP questions its function as a guanine nucleotide exchange factor for Rheb. *FEBS Lett.* 582, 3005-3010.

Rhee, S.G., Kang, S.W., Netto, L.E., Seo, M.S., Stadtman, E.R. (1999) A family of novel peroxidases, peroxiredoxins. *Biofactors.* 10, 207-209.

Rho, S.B., Lee, J.H., Park, M.S., Byun, H.J., Kang, S., Seo, S.S., Kim, J.Y., Park, S.Y. (2011) Anti-apoptotic protein TCTP controls the stability of the tumor suppressor p53. *FEBS Lett.* 585(1), 29-35.

Rid, R., Onder, K., Trost, A., Bauer, J., Hintner, H., Ritter, M., Jakab, M., Costa, I., Reischl, W., Richter, K., Macdonald, S., Jendrach, M., Bereiter-Hahn, J., Breitenbach, M. (2010) H(2)O(2)-dependent translocation of TCTP into the nucleus enables its interaction with VDR in human keratinocytes: TCTP as a further module in calcitriol signaling. *J. Steroid Biochem. Mol. Biol.* 118(1-2), 29-40.

Schroeder, J.T., Lichtenstein, L.M., MacDonald, S.M. (1997) Recombinant histamine-releasing factor enhances IgE-dependent IL-4 and IL-13 secretion by human basophils. *J. Immunol.* 159, 447–452.

Sternberg, N., Hamilton, N. (1981) Bacteriophage P1 site-specific recombination: I. Recombination between loxP sites. *J. Mol. Biol.* 150,467-486.

Susini, L., Besse, S., Duflaut, D., Lespagnol, A., Beekman, C., Fiucci, G., Atkinson, A.R., Busso, D., Poussin, P., Marine, J.C., Cavarelli. J., Moras, D., Amson, R., Telerman, A. (2008) TCTP protects from cell death by antagonizing bax function. *Cell Death Differ.* 15(8), 1211-1220.

Thaw, P., Baxter, N.J., Hounslow, A.M., Price, C., Waltho, J.P., Craven, C.J. (2001) Structure of TCTP reveals unexpected relationship with guanine nucleotide-free chaperones. *Nat. Struct. Biol.* 8, 701–704.

Thiele, H., Berger, M., Skalweit, A., Thiele, B. J. (2000). Expression of the gene and processed pseudogenes encoding the human and rabbit translationally controlled tumour protein (TCTP). *European Journal of Biochemistry*, *267*, 5473-5481.

Tsarova, K., Yarmola, E.G., Bubb, M.R. (2010) Identification of a cofilin-like actin-binding site on translationally controlled tumor protein (TCTP). *FEBS Lett.* 584(23), 4756-4760.

Tsutsui, H., Kinugawa, S., Matsuhima, S. (2008) Oxidative Stress and Mitochondrial DNA Damage in Heart Failure. *Circ. J.* Suppl A, A-31 – A-37.

Tuynder, M., FIucci, G., Prieur, S., Lespagnol, A., Geant, A., Beaucourt, S., Duflaut, D., Besse, S., Susini, L., Cavarelli, J., Moras, D., Amson, R., Telerman, A. (2004) Translationally controlled tumor protein is a target of tumor reversion. *Proc. Natl. Acad. Sci. USA*. 101(43), 15364-15369.

Warner, J.A., Pienkowski, M.M., Plaut, M., Norman, P.S., Lichtenstein, L.M. (1986) Identification of histamine releasing factor(s) in the late phase of cutaneous IgE mediated reactions. *J. Immunol.* 136, 2583–2587.

Wen, S-T and Van Etten, R.A. (1997) The pag gene product, a stress-induced protein with antioxidant properties, is an Abl SH3- binding protein and a physiological inhibitor of c-Abl tyrosine kinase activity. *Genes Dev.* 11, 2456–2467.

Woo, H.A., Chae, H.Z., Hwang, S.C., Yang, K.S., Kang, S.W., Kim, K, and Rhee, S.G.(2003) Reversing the inactivation of peroxiredoxins caused by cysteine sulfinic acid formation. *Science.* 300, 653–656.

Wood, Z.A., Schroder, E., Harris, J.R., Poole, L.B. (2003) Structure, mechanism and regulation of peroxiredoxins. *Trends Biochem. Sci.* 28, 32–40.

Wu, P.S., Yang, C.Y., Yen, J.J., Chou, C.H., Wang, C.K., Lai, Y.G., Liao, N.S., Yang-Yen, H.F. (2009) Critical roles of translationally controlled tumor protein in the homeostasis and TCR-mediated proliferation of peripheral T-cells. *J. Immunol.* 183(4), 2373-2381.

Yarn, F.R. (2002) Plk phosphorylation regulates the microtubule-stabilizing protein TCTP. *Mol. Cell. Biol.* 22, 6209-6221.

Yang, Y., Yang, F., Xiong, Z., Yan, Y., Wang, X., Nishino, M., Mirkovic, D., Nguyen, J., Wang, H, Yang, X-F. (2005) An N-terminal region of translationally controlled tumor protein is required for its antiapoptotic activity. *Oncogene.* 24, 4778-4788.

Yenofsky, R., Cereghini, S., Krowczynska, A., Brawerman, G. (1983) Regulation of mRNA utilization in mouse erythroleukemia cells induced to differentiate by exposure to dimethyl sulfoxide. *Mol. Cell. Biol* 3, 1197–1203.

Yoneda, K., Rokutan K., Nakamura, Y., Yanagawa, H., Kondo-Teshima, S., Sone, S. (2004) Stimulation of human bronchial epithelial cells by IgE-dependent histamine-releasing factor. *Am. J. Physiol. Lung. Cell. Mol. Physiol.* 286(1), L174-181.

Zhang, D., Li, F., Weidner, D., Mnjoyan, Z.H., Fujise, K. (2002) Physical and Functional Interaction between Myeloid Cell Leukemia 1 Protein (MCL1) and Fortilin: The potential role of MCL1 as a fortilin chaperone. *J. Biol. Chem.* 277(40), 37430-37438.

Zhang, J., de Toledo, S.M., Pandey, B.N., Guo, G., Pain, D., Li, H., Azzam, E.I. (2012) Role of the translationally controlled tumor protein in DNA damage sensing and repair. *Proc. Natl. Acad. Sci. USA.* 109(16), E926-933.

Zinszner, H., Kuroda, M., Wang, X., Batchvarova, N., Lightfoot, R.T., Remotti, H., Stevens, J.L., and Ron, D. (1998). CHOP is implicated in programmed cell death in response to impaired function of the endoplasmic reticulum. *Genes Dev*. 12, 982-995.

VITA

Abhijnan Chattopadhyay was born on June 3, 1983 in Kolkata (erstwhile Calcutta), West Bengal, India as the only child of Bijoy and Projnaparamita Chatterjee. Abhijnan attended South Point School from kindergarten through fifth grade and South Point High School from sixth grade through twelfth grade. He passed the Secondary Examination in the year 2000 and was placed 21st out of over 550,000 candidates. Two years later, he passed the Higher Secondary Examination, placing 150th out of over 350,000 students. For both these achievements, he received a National Certificate of Merit from the Government of India. Abhijnan then attended Presidency College, Kolkata (now Presidency University) affiliated with the University of Calcutta and earned a Bachelor of Science degree in 2005, majoring in Chemistry and securing a rank of 16th out of over 800 students in the process. In 2007, Abhijnan graduated with a Master of Science degree in Biochemistry from the University of Calcutta and placed 5th out of 48 successful candidates on the merit list. He joined the Biochemistry and Molecular Biology Graduate Program at the University of Texas Medical Branch in Galveston (UTMB) in the Fall of 2007.

Throughout his graduate career at UTMB, Abhijnan received multiple awards including the Jane Welsh Award for Excellence in Cardiovascular Research (2010), the Rose and Harry Walk Research Award (2011), the Barbara Bowman Award (2011) and the Biological Chemistry Student Organization (BCSO) Student Award (2012). Additionally, in the Spring of 2012, Abhijnan was nominated into Who's Who Among Students in American Colleges and Universities.

Abhijnan can be contacted through his parents at 83/4A Ballygunge Place, Kolkata – 700019, West Bengal, India.

This dissertation was typed by: Abhijnan Chattopadhyay